


2018

An Interdisciplinary Approach To The Target Elucidation of Novel Antibiotic 31G12

Larissa A. Walker
University of Montana

Let us know how access to this document benefits you.

Follow this and additional works at: <https://scholarworks.umt.edu/etd>

 Part of the [Bioinformatics Commons](#), [Microbiology Commons](#), and the [Organic Chemistry Commons](#)

Recommended Citation

Walker, Larissa A., "An Interdisciplinary Approach To The Target Elucidation of Novel Antibiotic 31G12" (2018). *Graduate Student Theses, Dissertations, & Professional Papers*. 11306.
<https://scholarworks.umt.edu/etd/11306>

This Thesis is brought to you for free and open access by the Graduate School at ScholarWorks at University of Montana. It has been accepted for inclusion in Graduate Student Theses, Dissertations, & Professional Papers by an authorized administrator of ScholarWorks at University of Montana. For more information, please contact scholarworks@mso.umt.edu.

AN INTERDISCIPLINARY APPROACH TO THE TARGET ELUCIDATION
OF NOVEL ANTIBIOTIC 31G12

By

LARISSA ANN WALKER

B.S. MICROBIOLOGY, UNIVERSITY OF MONTANA, MISSOULA, MT, 59812

Thesis

Presented in partial fulfillment of the requirements
for the degree of

Master of Science
In Microbiology

The University of Montana
Missoula, MT

January 2019

Approved by:

Scott Whittenburg, Dean of the Graduate School
Graduate School

Dr. Nigel Priestley, Committee Chair
Department of Chemistry

Dr. Michael Minnick, Committee Member
Division of Biological Sciences

Dr. Stephen Lodmell, Committee Member
Division of Biological Sciences

An interdisciplinary approach to target elucidation of novel triazole antibiotic 31G12

Chairperson: Dr. Nigel Priestley, Department of Chemistry

Staphylococcus aureus is a Gram-positive bacterial pathogen responsible for nosocomial and community-acquired infections that can quickly acquire antibiotic resistance. We have identified a novel triazole antimicrobial 31G12 based on the natural product core of nonactin isolated from the fermentation of *Streptomyces griseus*, that is active against many Gram-positive bacteria as well as antibiotic resistant methicillin-resistant *S. aureus* and vancomycin-resistant *Enterococcus*. The synthesis and characterization indicate that 31G12 exists as a mixture of two rotamers at room temperature and displays bacteriostatic activity against *S. aureus* with moderate mammalian cell toxicity. We have currently identified potential protein targets of 31G12 in *S. aureus* via an interdisciplinary approach to the target elucidation. First, a chemical proteomic strategy using photoaffinity labeling revealed a potential target protein at approximately 110 kDa when visualized via western blot and in-gel scans. Second, whole-genome sequencing and a bioinformatics approach revealed two potential proteins, thioredoxin-fold protein and L11 methyltransferase to be good candidates based on dose-response curves. Although the mode of action has not been established, this work provides a rational framework to expand the efficacy of this novel class of antimicrobials through structure-based drug design to improve potency against Gram-positive bacteria and reduce mammalian cell toxicity.

ACKNOWLEDGMENTS

Thank you to everyone who has supported me on my journey through graduate school in pursuit of my master's degree. I am incredibly grateful to my advisor Dr. Nigel Priestley for all his help and encouragement throughout my time with his lab. Thank you to my committee members for all your supervision and guidance not only through my graduate studies but also during my time as an undergraduate. Thank you to my lab mates for being there through this crazy journey. A special thank you to Jeremy and his mentorship in the lab and always being an ear for me.

Hoody, thank you so much for everything that you have helped me with through undergrad and graduate school. This project and my sanity would not have made it this far without you here. I want to thank my parents for always showing me support and encouraging my higher education. Of course, I want to thank my husband, Alex, for always being there for me through this roller coaster. It's been a great trip!

I also want to thank the numerous people who have helped throughout this project. Jim and Linda for showing me how to make the mutant clones. Dan and Laura for not only allowing me to use their instrument but helping me trouble-shoot my western blots. Margie for allowing me to use their plate reader. Dr. Heidi Crosby for suppling me with the *S. aureus* host strain and the plasmids. Both UM Genomics Core and WSU Sequencing for the sequencing of the genomes. Everyone in the Bowler lab for always allowing me to come in and get help and use of their UV/Vis. This project would not have been possible without all of their help.

TABLE OF CONTENTS

ABSTRACT.....	ii
ACKNOWLEDGEMENTS.....	iii
TABLE OF CONTENTS.....	iv
LIST OF FIGURES.....	v
LIST OF TABLES.....	vi
LIST OF SCHEMES.....	vii
LIST OF ABBREVIATIONS.....	viii
Chapter I: Introduction	
Public Health Concerns.....	1
Bacterial Acquisition of Antibiotic Resistance.....	2
Origin and History of Antibiotics.....	3
Modern Drug Discovery Methods.....	6
Target Elucidation Strategies.....	7
Nonactin.....	8
Purpose of Research.....	9
Chapter II: 31G12 Synthesis, Characterization and Resistance to <i>S. aureus</i>	
Introduction.....	10
Materials and Methods.....	12
Results.....	14
Discussion.....	23
Chapter III: 31G12-Based Photoaffinity Probe for Target Elucidation	
Introduction.....	27
Materials and Methods.....	29
Results and Discussion.....	31
Limitations and Future Directions.....	41
Chapter IV: A Bioinformatic Approach to Target Elucidation of 31G12	
Introduction.....	43
Materials and Methods.....	45
Results.....	47
Discussion.....	57
Chapter V: Conclusions	63
Chapter VI: Synthesis Experimental	
Synthesis of 31G12.....	66
Synthesis of Probe JH-7-088.....	70
Synthesis of Tag JH-7-022.....	75
Appendix A: Supplementary Information	77
Appendix B: Selected NMR Spectra for Synthesized Compounds	93
References	117

LIST OF FIGURES

Chapter II

Figure 2.1: Conversion of methyl nonactate into nonactic scaffold and 31G12.....	10
Figure 2.2: Structure for macrocyclic ring of nonactin and enantiomers methyl (\pm)-nonactate and Methyl (\pm)-homo nonactate.....	14
Figure 2.3: Retrosynthetic analysis of 31G12.....	15
Figure 2.4: Methyl resonance peaks of 31G12 in room temperature ^1H NMR.....	17
Figure 2.5: Observed variable temperature ^1H NMR of 31G12 in DMSO- d_6	18
Figure 2.6: Colorimetric resazurin MIC assay for 31G12 against <i>S. aureus</i>	20
Figure 2.7: Turbidity-based MIC assay for 31G12 against <i>S. aureus</i>	21
Figure 2.8: Observed growth of <i>S. aureus</i> after sub-culturing into drug free media.....	21
Figure 2.9: Optically determined MIC for Penicillin G against <i>S. aureus</i>	21
Figure 2.10: Observed growth of <i>S. aureus</i> after sub-culturing into drug free media.....	21
Figure 2.11: Determination of MBC for 31G12 against <i>S. aureus</i>	22

Chapter III

Figure 3.1: Structures of 31G12 derived Photoaffinity Probes and Reporter Tag.....	32
Figure 3.2: Glucose-6-Phosphate Dehydrogenase enzyme assay.....	31
Figure 3.3: Western Blot of photolabeled proteins.....	34
Figure 3.4: Western Blot of BSA controls.....	35
Figure 3.5: UV-VIS spectra of irradiated probe JH-7-088.....	36
Figure 3.6: Concentration-dependent photolabeling.....	37
Figure 3.7: Densitometry measurements of concentration-dependent photolabeling.....	37
Figure 3.8: Competitive 31G12 displacement of probe JH-7-088.....	38
Figure 3.9: Photoaffinity labeling using fluorescent tag azide-fluor 545 and BSA controls.....	39
Figure 3.10: Labeling of <i>S. aureus</i> preparative experiment.....	40

Chapter IV

Figure 4.1: The various assembly strategies offered in PATRIC.....	44
Figure 4.2: Proteomic profiling comparisons between parental and drug-resistant strains.....	49
Figure 4.3: The high-quality SNP variants reported using PATRIC variation analysis.....	50
Figure 4.4: Dose response curves of each transformed mutant.....	56
Figure 4.5: The workflow for variation analysis to determine genetic SNPs.....	57

Appendix A: Supplementary Information

Figure 1: Observed cooling of 31G12 variable temperature ^1H NMR in DMSO- d_6	77
Figure 2: Amino acid sequence alignment for WT, TZNB, TZNP.....	78
Figure 3: Map of pCM29.....	92

LIST OF TABLES

Chapter II

Table 2.1: MIC of 31G12 against Gram-positive bacteria.....10

Table 2.2: MIC values for 31G12.....19

Table 2.3: Mammalian cell viability with 31G12 treatment.....23

Chapter III

Table 3.1: MIC values for 31G12 and photoaffinity probes.....32

Table 3.2: List of proteins identified and calculated molecular weights by nanoLC-MS/MS.....41

Chapter IV

Table 4.1: Statistics for whole-genome sequencing.....48

Table 4.2: The 23 high-quality variants reported by PATRIC from TZNB.....51

Table 4.3: Six potential target proteins from TZNB.....52

Table 4.4: Predicted amino acid changes in six potential proteins.....53

Table 4.5: Confirmed amino acid mutations.....54

Table 4.6: EC₅₀ sensitivity to 31G12.....55

Appendix A: Supplementary Information

Table 1: List of strains and plasmids.....90

Table 2: List of primers and their respective protein/gene.....91

LIST OF SCHEMES

Scheme 2.1: Synthesis of key intermediate 5	15
Scheme 2.2: Synthesis of key intermediate 8	16
Scheme 2.3: Synthesis of final compound 31G12.....	16

LIST OF ABBREVIATIONS

µg- Microgram
µM- micromolar
¹³C NMR- Carbon Nuclear Magnetic Resonance
¹H- Proton Nuclear Magnetic Resonance
55/2052- *S. aureus* 55/2053, parental strain to TZNP
Abs- Absorbance
Amp- Ampicillin
AMR- Antimicrobial Resistance
BSA- Bovine Serum Albumin
CFU- Colony Forming Unit
CH₂Cl₂- Dichloromethane
CHCl₃- Chloroform
Cm- Chloramphenicol
COCl₂- Oxalyl Chloride
Cu- Copper
CuSO₄- Copper Sulfate
d- doublet
Da- Dalton
DCM- Dichloromethane
dd- doublet of doublets
DMAP- 4-dimethylaminopyridine
DMSO- Dimethyl Sulfoxide
EC₅₀- Half Maximal Effective Concentration
Et₃N- Triethylamine
EtOAc- Ethyl Acetate
G6PDH- Glucose-6-Phosphate Dehydrogenase
HGT- Horizontal Gene Transfer
HRP- Horseradish Peroxidase
h- hours
IC₅₀- Half-maximal Inhibitory Concentration
Inoc.- Inoculum
kDa - Kilodalton
LC/MS- Liquid Chromatography/ Mass Spectrometry
LiOH- Lithium Hydroxide
m/z- Mass to Charge Ratio
MBC- Minimum Bactericidal Concentration
MeOH- Methanol
mg- Milligram
MHz- Mega Hertz
MIC- Minimum Inhibitory Concentration
min- minute
mL- Milliliter
mmol- Millimole
MNPs- Multiple Nucleotide Polymorphisms

MRSA- Methicillin Resistant *Staphylococcus aureus*
MS- Mass Spectrometry
NaBH₄- Sodium Borohydride
NaHCO₃- Sodium Bicarbonate
NaN₃- Sodium Azide
NB- Nutrient Broth
nm- Nanometer
NMR- Nuclear Magnetic Resonance
O.D.- Optical Density
o/n- Over Night
OTs- Tosylate
PAL- Photoaffinity Labeling
PATRIC- Pathosystems Resource Integration Center
PBP- Penicillin Binding Proteins
Pd/C- Palladium on Carbon
PDD- Phenotype-based Drug Discovery
ppm- Parts per Million
q- Quartet
QTOF- Quadrupole Time-of-flight Mass Spectrometry
rt- Room temperature
s- Singlet
SAR- Structure Activity Relationship
SNPs- Single Nucleotide Polymorphisms
t - Triplet
TBS- Tris-Buffered Saline
^tBuOH- tert-Butyl Alcohol
TDD- Target-based Drug Discovery
TEA- Triethylamine
TFA- Trifluoroacetic Acid
THF- Tetrahydrofuran
TSB- Tryptic Soy Broth
TTBS- Tween Tris-Buffered Saline
TZNB- 31G12 resistant *S. aureus*, Triazole Nonactate Broth
TZNP- 31G12 resistant *S. aureus*, Triazole Nonactate Plate
VRE- Vancomycin Resistant *Enterococcus*
WT- Wild Type *S. aureus* 13709, parental strain to TZNB

CHAPTER 1. Introduction

Public Health Concerns

Antimicrobial resistance has become a global health concern.¹ Antimicrobial resistance is defined as resistance of a microorganism to an antimicrobial against which it was originally sensitive. Today, most of the infectious agents of concern to the public health have become antimicrobial resistant. The United States Center for Disease Control and Prevention (CDC) estimates that infections caused by AMR bacteria resulted in two million cases of illness and 23,000 deaths in the U.S. annually. The current AMR pandemic has been suggested to be caused by overprescribing and overuse of antimicrobials in hospitals, agriculture, and livestock settings and also the lack of viable drug alternatives.^{1,2} The lack of discovery of new classes of antibiotic threatens to continue the AMR pandemic. Pharmaceutical companies are often reluctant to invest in antimicrobial research and development due to the unfavorable returns- on- investment therefore placing the burden of new development on private companies.³ The BARDA Combating Antibiotic Resistant Bacteria Biopharmaceutical Accelerator has partnered with public-private companies to provide funding to address the growing need for new antimicrobials.

The World Health Organization (WHO) has listed six high-priority bacteria that includes methicillin-resistant *Staphylococcus aureus* (MRSA). *S. aureus* colonizes between 30% and 50% of the skin or nasopharynx.⁴ The SENTRY Antimicrobial Surveillance Program demonstrated that *S. aureus* was the most prevalent cause of nosocomial and community-acquired bloodstream infections, skin and soft tissue infections, and pneumonia. This can be partly attributed to the survivability of *S. aureus* in acidic, high salt concentration, and wide-temperature variation environments.⁵ Before the introduction of antimicrobials, the mortality rate of invasive infections was approximately 90%.⁶ Resistance to penicillin was noted soon

after its first clinical trials in the 1940s.⁷ This rapid acquisition of resistance soon led to the isolation of MRSA almost immediately after the introduction of methicillin. The CDC reported that after the introduction of MRSA into a hospital, 87.5% of hospital's retain persistent MRSA isolates.⁸ Resistance to the last resort antimicrobial, vancomycin, was first documented in 1997 making certain strains of *S. aureus* resistance to all antimicrobials developed.⁹ There is a pressing need for development of new antimicrobials to combat the treat of AMR and tackle this serious public health challenge.

Bacterial Acquisition of Antibiotic Resistance

The emergence of antibiotic resistance closely mirrors that of the discovery of antibiotics due to the bacterial genetic plasticity to develop resistance. The cause for this new era of resistance can be seen in the overuse, inappropriate prescribing, extensive agricultural use, availability of few new antibiotics and regulatory barriers.¹⁰ In order for bacterial to persist in threatening environments when exposed to antibiotics they use two major strategies of gaining resistance to adapt to the environment, including genetic or mechanistic bases of antimicrobial resistance.

In the presence of an antimicrobial a bacterium can acquire foreign DNA coding for resistance through horizontal gene transfer (HGT) or develop mutations in genes often associated with the mechanisms of action at a cost to cell fitness.¹¹ HGT proceeds through three strategies, including transformation (incorporation of naked DNA), transduction (phage mediated) and conjugation (bacterial "sex"). To counter antibiotics with different mechanisms of action, bacteria have evolved multiple mechanisms of drug resistance for continued survival. Antibiotic resistance mechanisms can be classified by the route involved in resistance, including; modification of the antimicrobial compound, prevention of the drug reaching the antibiotic

target, changes and/or bypass of target site and global cell adaptive processes.¹¹ Modification of the antibiotic molecule is achieved by adding specific chemical moieties such as acetylation, phosphorylation, and adenylation which create steric hindrance at the active site on the target or enzymatic destruction of the antibiotic molecule itself. Many antibiotic targets reside within the cell and molecules must therefore penetrate the cell to exhibit their effects. Bacteria have combated these mechanisms of action by decreasing the uptake of the molecule or by the production of efflux pumps to extrude the compound from the cell. A common strategy of bacteria is to modify the target site to decrease affinity for the antibiotic molecule or prevent the antibiotic from binding altogether to protect the target site. Modification of the target site can include point mutations in the respective gene, enzymatic alterations of the binding site through addition of different moieties or bypassing the original target. The last adaptation utilized by bacteria is global cell adaptation in which bacteria evolve to cope with the stressful situations without disrupting vital cellular processes.

Origin and History of Antibiotics

Antimicrobials have saved countless number of lives and helped to control infectious diseases. Antimicrobials have been used for millenia to treat infections, nevertheless the beginning of the “modern antibiotic” era was established with the discovery of penicillin in 1928 by Alexander Fleming.^{10,12}

Between 1930 and 1962 more than twenty novel classes of antibiotics were discovered. The most common classification scheme is based on their molecular structure, mode of action, or spectrum of activity.¹³ Some common classes of antibiotics include beta-lactams, macrolides, tetracyclines, quinolones, aminoglycosides, sulfonamides, glycopeptides and Oxazolidinones.

Beta-lactams were the first class of antibiotics to be discovered. They are classified

based on their cyclic amid composed of 3-carbons and 1-nitrogen that interferes with bacterial cell wall synthesis to either kill or inhibit growth. Beta-lactam antibiotics bind to penicillin-binding proteins (PBP), which are responsible for cross linking peptide units during peptidoglycan synthesis.¹⁴ The most common antibiotics of this class include penicillins, cephalosporins, monobactams and carbapenems.

Macrolides are metabolic products first isolated from the soil dwelling bacteria *Saccaropolyspora erythraea*, and are characterized by 14-, 15-, or 16-membered macrocyclic lactone rings with pendant carbohydrates. These antibiotics inhibit protein synthesis by binding to the ribosome, thereby preventing the addition of subsequent amino acids to the growing polypeptide chains.¹⁵ Antibiotic examples include erythromycin, azithromycin, and clarithromycin.

Tetracyclines, like macrolides, were first isolated from soil bacterium genus *Streptomyces* by Benjamin Duggar.¹⁶ These antibiotics target the ribosome to disrupt protein synthesis similar to macrolides. This class of antibiotics displays a broad-spectrum of activity against both Gram-positive and Gram-negative bacteria¹⁷. These antibiotics can be separated into different generations, depending on whether they were obtained by biosynthetic methods, semi-synthetic derivatives or total synthesis. First generation tetracyclines include tetracycline, oxytetracycline; second includes generation doxycycline methacycline; and third generation is exemplified by tigecycline.¹⁸

Quinolones were accidentally discovered during development of antimalarial chemotherapies based on the quinine structure. The bicyclic core structure has multiple functional groups, but the greatest improvement in biological activity made by the addition of fluorine at C6 to generate the fluoroquinolones and a more broad spectrum antibiotic.¹⁹

Although the mechanisms of action are not well understood, it is accepted that quinolones inhibit DNA synthesis by binding to the complexes formed between DNA and gyrase or topoisomerase.²⁰

Aminoglycosides, like other antibiotics, were first isolated from soil *Actinomycetes* and have been used extensively against *Mycobacterium tuberculosis*. These compounds are composed of 3-aminosugars connected by glycosidic bonds and inhibit protein synthesis by binding to the ribosomal subunits.²¹ While these antibiotics have been shown to be highly toxic, they are still commonly used due to their broad-spectrum activity. Commonly used antibiotics include gentamicin, neomycin and tobramycin.

The first effective clinically used antibacterial drugs were the sulfonamides, discovered in 1935 by Gerhard Domagk. Sulfonamides are structurally related to *p*-aminobenzoic acid which is used in the synthesis of folic acid, leading to the mechanism of action that inhibits tetrahydrofolic acid synthesis²².

Glycopeptides were initially isolated from soil *Actinomycetes* but current antibiotics are semi-synthetic and contain the core of a cyclic peptide of seven amino acids, in which two are bound to sugars²³. These bulky structures inhibit bacterial cell wall peptidoglycan synthesis by binding to the outside of the cell wall.²⁴ These antibiotics tend to have high toxicity and include vancomycin and teicoplanin.

The newest class of synthetic antibiotics are the oxazolidinones which include linezolid. The mechanism of action is not fully understood for this class but evidence suggests that inhibition of protein synthesis by binding to the ribosome occurs in this broad-spectrum antibacterial.^{25,26}

Modern drug discovery methods

As previously discussed, the source of many antibiotics has been from soil-dwelling microbes whose metabolites possess antimicrobial activity. From the natural products, the compounds are synthetically modified to create new generations but the majority retain the same mechanism of action. Today the increasing threat of increasing highly resistant bacteria calls for an urgent need for new antibiotics. Three different approaches have been applied for new drug discovery: bioactivity-guided screening of crude extracts produced from microorganisms, chemical screening based on biological screening of chemical libraries, and target-oriented screening that exploits known molecular targets.^{27,28}

Natural products have been a major driving force for drug discovery since the antibiotic Golden era from 1920-1940's. These small-molecule metabolites are used as the basis for combinatorial chemistry libraries which demonstrate increased hit rates in biological screening campaigns.²⁹ Benefits of these natural products include the complex molecular structures, stereogenic centers and ability to interact with multiple proteins which is difficult to achieve with solely synthetic antimicrobials.³⁰ In order to enhance the bioactivity of natural products, the biologically-relevant core is used as a scaffold for the synthetic addition of different functional groups to produce compound libraries. These compounds are then biologically screened and scored from increasing to decreasing activity and further chemical modifications are made to the compounds in iterative rounds of development. The success of these chemical libraries depends on the screening of hundreds of thousands of compounds that may require combinatorial multi-step synthetic chemistry to produce.

Another approach to new drug discovery is *in silico* screening of target-oriented

structures. This approach utilizes structure activity relationships (SAR) that aim to improve potency, reduce toxicity and enhance bioavailability.³¹ Although these computational methods cannot replace medicinal synthetic chemistry, computational methods can explore active sites to elucidate and optimize biologically active structures. These methods can also be used in screening campaigns against microbial specific targets thus reducing the toxicity to humans. However, a major downfall is that these methods often require a 3D representation of the protein to be used in computation analysis.

Target Elucidation Strategies

Historically there have been two main approaches to target elucidation in drug discovery; those being phenotype-based drug discovery (PDD) and target-based drug discovery (TDD). In the phenotype-based approach, an assay is first developed to screen a library of compounds for an observable phenotypic change, such as fluorescence based resazurin reduction assay to monitor cell viability.^{32,33} From these libraries, the top candidates are then used for target deconvolution and ultimately target identification. An advantage of phenotypic screening is that it does not rely on knowing the target and it is capable of testing complex biological mechanisms that may include multiple targets.³⁴ A downfall of PDD is that the flow scheme from hit to target elucidation tends to be more complicated and nonlinear due to the unknown target(s) of the tested compounds.³⁵

Target-based drug design has been broadly used in the post-genomic era for target elucidation. Unlike PDD, TDD is hypothesis driven based on specified molecular targets, which have been elucidated from bioinformatics to have an important role in disease.^{36,35} Drugs can then be designed using a SAR approach and later screened in target-specific assays to determine drug hits and leads.³³ A downfall of TDD approaches is the dependence on molecular biology

for protein purification or creation of cell lines that overexpress the target and therefore the assays are based on these recombinant proteins.³⁵ A pitfall of drug discovery is the target validation which links the specific molecular target to the *in vivo* model and indicates drug efficacy.^{35,37} Whether the target elucidation strategy is phenotype or target-based, both methods are vital to the production of new molecular targets that will aid in the improvement of drug discovery.

Nonactin

Natural products serve as an important scaffold for the development of new antimicrobials with a diverse array of properties. Nonactin is a macrotetrolide antibiotic, produced by soil-dwelling *Streptomyces griseus*. The macrocyclic ring consist of two units of (+)—nonactate and two units of (-)—nonactate in an altering arrangement of (+)-(-)-(+)-(-), such that nonactin is achiral.³⁸ Nonactin can be separated into its monomeric methyl nonactate by methanolysis of nonactin followed by resolution using *Rhodococcus* under aerobic and anaerobic conditions.³⁹ This methyl nonactate core is the scaffold for a highly diverse combinatorial library that displays a range of pharmacological activity against both Gram-negative and Gram-positive bacteria.³⁸ This library can further be broken down into the heterocyclic compounds of 1,2,3-triazoles prepared from the copper catalyzed cycloaddition of terminal alkynes and azides, Figure 2.2 key intermediate **5** and **16**, and amide bond formation prepared from an acyl chloride and amine, Figure 2.2 key intermediate **5** and **8**.

Further investigation using biological screening of triazole compounds suggested that the complex stereochemistry of the nonactin core contributed to its selective antibiotic activity.⁴⁰ It was demonstrated that the (+)—nonactic acid, not the (-)—nonactic acid contributed to the observed antimicrobial killing. Through the biological screening of a large library of nonactic

acid analogs against Gram-positive and Gram-negative bacteria it was discovered that the library consisted of compounds active against vancomycin-resistant *E. faecalis* (VRE) and methicillin-resistant *S. aureus* (MRSA). The screening campaigns yielded the compound 31G12, which had the greatest biological activity was selected for further studies involving target elucidation.

Purpose of Research

The emergence of resistant strains of bacteria, the limited number of new antibiotics brought to market, and the declining interest from medical companies into new antibiotic development has raised concern for the future of treatment of bacterial infections.^{41,42} With the number of multidrug-resistant bacteria ever increasing, the pursuit of new antibiotics with novel modes of action needed to combat infections. Our lab has previously used a natural product core scaffold, nonactin, to synthesize a library of compounds with varying degrees of activity. From this library of compounds, 31G12 showed the most potent killing of Gram-positive bacteria and was selected for further studies to elucidate the mechanism of action. However, the mechanisms of action for these new antibiotics still remains a mystery. Herein lies the genesis of my research on finding the mechanism of action for novel triazole antibiotic 31G12. This project was approached using multiple methods of target elucidation, including photoaffinity probe labeling and bioinformatics. The hypothesis is that these novel antibiotics, which are selective against VRE and MRSA, will yield a novel mechanism of action and novel class of antimicrobials to contribute to the field of antimicrobial development.

CHAPTER II: 31G12 Synthesis, Characterization and Resistance to *S. aureus*

Introduction

Bacterial infections have become a serious public health threat.¹ Antimicrobial resistance (AMR) in bacterial pathogens has led to increased infections and mortality rates worldwide.⁴³ The current AMR pandemic has been suggested to be caused by overprescribing and overuse of antimicrobials in hospitals, agriculture, and livestock settings and the lack of viable drug alternatives.^{1,2} The lack of new classes of antibiotic discovery threatens to continue the AMR pandemic. *Staphylococcus aureus* is a Gram-positive bacteria and a major cause of nosocomial and community acquired infections.⁴⁴ This bacteria is the leading cause of bacteremia and infectious endocarditis as well as skin, soft tissue, and device-related infections.⁴⁵ The emergence of methicillin-resistant *S. aureus* (MRSA) has complicated treatment options for such infections.⁴⁶ *Enterococcus faecalis* is a Gram-positive bacterium and is commonly an opportunistic pathogen and cause of nosocomial infections.⁴⁷ A last resort treatment for Gram-positive bacteria is vancomycin. The emergence of vancomycin-resistant enterococcus (VRE) and vancomycin-resistant *S. aureus* has further limited treatment options.^{47,48} It has become clear that multidrug resistance is spreading at an alarming rate.⁴³ Unfortunately, the need for new antibacterial therapeutics has not been met, with only five new classes of antibiotics marketed since 2000.⁴⁹ During the golden-era of antimicrobial discovery, antibiotics were initially isolated from natural products. Many natural products possess complex stereochemical centers, and their structures can be used as scaffolds to develop novel, semi-synthetic antimicrobial agents.⁵⁰

The ability to identify new, potential targets in Gram-positive bacteria that can be used in

therapeutic intervention will contribute to the pressing need for new antibacterial therapeutics.⁵¹ In the search for new therapeutics, our interest in a natural product-derived combinatorial library was based on the macrotetrolide antibiotic nonactin.⁵² Nonactic acid provides a unique scaffold with the C-8 alcohol and C-1 ester functional groups (Figure 1.1) that allow for easy diversification. The conversion of the C-8 alcohol into an azide allows the use of Cu-catalyzed cycloaddition chemistry for easy elaboration, and the C-1 ester can readily be converted to numerous amide derivatives (Figure 1.1).⁵² Through structure activity relationship studies of the triazole combinatorial library, we have identified a lead antibacterial compound 31G12 ((*S*)-2-((2*S*,5*R*)-5-((*R*)-2-(4-((4-(4-chlorophenyl)piperidin-1-yl)methyl)-1*H*-1,2,3-triazol-1-yl)propyl)tetrahydrofuran-2-yl)-*N*-(3,4-dichlorophenethyl)-*N*-(thiazol-5-ylmethyl)propenamide), that is biologically active against multiple species of bacteria including human pathogens such as *S. aureus*, *E. faecalis* and drug-resistant MRSA and VRE (Table 1). Our hypothesis is that the biological activity is due to a different mode of action relative to currently available antibiotics. This study discusses the synthesis of the novel antibiotic 31G12 and its chemical and biological characterization. *S. aureus* was used as a model pathogen to investigate the antimicrobial properties of 31G12, including attempting to elucidate the target. The antibacterial characteristics of 31G12 were further investigated in order to classify this novel antibiotic as bacteriostatic against *S. aureus* with moderate toxicity to mammalian cells.

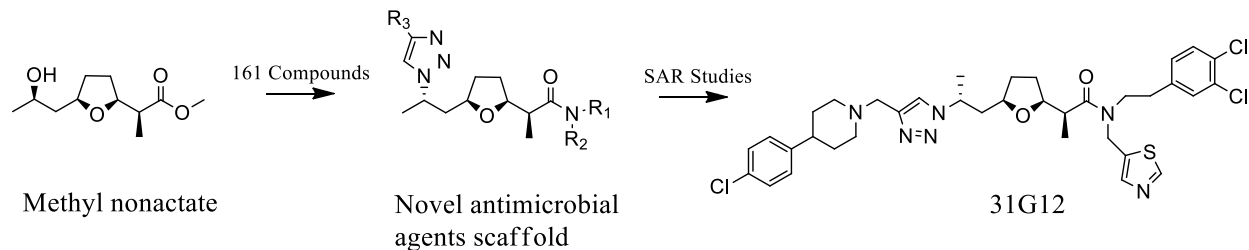


Figure 2.1: The conversion of starting material methyl nonactate into the nonactin acid scaffold with substituted triazole ring and an amide bond used in synthesis of a combinatorial library of 500 compounds. The structure activity relationship studies (SAR) yielded compound 31G12 as the top lead for further studies in determining the mode of action.

Table 2.1: Minimum inhibitory concentrations (μM) of lead compound 31G12 against Gram-positive bacteria for.

Compound	<i>S. aureus</i>	<i>B. anthracis</i>	<i>E. faecalis</i>	<i>B. subtilis</i>	MRSA	VRE
31G12	4	4	16	2	4	16

Materials and Methods

Synthesis of 31G12. Solvent and other reagents were ACS grade and used without purification, unless otherwise noted. All reactions were run under an argon atmosphere. Water was distilled water obtained from laboratory tap. Full synthesis experimental details can be found in Chapter VI: Synthesis Experimental.

Variable-Temperature NMR Experiment.⁵³ For ^1H NMR experiments 31G12 was dried *in vacuo* for several days before sample preparation. A sample was prepared by dissolving approximately 3 mg in CDCl_3 . Variable-temperature NMR measurements were performed on an Agilent 400-MHz NMR Spectrometer.

Strains. Bacterial strains used were derived from *Staphylococcus aureus* 13709 (WT). Bacteria were routinely grown in nutrient broth and nutrient agar plates at 37°C , unless otherwise

indicated. Mutants were selected by screening on increasing concentrations of 31G12 in nutrient broth and designated TZNB (TriaZole Nonactate Broth). *S. aureus* TZNP (TriaZole Nonactate Plate) was previously isolated from 31G12 nutrient agar plates from an unknown parent strain.

Colorimetric MIC Assays. Antimicrobial susceptibility was measured according to the Clinical and Laboratory Standards Institute's guideline for Standard Micro-dilution broth assay using a final inoculum of 1×10^5 CFU/0.1 mL in nutrient broth (Bacto)⁵⁴. The MIC was defined as the lowest concentration of visually inhibited growth monitored colorimetrically using 0.3% resazurin after 6 h of incubation at 37°C.

Turbidity MIC Assays. Overnight cultures were plated in a Corning 96-well plate using an inoculum of 1×10^5 CFU/100 μ L in TSB. The test compound was twofold serially diluted in DMSO and added to each well to a final concentration of 2% DMSO, and plates were incubated at 37°C for 18 h. The optical density of the plates was then read on a SpectraMax M5 plate reader at a 600 nm wavelength. The MIC was defined as the lowest concentration of the drug corresponding to the visually inhibited growth monitored.

Bacteriostatic Activity. Overnight cultures of *S. aureus* 13709 were used to inoculate 1 mL TSB in culture tubes to a final inoculum of 1×10^6 CFU/mL. The test compounds were twofold serially diluted in DMSO and 20 μ L were added to each tube to a 2% final concentration of DMSO, and the tubes were incubated at 37°C, 225 rpm for 12 h. The MIC was defined as the lowest concentration of drug corresponding to visually inhibited growth. In order to eliminate carry-over, 10-fold dilution series was prepared for each sample in sterile TSB, and 100 μ L of these dilutions were plated on TSA and incubated overnight at 37°C, after which the CFU/mL was calculated. From the remaining test samples, 100 μ L were inoculated into 1 mL TSB with no drug and grown at 37°C, 225 rpm for 12 h. Penicillin served as a bactericidal drug control.

Mammalian Cell Toxicity. Cell culture and drug treatment. MCF7 and MCF10A, breast cancer cells, and HEPG2, liver carcinoma cells, were obtained from ATCC (USA). All cells were maintained in Dulbecco's modified essential medium (DMEM) (Gibco, CA, USA) supplemented with 10% fetal bovine serum, 100 Units/mL penicillin and 100 µg/mL streptomycin at 37°C in a 5% CO₂ atmosphere (Gibco). Compound 31G12 was prepared at 1000 µM, dissolved in suitable media and serial diluted in 96-well assay plates (Greiner). After 24 h of growth, 10 µL of 0.3% resazurin was added to each well and the MIC was measured via fluorescence at 560 nm excitation/ emission 590 nm using a SpectroMax M5

Results

Synthesis of 31G12

The methyl nonactate starting material for synthesis of 31G12 was obtained as previously described.⁵² Briefly, nonactin and its homologue monactin were obtained from a fermentation of *Streptomyces griseus* as a mixture (Figure 2.2). Methanolysis of the mixture using *Rhodococcus* generated the methyl esters methyl(±)-nonactate **1** and methyl(±)-homononactate **2**. The methyl esters were then separated by column chromatography, yielding purified homologues **1** and **2**.

Methyl (±)-nonactate **1** was used as the starting scaffold for 31G12.

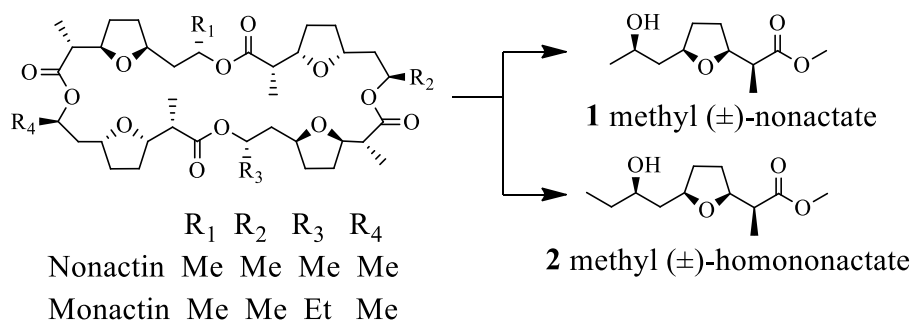


Figure 2.2: Structure for macrocyclic ring of nonactin and homologue monactin, which yield a mixture of methyl (±)-nonactate **1** and methyl (±)-homononactate **2** after methanolysis.

The retrosynthetic analysis of 31G12 is shown in Figure 2.2, involving key intermediates **5**, **8**, and **16**.

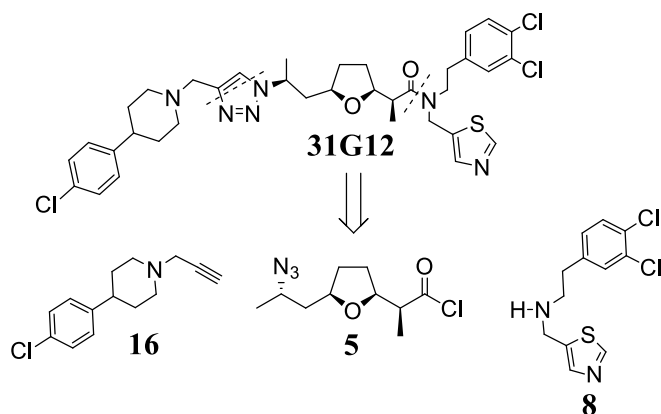
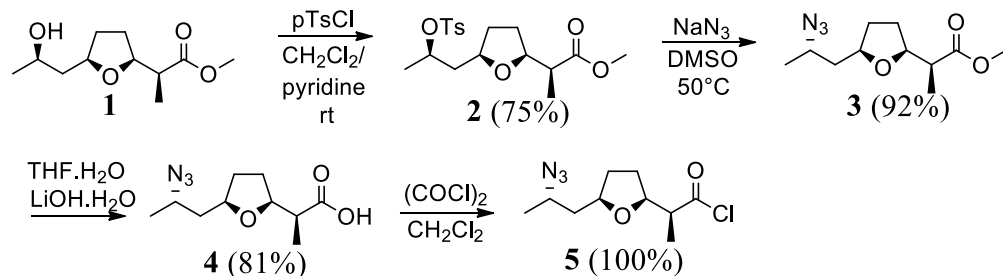


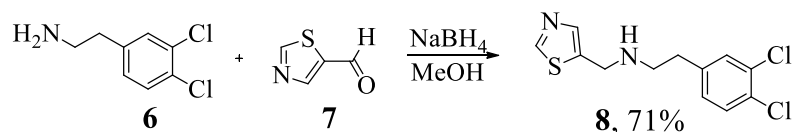
Figure 2.2: Retrosynthetic analysis in synthesis of 31G12.

Synthesis of 31G12

The first step of the synthesis of key intermediate **5** (Scheme 2.1) was tosylation of the C-8 alcohol of methyl nonactate **1** yielding **2**. Reaction of **2** with sodium azide yielded **3**, possessing inverted stereochemistry at C-8. Hydrolysis of the ester yielded **4** which was subsequently converted with oxalyl chloride into acid chloride **5**. Amine **8** was synthesized by reductive amination of commercially available **6** and **7** (Scheme 2.2).

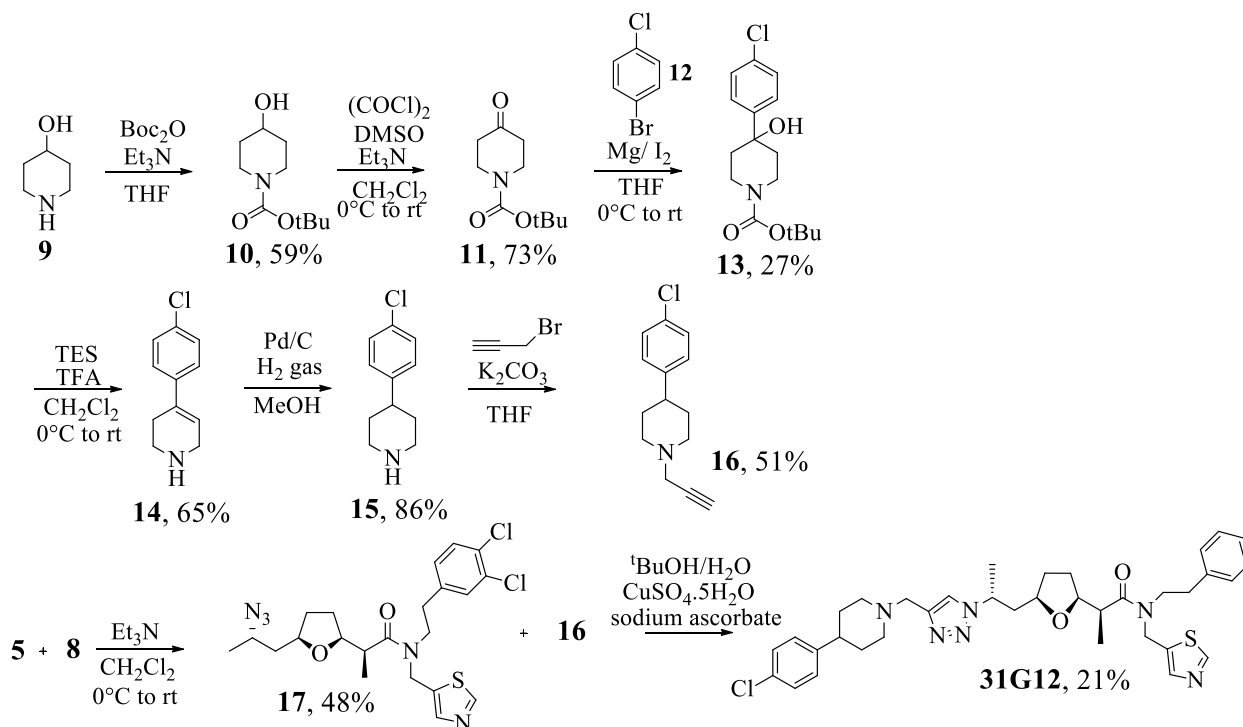


Scheme 2.1: Synthesis of key intermediate **5** from starting material methyl nonactate with reaction yields reported in percent.



Scheme 2.2: Synthesis of key intermediate **8** from commercially available **6** and **7** with reaction yields reported in percent.

For the synthesis of **16** (Scheme 2.3), commercially available amine **9** was first Boc protected yielding **10**, followed by a Swern oxidation to yield ketone **11**. A Grignard reaction between **11** and **12** produced tertiary alcohol **13**. Addition of TFA to **13** simultaneously dehydrate and deprotect yielded alkene **14**. Palladium catalyzed reduction of **14** followed by propargylation at the amine position afforded key intermediate **16**. The amide bond formation between **4** and **9** yielded **17**. The final step was Cu-catalyzed alkyne-azide cycloaddition between **16** and **17** to afford compound 31G12.



Scheme 2.3: Synthesis of 31G12 with reaction yields indicated in percent.

31G12 exists as two rotamers

A variable temperature ^1H NMR was performed to investigate whether double signals from the methyl groups in the NMR were due to rotamers or diastereomers. Two methyl resonances were seen at 0.76 and 0.88 ppm with an intensity ratio of (2.5:1) (Figure 1.3 **A**). In addition, two more methyl resonances were seen at 1.40 and 1.48 ppm (Figure 1.3 **B**). The results showed that at increasing temperatures, the methyl peaks coalesced from two peaks for each methyl group into one peak for each methyl group **A** and **B**. The coalescing of peaks is due to the methyl groups existing as rotamers rather than diastereomers. The coalesced peaks return to the initially observed patterns as the temperature is cooled (Appendix A Figure 1), further illustrating that 31G12 exists as a mixture of two rotamers.

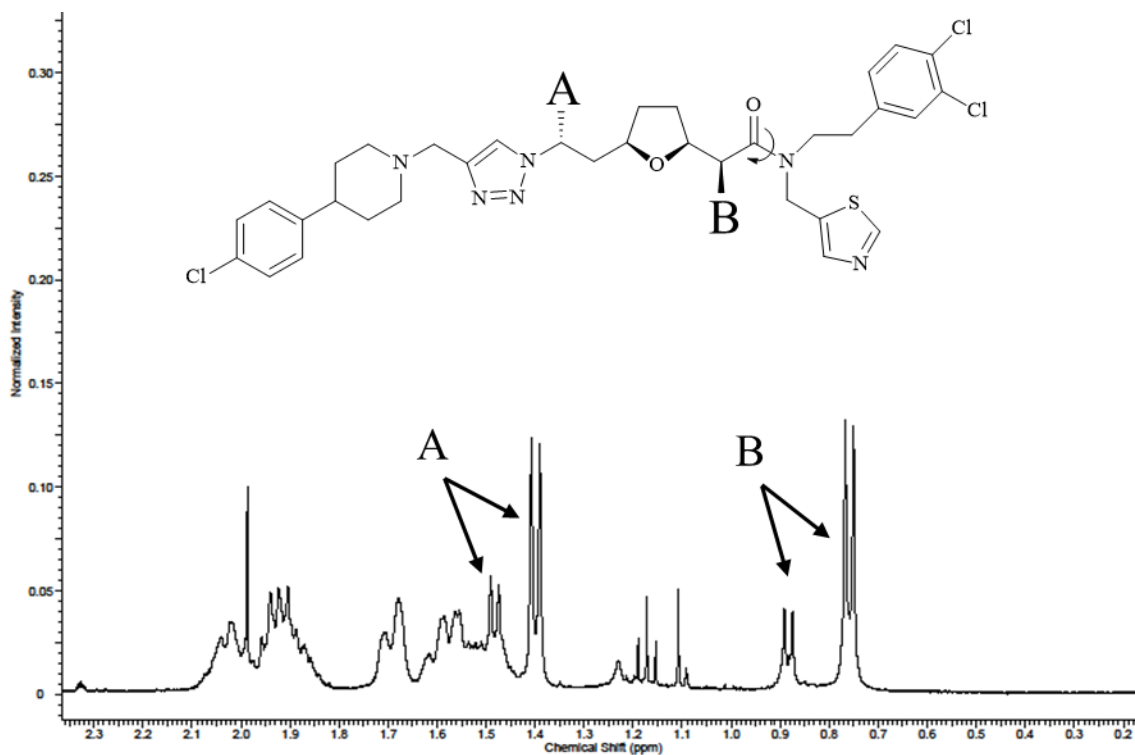


Figure 2.4: Two sets of methyl resonance peaks (A and B) indicated with blue arrows in the room temperature ^1H NMR of 31G12.

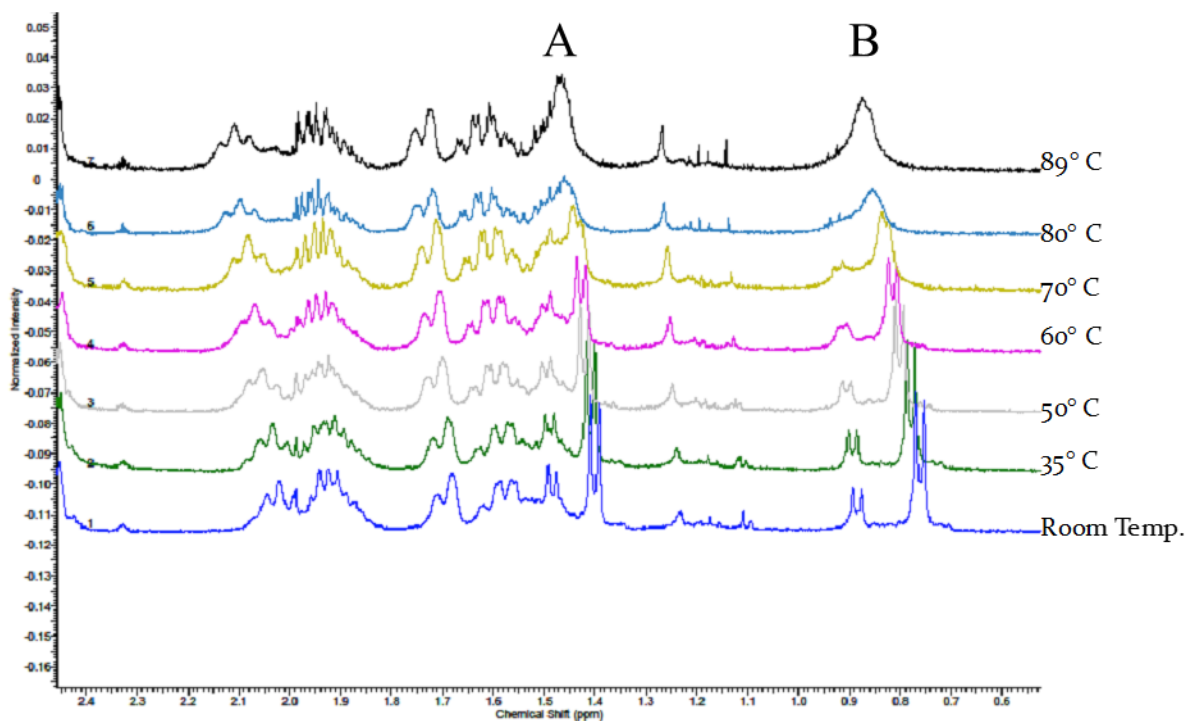


Figure 2.5: Observed variable temperature ^1H NMR (400 MHz) of 31G12 in DMSO-d_6 .

Selecting for mutants of *S. aureus* Resistant to 31G12

To conduct target elucidation studies with 31G12, two different strains of *S. aureus* were selected for resistance to 31G12. *S. aureus* 13709 (WT) was used as the parent strain for screening of 31G12 resistant mutants. The selection of *S. aureus* 31G12 resistant mutant TZNB (TriaZole Nonactate Broth) was obtained by initially inoculating WT at the MIC (4 μM) and growing overnight. Each day the culture was diluted to 1×10^5 cfu/mL in 3 mL triplicates with an increasing concentration of 31G12 in 2% DMSO to a final concentration of 125 μM of 31G12. From these cultures, glycerol stocks were made and designated *S. aureus* TZNB.

S. aureus 31G12 resistant mutant TZNP (TriaZole Nonactate Plate) was previously isolated by Dr. Priestley, using the same method previously described but using increasing

concentrations of 31G12 on nutrient agar plates for screening.

Confirmation of 31G12 Resistant *S. aureus* TZNB and TZNP

MIC data for 31G12 are shown in Table 1.2 and indicate that both TZNB and TZNP mutants have the same MIC values for the colorimetric and turbidity assays. These MIC values are >62 times the MIC for the WT and therefore suggest resistance of both mutants. The isolates of TZNB and TZNP were tested for resistance against 31G12 using the colorimetric resazurin reduction assay, which is dependent on measuring active metabolism via reducing resazurin into resorufin product (Figure 2.6)³². The color change from deep purple to pink indicates that cells are metabolically active and therefore not affected by the presence of the drug. TZNB and TZNP resistance to 31G12 was also tested by optically measuring the turbidity to determine the MIC. The increase in turbidity correlates with increased resistance due to the resistant strains being less inhibited by the presence of drug. Again, both TZNB and TZNP showed resistance to 31G12 up to 500 μ M (Table 2.2). From these isolates only one was selected for use in downstream applications in target elucidation.

Table 2.2: MIC values (μ M) for 31G12.

<i>S. aureus</i>	Colorimetric	Optically
Wild Type	4	8
TZNB	500	500
TZNP	500	500

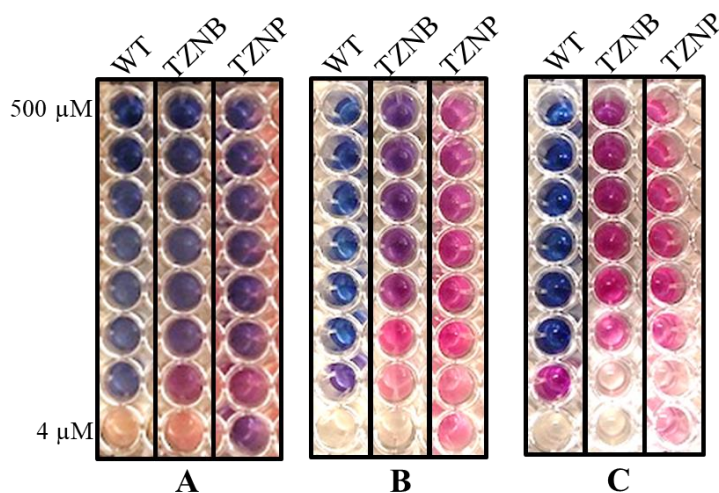


Figure 2.6: Colorimetric resazurin MIC assay for the effect of 31G12 (4-500 μM) against *S. aureus* after development for 5 mins (A), 30 mins (B) and 60 mins (C).

Bacteriostatic Activity of 31G12.

Compound 31G12 can be classified as a bacteriostatic antimicrobial agent against *S. aureus*. When *S. aureus* was initially grown at varying concentrations of 31G12, the MIC measured optically was determined to be 8 μM (Figure 2.7), and when treated bacteria were sub-cultured into drug free media it resulted in growth of all samples (Figure 2.8). Penicillin G is a known bactericidal antibiotic with a MIC of 15.6 $\mu\text{g}/\text{mL}$ (Figure 2.9), and when treated cells were sub-cultured into drug free media resulted in no growth between 31.25-1000 $\mu\text{g}/\text{mL}$ (Figure 2.10). Compound 31G12 was also tested for cidalty by determining if the minimum bactericidal concentration (MBC) was no more than fourfold higher than the MIC and resulted in a 3_{\log} reduction of the initial inoculum (Figure 2.11). It was determined that up to 125 μM there was no observable 3_{\log} reduction of the initial inoculum and this suggests that 31G12 is a bacteriostatic, not bactericidal antimicrobial.

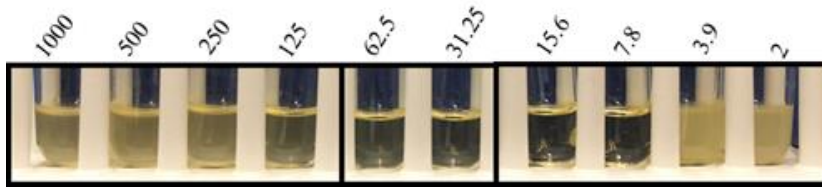


Figure 2.7: MIC of 31G12 (μM) against *S. aureus* 13709 (WT) determined optically after 12 hrs.

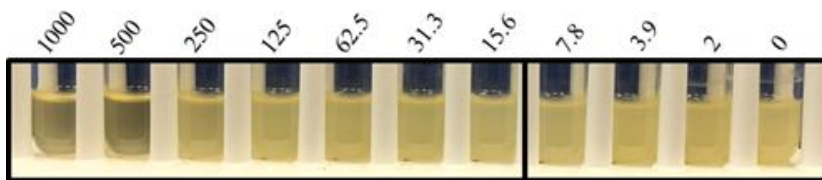


Figure 2.8: Observed growth of *S. aureus* 13709 (WT) after sub-culturing into drug free media and grown for 12 hrs.

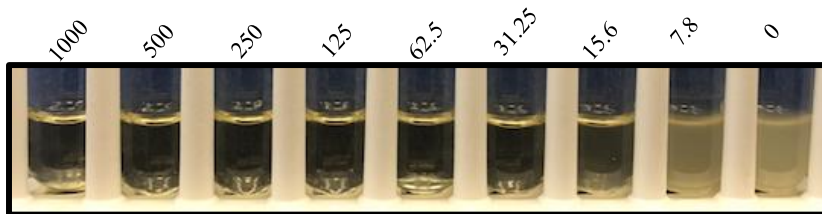


Figure 2.9: MIC of Penicillin G ($\mu\text{g/mL}$) against *S. aureus* 13709 (WT) determined optically after 12 hrs.

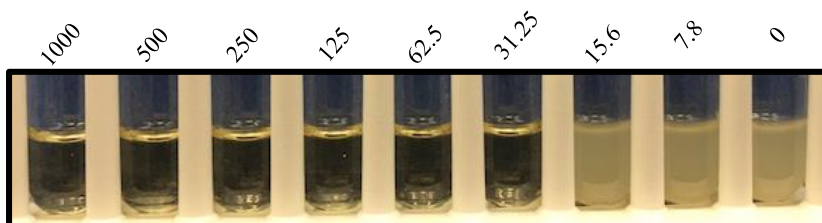


Figure 2.10: Observed growth of sub-cultured *S. aureus* 13709 (WT) after sub-culturing into drug free media and grown for 12 hrs.

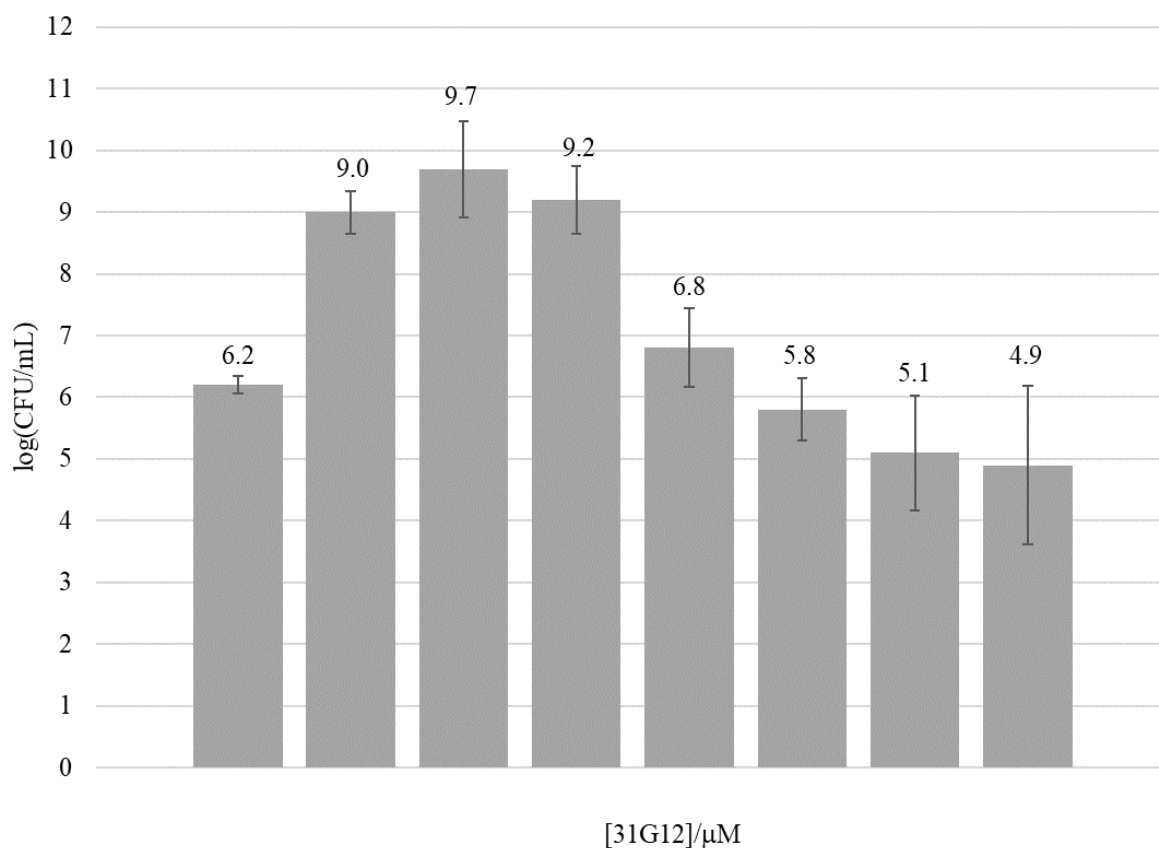


Figure 2.11: Viable bacteria count log(CFU/mL) of *S. aureus* after 12-hour exposure to varying concentrations of 31G12 compared to the initial inoculum (Inoc.) to determine MBC.

Mammalian Cytotoxicity

The half-maximal (50%) inhibitory concentration (IC_{50}) was determined for 31G12 using three different mammalian cell lines. As previously described, the use of resazurin to monitor cellular respiration can be used to determine the cytotoxic effects of chemotherapeutic agents. Screening of mammalian cell lines showed that 31G12 reduced cell viability by 50% at 22 μM and 13.65 μM for the breast cell lines and 7.8 μM for the liver cells (Table 2.3). This indicates that 31G12 is moderately toxic to mammalian cells.

Table 2.3: Mammalian cell viability with 31G12 treatment (n=2).

Cells	IC ₅₀ /μM
MCF7	22.01 ± 0.7
MCF10A	13.65 ± 4.2
HEPG2	7.793 ± 1.2

Discussion

The novel antimicrobial 31G12 was synthesized in a thirteen-step synthesis and determined to exist as a rotamer as determined by variable temperature NMR. The drug displays bacteriostatic activity against Gram-positive *S. aureus* and is moderately toxic to mammalian cells. The drug was used to select for drug-resistant *S. aureus* and resulted in the isolation of two resistant strains TZNB and TZNP, which were used in downstream applications for target elucidation.

The thirteen-step synthesis and relatively low yield to synthesize 31G12 are not ideal when trying to bring a new drug to market. However, it was later determined that compound **15** was commercially available which eliminated five steps from the overall synthesis and allowed for faster synthesis and higher yields of 31G12. Since the drug is not commercially available, the ability to produce drug faster is beneficial when the stock quantity is limited, and more drug was needed for other analyses.

Although 31G12 has only two methyl groups, four methyl resonances were observed in the ¹H NMR at room temperature in DMSO-d₆, which can complicate the analysis of reaction products. Our hypothesis was that the additional resonances were due to the presence of rotamers at the amide bond. To investigate this hypothesis, a variable temperature ¹H NMR was performed at increasing temperatures, which allows for rotation around the amide bond. The two doublets for methyl group **B** (0.75 and 0.88 ppm) and two doublets for methyl group **A** (1.40 and

1.48 ppm) are most likely due to the existence of rotamers around the amide bond present in 31G12 (Figure 2.4).

The chemical shift difference between the two doublets for methyl group **A** (0.08 ppm) is smaller than that of the chemical shift difference between **B** (0.12 ppm). The rationale for the larger chemical shift difference seen for methyl group **B** is that it is closer to the amide bond. The rotation around the amide bond can be seen as individual peaks coalescing into a single peak at increased temperatures. The results showed that at increasing temperatures, the methyl peaks coalesced from four resonances into two resonances, one for **A** and one for **B**. This suggests that these peaks are due to rotamers rather than being diastereomers. The coalesced peaks return to the initial methyl groups peaks as the temperature is cooled (Appendix A Figure 1) further illustrating that this compound is a mixture of two rotamers. The distinction between a compound comprised of rotamers or diastereomers is biologically important because diastereomers can display as two different compounds in a biological system. Drug targets are often enantioselective towards their binding partners and differences in stereochemistry may affect the ability of the drug to elicit its toxic effects in the cell⁵⁵. Optimization of synthesis and characterization of stereochemistry should be established early in drug development in order to reduce time and cost.

The classical approach to target elucidation of novel antibiotics involves the identification of a gene(s) causing a resistant phenotype by genetic or biochemical strategies using resistant clones.⁵⁶ In this study, we used *S. aureus* for generation of 31G12 resistant clones through two different methods. The initial method by Dr. Priestley involved gradually increasing concentrations of 31G12 on plates and selecting for colonies that displayed phenotypic resistance to 31G12. The resulting strain was designated TZNP (TriaZole Nonactate

Plate). The process was then repeated by gradually increasing the concentration of 31G12 in liquid media to select for mutants designated as TZNB (Triazole Nonactate Broth). This gradient method applies maximal selection pressure and resulted in generation of highly resistant strains which were confirmed using two different MIC assays. These assays showed that TZNB and TZNP both had MICs that were >62 times that of the wild-type strain. However, some considerations were taken into account when using strains TZNP and TZNB for downstream application in target elucidation. Firstly, TZNB was generated directly from reference strain *S. aureus* 13709 but the reference strain for TZNP was unknown. This information is critical for bioinformatic approaches to identify single nucleotide polymorphisms (SNPs) from whole genome sequencing that could contribute to resistance. Secondly, by using a gradual gradient for isolation, an increased number of mutations other than those responsible for conferring resistance to 31G12 may have occurred. These additional mutations could be explained by selection pressure on fitness from exposure to low levels of drug over an extended period of time, as opposed to selecting for resistant phenotypes using an initial high concentration of drug without a gradual gradient. An example of this is seen in the study done by Jahn et Al. using *E. coli* as a model organism.⁵⁷ Lastly, 31G12 has limited drug solubility in liquid and solid media. This can be seen in Figure 2. at concentrations >62.5 μ M where the drug has precipitated from solution and closely resembles growth when measuring the MIC optically. Drug solubility is important for bioavailability, especially via oral administrations and future experiments should include formulation to increase the solubility of 31G12 and structure based drug design studies to improve drug solubility.⁵⁸

The core structure of 31G12 is derived from the macrolide antibiotic nonactin. It was determined that 31G12 is a bacteriostatic antibiotic. When *S. aureus* was initially grown in

varying concentrations of 31G12 and then sub-cultured into drug-free media, growth was observed in all samples, suggesting that 31G12 is bacteriostatic. The result is consistent with literature which states that bacteriostatic antibiotics prevent bacterial growth and reproduction without killing them.⁵⁹ When the antibiotic pressure is removed the bacteria will continue to grow. This is in comparison to known bactericidal antibiotics such as Penicillin G. A bactericidal antibiotic kills the bacteria and therefore when sub-cultured into drug-free media no growth will occur, as seen in Figure 2.10. An antimicrobial is considered bactericidal if the minimum bactericidal concentration (MBC) is not more than fourfold higher than the MIC and the viable cell count results in a 3_{log} reduction of the initial inoculum.^{59,60} It was observed that growth with 31G12 results in less than a 3_{log} reduction of the initial inoculum (Figure 2.11) at concentrations up to fourfold the MIC, which again suggests that 31G12 is a bacteriostatic antimicrobial.

It is important in antimicrobial drug discovery to assess mammalian cytotoxicity for a better understanding of the pharmacological and biological characteristics of 31G12.⁶¹ Cytotoxicity of 31G12 to mammalian cells was demonstrated using three different cell lines and 31G12 was shown to have moderate toxicity. This result is important for initial screening of drugs before *in vivo* efficacy, pharmacokinetic, and pharmacodynamic studies are done using mouse models. It is also important to determine a baseline IC₅₀ for future structure-based drug design based on the mode of action for 31G12, which will involve decreasing the toxicity to mammalian cells to create a more selective antimicrobial.

In conclusion, from our combinatorial library of nonactin derived antimicrobials, 31G12 was selected for further studies due to its low MIC value against Gram-positive and antibiotic-resistant bacteria. The synthesis and characterization indicated that 31G12 is a pure compound,

although containing a mixture of two rotamers, and was used to select for *S. aureus* resistant mutants TZNB and TZNP, which will be used in subsequent studies for target elucidation. Compound 31G12 was determined to have bacteriostatic activity with moderate cell toxicity. Subsequent studies were focused on finding the mode of action for 31G12.

CHAPTER III. 31G12-BASED PHOTOAFFINITY PROBE FOR TARGET ELUCIDATION

Introduction

Photoaffinity labeling (PAL) was first introduced in the early 1960s by Frank Westheimer and is used to study protein-ligand interactions, elucidation of protein structures, and identification of novel or alternative binding sites in proteins.^{62,63} PAL can be used in complex mixtures, such as protein lysates, to identify target proteins to elucidate their mode of action. The design of the photoaffinity probe should be structurally similar to the parent compound with the exception of incorporation of a photoreactive group and alkyne tail. The most ideal PALs would be stable in the dark at a range of pHs and display the same activity, or MICs, compared to that of the parent compound.⁶²

The photoreactive group of the photoaffinity probe is activated upon irradiation to form a reactive intermediate that rapidly binds with the nearest molecule. This irreversible covalent binding of the photoreactive group is hypothesized to occur in the same binding pocket of the target protein as the parent compound while causing minimal damage to biological molecules which remain intact during isolation and detection of the target protein.⁶⁴ Commonly used photoreactive groups are phenylazides, phenyldiazirines and benzophenones, which produce the reactive intermediates of a nitrene, a carbene, and a diradical, respectively. However, the most commonly used photoreactive group is the trifluoromethyl aryldiazirines due to its high chemical stability and the wavelength required for activation. The diazine is quickly converted to the carbene intermediate upon irradiation which may minimize nonspecific binding but can also be rapidly quenched by solvent molecules. Around 30% of the diazine isomerizes to the diazo derivative upon irradiation; the diazo can also decompose to the carbene, yet quite slowly.^{62,65}

The reporter tag of the photoaffinity probe is essential to facilitate the isolation and visualization of target molecules. The alkyne tail of the photoaffinity probe is used to attach a reporter tag with an azide side group via the Cu-catalyzed alkyne azide cycloaddition (“click chemistry”). The biotin affinity tag is commonly used in PAL due to its high affinity toward streptavidin.⁶² However, the interaction between biotin and avidin is the strongest non-covalent interaction between a protein and ligand thus limiting its utility; harsh conditions are required to break the streptavidin-biotin bonds such as those used during target protein dissociation and elution for isolation.^{66,67} Other reporter tags include the use of fluorophores such as fluorescein, BODIPY (dipyrromethene boron difluoride), rhodamine, cyanine dyes and NBD (nitrobenz-2-oxa-1,3-diazole). Rhodamine is inexpensive and hydrophobic allowing it to penetrate the cell membranes but photobleaching is a drawback to its use.

After live cells or lysates have the PAL and reporter tag attached to the target, the samples are separated on SDS-PAGE gels and probed for labeled proteins using Western blot or in-gel scans. Alternatively, the labeled proteins can be isolated using affinity purification and then separated on a SDS-PAGE gel. Proteins are then excised from the gel and digested for sequencing using MS to determine the identity of the protein. A drawback of PAL is nonspecific cross-linking of the probe and therefore adequate controls need to be present. However, PAL has been shown to identify off-target interactions in cells through *in vitro* screening which can aid in SAR studies or identification of multiple targets within the cell as seen in Eirich *et al.*⁶⁸ There have been many published example of the use of PAL, which demonstrates the importance of the method in medicinal chemistry and drug discovery and highlights the wide scope of probe designs, photophores and reporter tags⁶². In this study, we used 31G12 based photoaffinity

probe JH-7-088 in conjunction with a biotin-streptavidin reporter tag for PAL, for target elucidation of the mode action for antibiotic 31G12.

Materials and Methods

Synthesis of Photoaffinity Probe JH-7-088 and Reporter Tag JH-7-088. Complete synthesis details can be found in Chapter VI: Synthesis Experimental.

Bacterial Strains. *Staphylococcus aureus* 13709 was maintained in TSB medium at 37°C.

MIC Assays. Antimicrobial susceptibility was measured according to the Clinical and Laboratory Standards Institute's guideline for Standard Micro-dilution broth assay using a final inoculum of 1×10^5 CFU/0.1 mL in nutrient broth (Bacto)⁵⁴. The MIC was defined as the lowest concentration of drug corresponding to the visually inhibited growth monitored colorimetrically using 0.3% resazurin after 6 h of incubation at 37°C.

Preparation of Proteomes. The proteomes of the bacterial strains were prepared from 50 mL BHB media harvested after 24 h growth by centrifugation for 15 min at 10,000g. The bacterial pellet was washed with PBS, resuspended in 5 mL PBS buffer with 5% glycerol, and lysed by sonication with a Branson 550 sonicator under ice cooling using a cycle of 9s on/9s off, 30% amp, for 15 minutes followed by centrifugation for 30 mins at 16,000g and concentrated using 3kDa Amicon Ultra-Centrifuge filters and stored at -20°C in 50% glycerol.

Glucose-6-Phosphate Dehydrogenase Assay. All reagents were obtained from Sigma-Aldrich. A standard reaction mixture contained 50 mM glycylglycine, 2 mM D-glucose-6-phosphate, 0.67 mM β -nicotinamide adenine dinucleotide phosphate and 10 mM magnesium chloride at pH 7.4. The final volume of the reaction mixture was 1.0 mL. The reaction was initiated by the addition of 0.01 units glucose-6-phosphate dehydrogenase or 50 ng of whole cell lysate. The enzyme activity and formation of NADPH was measured spectrophotometrically at 340 nm at 25°C.

***In Vivo* Labeling Experiments.** The protocol for labeling experiments adapted from Sieber⁶⁸ and Taunton⁶⁹. Proteomes were adjusted to a final concentration of 1.5 mg/mL by dilution in RNase free water. Labeling was initiated by the addition of 1 μ L (1 mM) probe JH-7-088 and incubated at 25°C for 15 min. Samples were irradiated in open microwell plates for 45 min with 366 nm UV light on ice. Following incubation, 2.5 μ L of 10% SDS (w/v) was added and vigorously vortexed and then 1 μ L (5mM) biotin reporter tag JH-7-022 was added immediately followed by 2.5 μ L catalyst mix (1.5 volumes 1.7 mM TBTA in 80% tert-butanol/20% DMSO, 0.5 volumes 50 mM CuSO₄, and 0.5 volumes 50 mM TCEP at pH 7.0) and gently vortexed. Samples were incubated at rt for 2 h then separated on a 4-10% gradient SDS-PAGE gel (Bio-Rad).

Preparative Experiments. A labeling experiment was carried out at 1.5 mg/mL (500 μ L) of proteome sample as described for *in vivo* labeling. After click chemistry, proteins were precipitated with acetone and stored at -20°C for 60 min prior to centrifugation (13,500g for 10 min). The precipitation was repeated twice. The pellet was air dried and rehydrated in 1% SDS with sonication then incubated with 1 mL avidin-agarose beads (Sigma-Aldrich) for 30 min at 25°C. The beads were washed with PBS, incubated with 8M Guanidine-HCl for 15 min at 25°C, washed three times with 500 μ L PBS and buffer exchanged in 3kDa Amicon Ultra-Centrifuge filters. Twenty microliters of 2x Laemmli buffer (Bio-Rad) was added to each sample which was resolved on a 4-10% SDS-PAGE gel. Protein was visualized with Brilliant Blue R250.

Western Blot. Proteome samples from *in vivo* labeling were transferred to 0.45 μ m nitrocellulose membranes (Bio-Rad). The membranes were dried at 25°C for 3 h then blocked overnight at 4°C in TTBS (20 mM Tris, 150 mM NaCl, 0.1% Tween 20) with 3% BSA and then washed once with TTBS. The membrane was incubated with High Sensitivity Streptavidin:HRP

(Pierce) at a 1:24,000 dilution in TTBS for 1 h at 25°C, then washed with TBS three times for a duration of ten mins. Blots were detected using Amersham ECL Prime Western Blotting Detection Reagent after incubation for 5 min at 25°C and exposed using a Fujifilm LAS-3000.

Mass Spectrometry and Proteomics. Bands from the preparative experiment were excised and sent to Alphalyse (Palo Alto, CA) for nanoLC-MS/MS and proteomic analysis. Briefly, protein samples were reduced and alkylated with iodoacetamide and tryptically digested. The samples were concentrated by Speed Vac lyophilization and redissolved for injection on a Acclaim PepMap 100 C18 column (2 μ m) for analysis on a Dionex nano-LC system and MS/MS on a Bruker Maxis Impact QTOF. The MS/MS spectra were used for a Mascot version 2.6.2 database search and in-house protein database search downloaded from SwissPort 2, UniPortTRMBL, and NCBI with a peptide mass tolerance of 10 ppm and fragment mass tolerance of 0.05 Da.

Results and Discussion

31G12 Based Photoaffinity Probes and Biological Evaluation

A 31G12-based photoaffinity probe was designed to identify and isolate proteins from *S. aureus* for the target elucidation of 31G12. We initially synthesized several 31G12-based photoaffinity probes with different structures (Figure 3.1). The first structural variation was the addition of a benzophenone or diazirine photoreactive group, which is required to covalently cross-link the probe to the protein target. Secondly, we varied the position of the alkyne tail which is required to attach the reporter tag via click chemistry. The variation of probe structures was essential to finding a modification of the original antibiotic that would be biologically active in photoaffinity labeling experiments.

To test the modified 31G12 probes for antibiotic potency, we tested their MIC against *S. aureus* WT and 31G12 resistant *S. aureus* TZNB and TZNP (Table 3.1). The most potent probe,

JH-7-088, displayed the same potency in *S. aureus* WT as 31G12, and was selected for PAL studies. We also synthesized a biotin reporter tag for western blot analysis and protein isolation. This tag was also tested for activity against *S. aureus* WT, TZNB, and TZNP and showed no activity (Table 3.1). This is ideal for use with the biologically active probe because the tag should have no activity that could confound the results of the labeling experiment.

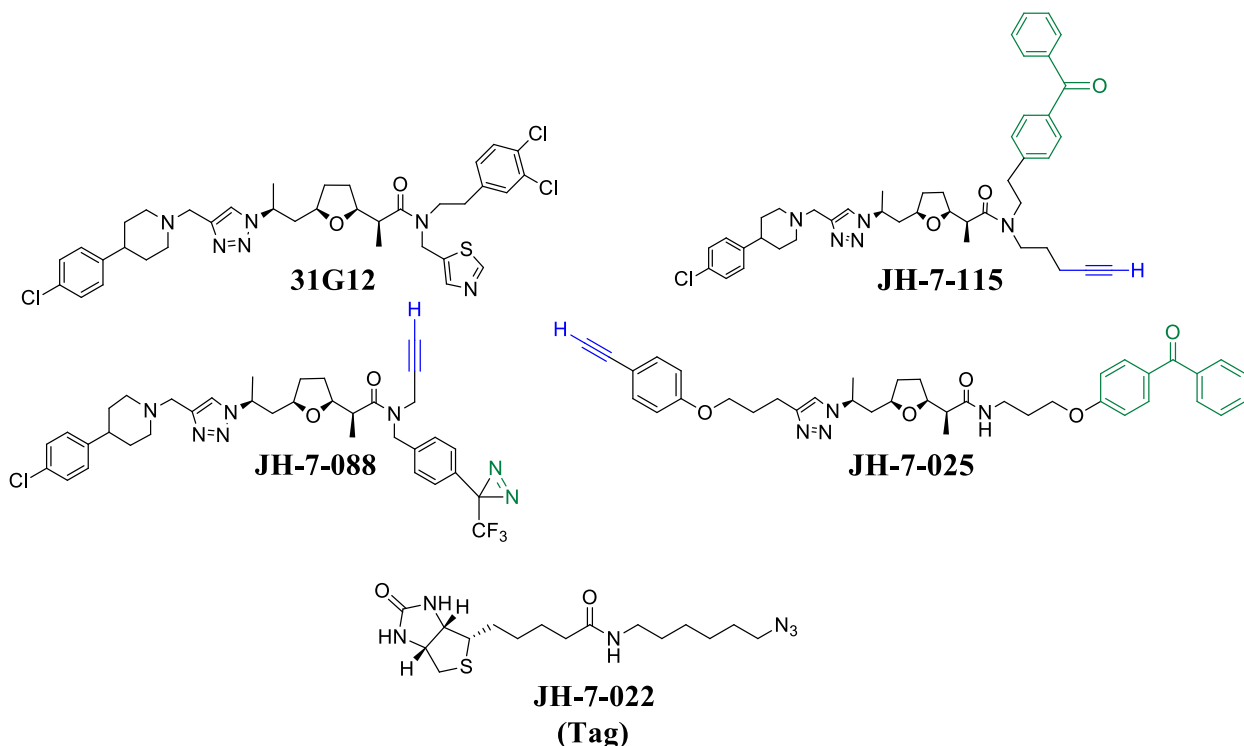


Figure 3.1: Structures of 31G12 derived Photo-Affinity Probes (JH-7-115, -088, -025) with photo-cross-linker (green), alkyne handle (blue) and Biotin Reporter Tag (JH-7-022).

Table 3.1: MIC values (μM) for 31G12 and PALs

Compound	<i>S. aureus</i> WT	<i>S. aureus</i> TZNP	<i>S. aureus</i> TZNB
31G12	<8	16	32
JH-7-022	>1000	>1000	>1000
JH-7-025	>1000	>1000	>1000
JH-7-088	<8	64	64
JH-7-115	250	1000	>1000

G6PHD Assay Demonstrates Active Enzymes in Cell Lysate

It is important in photolabeling that proteins retain their native conformations for *in vitro* labeling to mitigate artificial labeling effects due to protein degradation and corresponding changes in enzyme activity. After proteome isolation, the lysate was tested for enzyme activity using a glucose-6-phosphate dehydrogenase (G6PDH) assay to assess the activity of known housekeeping enzyme, glucose-6-phosphate dehydrogenase, that is present in all cells. The protein lysate for both WT and TZNB displayed similar kinetics curves when compared to the control (Figure 3.2) and suggesting that the proteins in the lysate were active and had retained the native conformations. This is crucial for protein visualization and isolation in target elucidation and determining off target effects for photoaffinity probes.

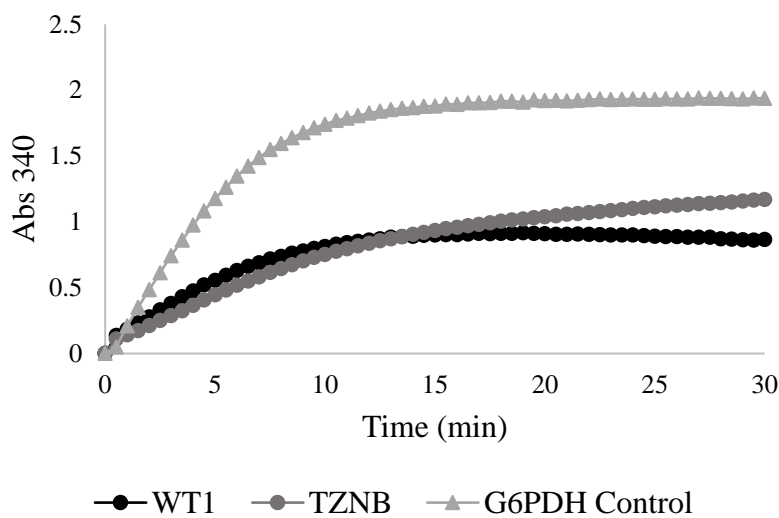


Figure 3.2: Glucose-6-phosphate dehydrogenase (G6PDH) enzymatic assay to assess for activity in cell lysates for *S. aureus* WT and TZNB compared to the control enzyme.

***In vitro* labeling with Photoaffinity Probe JH-7-088**

To test labeling properties and establish an efficient protocol for *in vitro* labeling we initially tested JH-7-088 with *S. aureus* WT and 31G12 resistant TZNB lysate. When using a Western blot to visualize results, we anticipated seeing a photoaffinity labeled protein present in

the WT lysate but absent in the TZNB lysate due to its resistance to both 31G12 and probe JH-7-088. However, this hypothesis was not supported by our initial results. All protein bands were present in both the WT and TZNB when photoaffinity labeled (Figure 3.3 A).

We sought to use the biotin-streptavidin reporter tag but, interestingly, found a strong non-specific biotin binding protein which interferes with both the streptavidin-agarose purification and western blot results. Initial western blot results (Figure 3.3 A) showed the strong background band in all lanes at approximately 100 kD and the probe labeling of five other proteins at approximately 25, 35, 50, 75 and 110 kD. These experiments were repeated using only WT lysate because there was no difference in protein detection between WT and TZNB lysates and to simplify the assay. The background band was present in all samples, and none of the other previously photolabeled proteins were present, except for the 110 kD protein band (Figure 3.3 B). This raised concern for target elucidation using a PAL system because of the inconclusive results. Therefore, further experimentation was needed to confirm that an efficient labeling protocol had been established, the diazirine was still intact on our probe required for cross-linking to the protein of interest, and determining if the 110 kD band is our protein of interest.

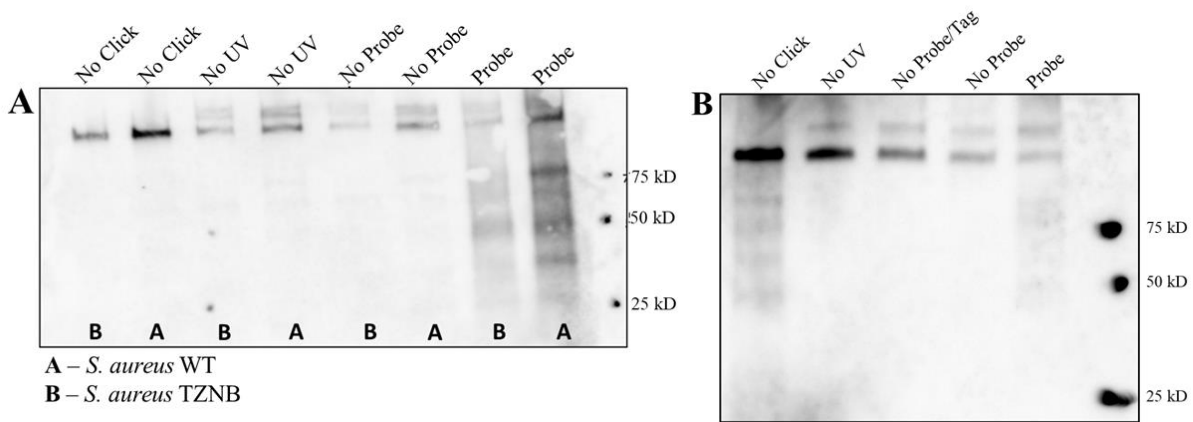


Figure 3.3: Initial Western blot of initial photolabeled proteins and controls (A) compared to repeated results (B).

BSA Controls to Establish Efficient Labeling Protocol

Due to the inconclusive results from the western blots, a biotinylated bovine serum albumin (BSA) and a BSA with an alkyne tail were used as controls to establish an efficient protocol for PAL. We purchased a biotinylated BSA to serve as a Western control for visualization when using streptavidin-HRP (Figure 3.4). To determine if the biotin tag JH-7-022 was being successfully added to probe JH-7-088 via click chemistry, we created a BSA with an alkyne tail (BSA-Alkyne) (Figure 3.4). These BSA controls were spiked into the lysate which underwent the photolabeling protocol. The background band from the lysate and the BSA-alkyne and biotinylated BSA bands at 66.4 kD were present on the western, indicating that our tag JH-7-022 was being successfully added via click chemistry to the BSA and probe, and that an efficient labeling protocol had been established.

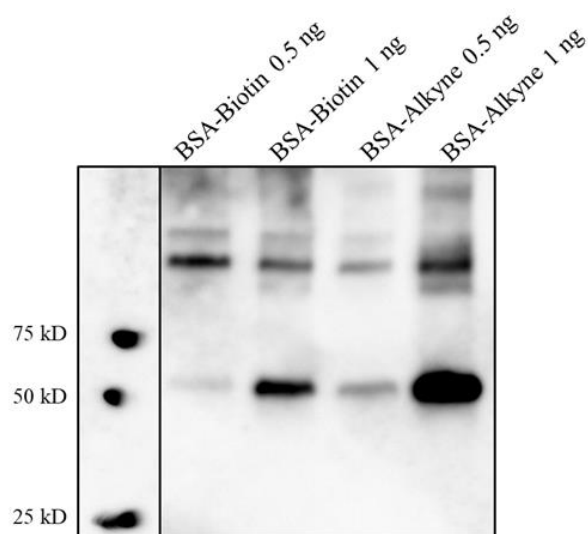


Figure 3.4: Western blot of BSA controls to establish an efficient labeling protocol.

UV/VIS Measurement of Probe Diazirine Activation

To determine the chemical stability of the diazirine in probe JH-7-088, we used photolysis in methanol for a fixed period of time and followed the diazirine activation spectrophotometrically. The diazirine showed an absorbance peak at 350 nm (Figure 3.5 D), which is consistent with other 3-trifluoro-methyl-3-aryldiazirines spectral properties.^{65,70-72} Upon irradiation the peak at 350 nm, decreases which indicates the conversion of the diazirine into other species. The peak at ~270 nm increases with irradiation time due to the rearrangement of the diazirine into its isomer (Figure 3.5 A → B). The conversion of the diazo into the carbene is relatively slow and can be monitored spectrophotometrically (Figure 2.5 B → C).⁷² Together these results indicate that the diazirine was still present on the probe and therefore should be generating the carbene and therefore covalently cross-linking to protein(s) in our PAL protocol.

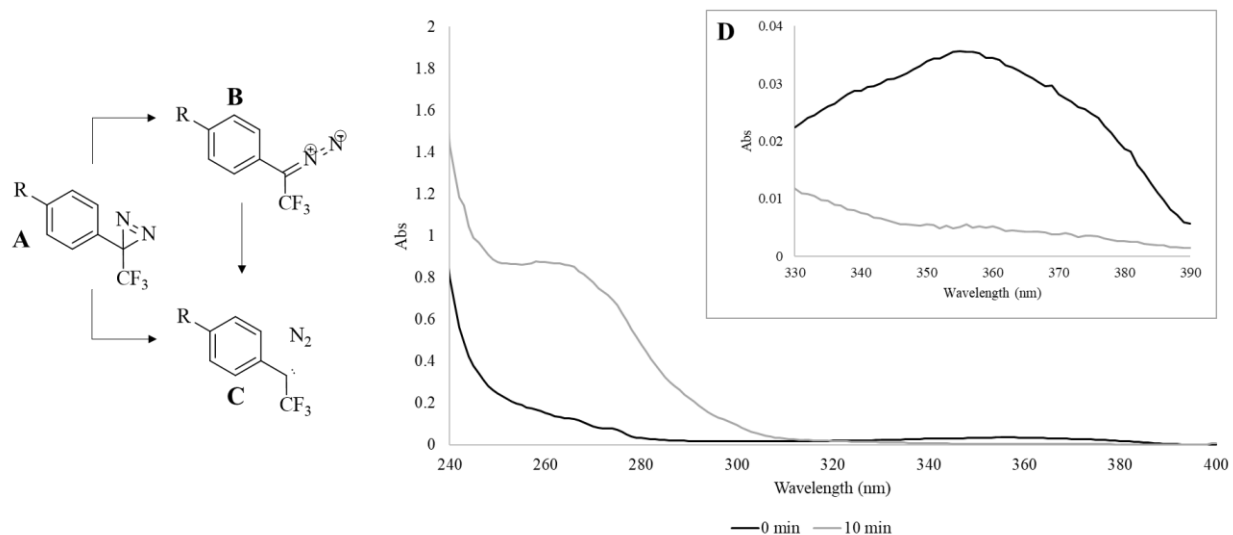


Figure 3.5: UV-Vis spectral changes that occurred upon irradiation of diazirine PAL JH-7-088 (A) in methanol converting in its isomer (B) and carbene (C). Insert (D) shows the absorbance changes between 330-390 nm, as a function of irradiation time for the diazirine conversion into its isomer.

Evaluation of Potential Photoaffinity Labeled Protein Target

In order to optimize the probe concentration and determine specific photoaffinity labeled proteins *in vivo*, the lysate was treated with varying concentrations of JH-7-088. The initial western blot showed a strong dose dependence for all labeled proteins while the background band at 100 kDa remains relatively the same in all samples (Figure 3.3). Again, when the experiment was repeated the protein bands below the 100 kDa background protein band failed to be detected (Figure 3.6). Using ImageJ to measure densitometry of the 110 kDa protein band in the repeated experiments, shows a dose dependence curve (Figure 3.7). This suggest that the target protein may correspond to this protein band at 110 kDa.

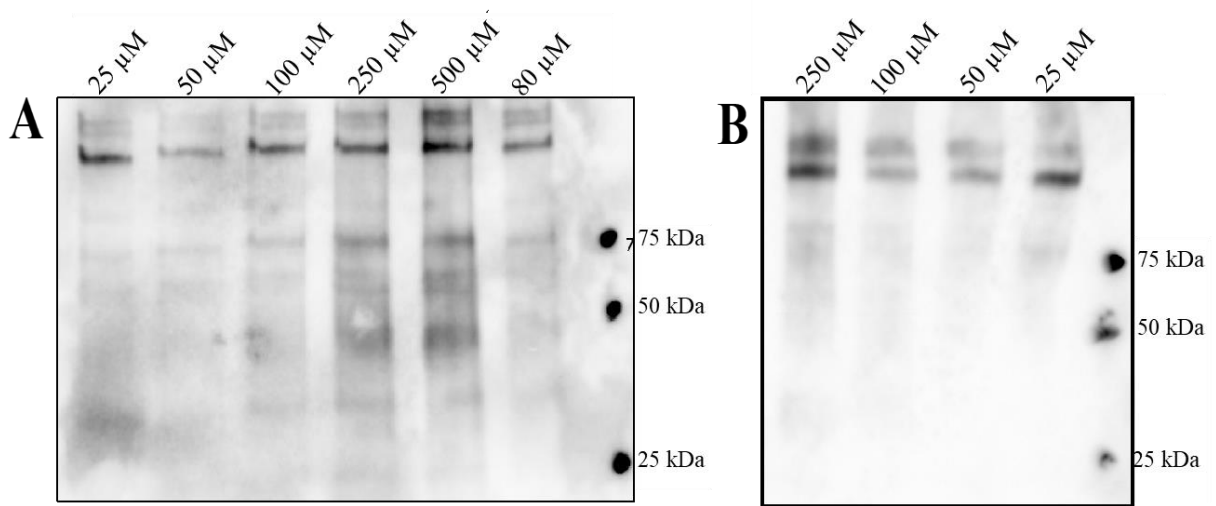


Figure 3.6: Labeling of cell lysate by concentration-dependence using JH-7-088 of the initial western blot (A) and repeated results (B).

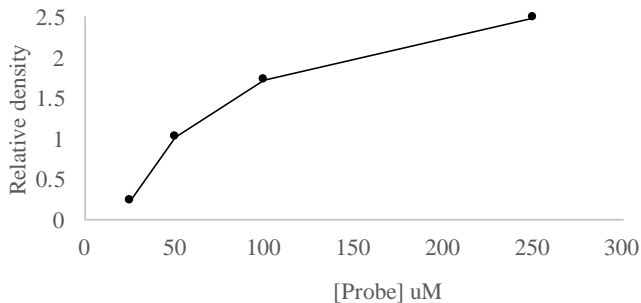


Figure 3.7: Densitometry measurements of the 110 kDa band from the repeated western shows a strong dose-response to increasing concentrations of JH-7-088 PAL.

To test the hypothesis that the 110 kDa protein was the target, we pre-treated the lysate with 31G12 prior to photoaffinity labeling with JH-7-088. Compound 31G12 should bind preferentially to the binding site of the target protein and therefore not allow JH-7-088 to bind. The western blot and densitometry analysis (Figure 3.8) showed that there was a ten-fold decrease in relative density in the samples pre-treated with 31G12 prior to labeling. This evidence also supports the hypothesis that our target protein corresponds to the 110 kDa band seen in the western blots.

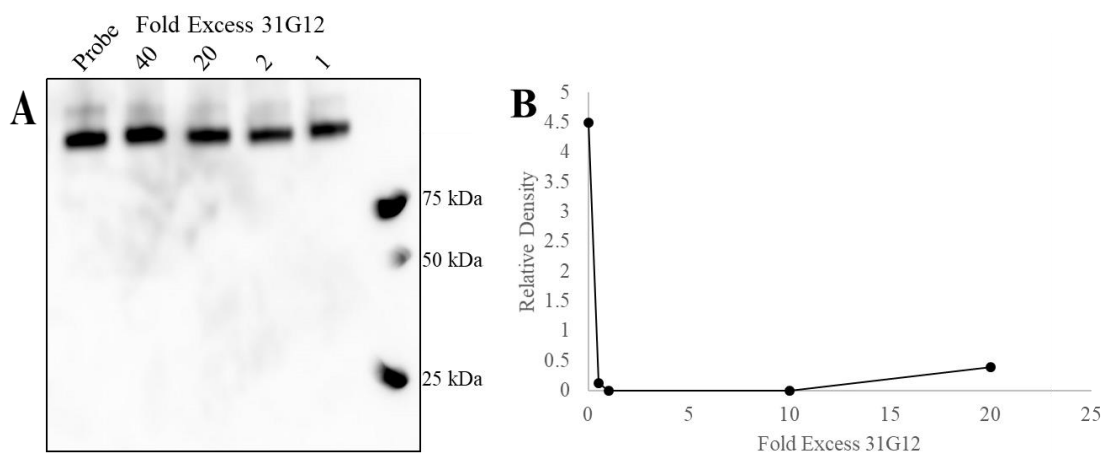


Figure 3.8: Competitive, concentration-dependent displacement of JH-7-088 by antibiotic 31G12 in labeling experiments via western blot (A) using cell lysate and densitometry measurements (B).

Preliminary Results

Since the potential target protein at 110 kDa is very close to the biotinylated background protein band at 100 kDa, isolation and visualization was difficult in PAL experiments.

Therefore, an alternative tag, Azide-fluor 545 (5-carboxytetramethylrhodamine-azide), was used instead of the biotin-streptavidin reporter tag. Azide-fluor 545 is a fluorescence based rhodamine tag, which can be visualized by scanning fluorimetry of SDS-PAGE gels. This approach eliminates the use of Western blots for protein visualization. Like the biotin tag JH-7-022, this tag also has an azide side chain used to attach to the probe via click chemistry. The preliminary results showed multiple bands (Figure 3.9) being labeled in both the probe and no probe samples. However, a band does appear at approximately 100 kDa in the probe sample as seen in the previous western blots. This band was absent from the no probe and 31G12 pre-treated samples. BSA-alkyne was used again as a click chemistry control and showed both the monomer at (66 kDa) and the dimer (132 kDa) being successfully labeled with the azide-fluor 545 tag. This suggests that we have established an efficient protocol for labeling proteins using the rhodamine tag and the protein at ~100 kDa is our target protein and possible target for 31G12.

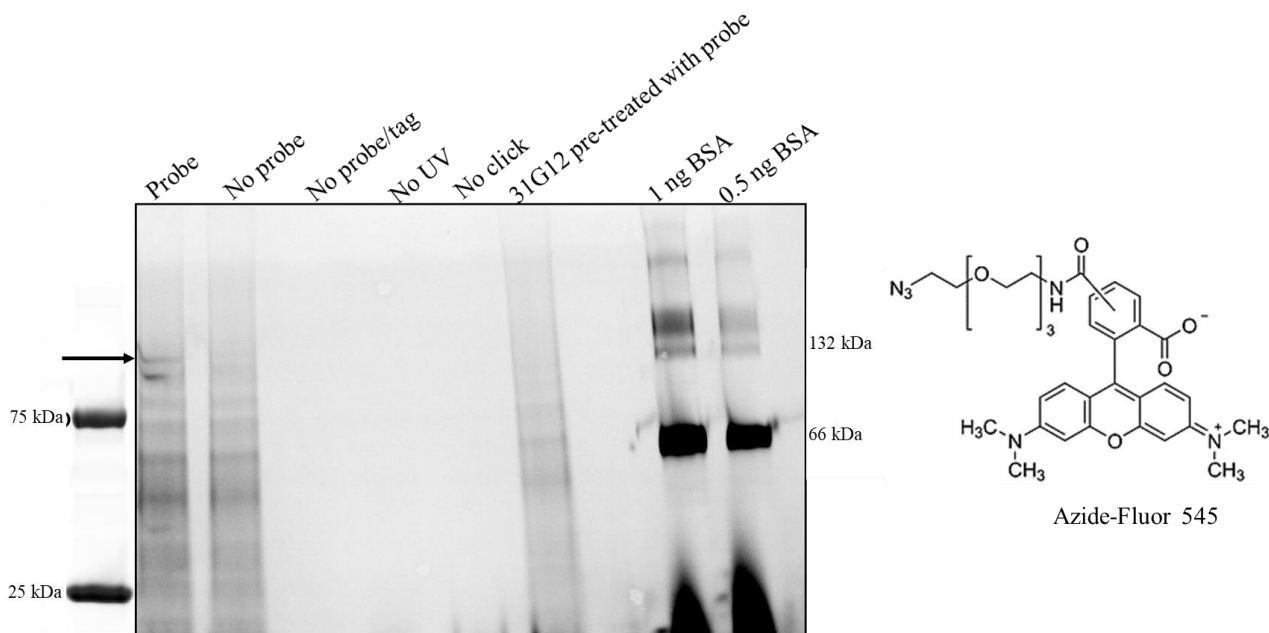


Figure 3.9: Photoaffinity labeling of *S. aureus* WT lysate using probe JH-7-088 tagged with azide-fluor 545 and BSA-alkyne-azide-fluoro 545 controls.

Preparative Scale PAL for LC-MS/MS Data Analysis

Based on the western blot results, we hypothesize that the target protein is going to be at the relative molecular mass in the SDS-PAGE gel as the background band after protein isolation using streptavidin-agarose, which correlates to the proteins seen at both 60 and 100 kDa. The SDS-PAGE gel shows three different bands of interest at around 37, 60, and 100 kDa with the biotinylated background proteins at approximately 60 and 100 kDa (Figure 3.10). Interestingly, the proteins seen at 37 and 60 kDa correspond to the initial western where these bands were also present. However, these bands were not reproducible on subsequent experiments. The band at 60 kDa was excised and sent to Alphalyse for multiple protein analysis via nanoLC-MS/MS. This protein band was chosen based on the fact that it was isolated from streptavidin-agarose beads, which indicates that these proteins were successfully labeled with probe JH-7-088.

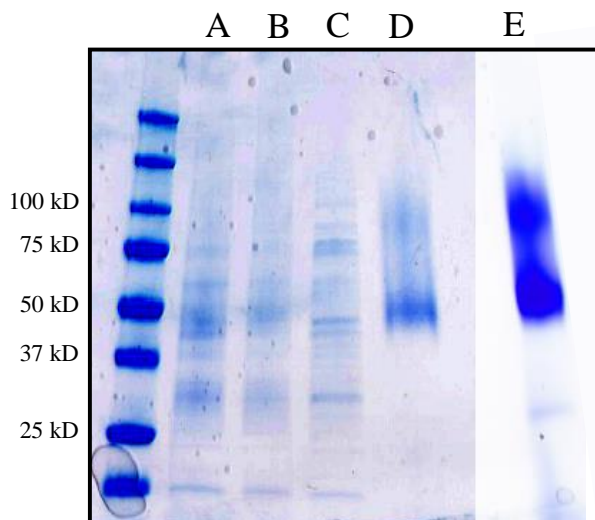


Figure 3.10: Labeling of *S. aureus* WT and TZNB preparative experiment. Protein sample after click chemistry (A), protein precipitation and pellet rehydration (B), cell lysate (C), non-specific binding to avidin-agarose (D) and recovered labeled proteins (E).

Protein Identification via nanoLC-MS/MS

To determine if the protein of interested isolated from the preparative scale PAL is present compared to that of the background proteins, we did a comparative analysis of the MS-MS spectra between results. The MS-MS spectra results from the protein were used in Mascot database search to identify similar proteins based on their peptide sequence and fragment mass to charge ratios. The results were scored using a probability-scoring algorithm and the best matches were reported as results. A positive identification was reported when two peptides have an Ions score above 35 or if a protein under 20 kDa has one peptide with an Ions score above 50. The reported results from Alphalyse indicated that there were 15 *S. aureus* proteins within the 60 kDa PAL band (Table 3.2). The background band was also sent to Alphalyse for protein identification and resulted in only one similar protein, the catalase protein, as the PAL analysis. Expected results were that the background analysis and PAL analysis would share more similar proteins and comparative analysis between results would narrow down the potential target proteins.

Table 3.2: List of protein identified and calculated molecular weight by nanoLC-MS/MS peptide sequencing and database search.

Protein Name	Calculated MW (kDa)
Elongation factor	43.1
Enolase	47.1
Dihydrolipoyl dehydrogenase	49.5
Formate-tetrahydrofolate ligase	49.5
Glutamine synthetase	51
2,3-biphosphoglucerate-dependent phosphoglycerate mutase	26.7
Glutamyl-tRNA(Gln) amidotransferase subunit A	52.9
Pyruvate kinase	63.2
1-pyrroline-5-carboxylate dehydrogenase	57
Catalase	58.3
Phosphoenolpyruvate carboxykinase	59.5
Ferritin	19.6
Inosine-5~monophosphate dehydrogenase	52.9
L-lactate dehydrogenase	34.5
30S ribosomal protein S5	17.7

Limitations and Future Directions

Currently, we have identified a potential target protein of the PAL assay to be at approximately 110 kDa, but further analysis is required for specific protein identification and target elucidation of 31G12. Future experiments using azide-fluor 545 instead of biotin-streptavidin will include a dose-dependent response, competitive 31G12 displacement and preparative scale protein isolation for LC-MS/MS analysis to further elucidate the protein of interest and mode of action for 31G12 by photolabeling.

A limitation of using the LC-MS/MS for protein identification in PAL is that the probe is covalently attached to our protein of interest. If this is true, the probe would add 1.092 kDa to the peptide fragment of the protein of interest and produce a different spectra. This difference in spectra would not be recognizable by a MASCOT database search and could possibly give false positive results. We plan to mitigate this problem with two different approaches. The first is by synthesizing a probe with an alanine residue attached to use as a standard in LC-MS/MS experiments. This will allow us to extract the spectral differences between Alanine and Alanine with the probe JH-7-088 attached. These data are then used to search the raw spectral data from Alphalyse to find a spectra similar to the probe and use this to identify the protein of interest. The second approach is to write a computer program that will scan through the spectra of both the background and PAL sample and extract the spectra that are not similar to one another. This should provide us with the spectra to use for protein identification.

CHAPTER IV. A BIOINFORMATIC APPROACH TO TARGET ELUCIDATION OF 31G12

Introduction

The search for new antibiotics with novel mechanisms of action remains a significant challenge to combat resistance to existing antibacterial therapies.^{73,74} Drug resistance is encoded in the bacterial genome through resistance-associated mutations or single-nucleotide polymorphisms (SNPs) and can serve as biomarkers in bacterial drug resistance profiles.⁷⁵ Besides SNPs that contribute to drug resistance in genes that encode for the protein target or drug-metabolizing enzyme, there are three other classes of genes that may confer a selective advantage against antimicrobials.⁷⁵ First, decreased permeability of membrane barriers or membrane-associated efflux systems can minimize exposure to the drug.⁷⁶ Secondly, compensatory mutations can offset the fitness costs of the initial mutation that confers resistance.⁷⁷ Third, bacteria with increased mutation rates can increase the rate at which beneficial mutations can occur in the presence of drug treatment providing a selective advantage.⁷⁸ Much effort has been made to identify candidate SNPs that give rise to molecular variants causing phenotypes, such as those associated with drug resistance, using databases and web resources.⁷⁹ Over the past decade, bioinformatic research has led to a better understanding of the effects of these molecular variants.⁷⁹

We investigated the use of genome sequencing and genome-wide association studies (GWAS) to identify SNPs and genes associated with resistance to 31G12 using an all-bacterial bioinformatics resource center, Pathosystems Resource Integration Center (PATRIC). PATRIC is an online resource that stores and integrates data such as genomics, transcriptomics, protein-

protein interaction, 3D protein structures, sequence typing data and associated metadata.⁸⁰ For utilization in comparative genomic analysis there are over 80,000 bacterial genomes which includes more than 6,000 antibiotic resistant genomes (as of August 2016). Genome assembly using Assembly RAST assembles short reads that are single or paired-end (Illumina) and long reads from filtered FASTQ files (PacBio) using base calling algorithms such as BayesHammer or Kmergeni and assembler such as Velvet, IDBA, Spades, MEGAHIT and MiniASM (Figure 4.1). A custom ARAST is used to evaluate and score the assemblies and frameworks.

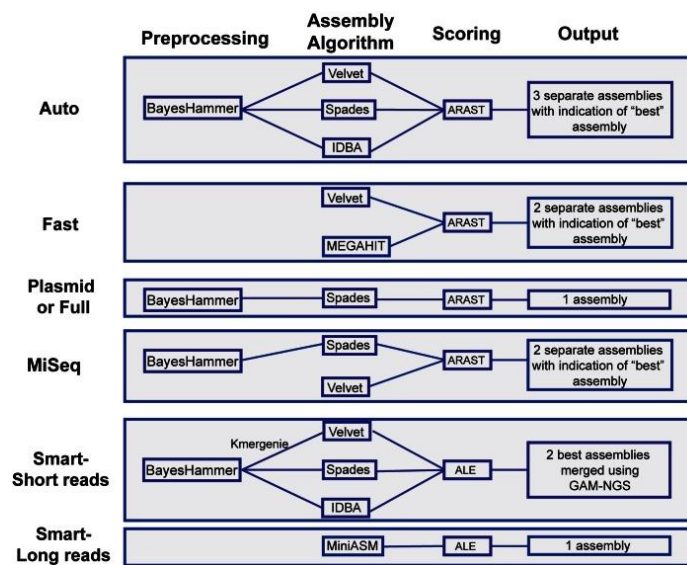


Figure 4.1: The various assembly strategies offered in PATRIC (reference).

RAST tool kit (RASTtk) is used for genome annotation which allows for comparative analyses of all genomes in PATRIC because they are processed identically so that comparisons can be made. PATRIC also offers a proteome comparison service that aligns multiple genomes to a reference genome in a bidirectional best BLASTP analysis.

The most useful tool for our investigation to identify SNPs is the use of the variation analysis service. Here multiple short or long read files are aligned against a reference genome to

which variation such as SNPS, Multiple Nucleotide Polymorphism (MNPs), insertions, and deletion with confidence scores and polymorphisms are reported. The variation analysis can be performed using different aligner programs such as BWA-mem and BWA-mem-strick, Bowtie, MOSAIK and LAST with variant caller algorithms FreeBayes and SAMtools.⁸⁰ The variant prediction can lead to false positives due to sequencing errors and misplacement during alignment but can be partially reduced by quality filtering.^{81–83} The high-quality genetic variants reported by PATRIC for 31G12 drug-resistant strain TZNB were then screened for resistance using traditional laboratory techniques to assess whether these biomarkers actually contribute to drug resistance and therefore provide the mode of action for 31G12.

Materials and Methods

Strains. Bacterial strains were derived from *Staphylococcus aureus* 13709 (WT). Bacteria were routinely grown in nutrient broth and nutrient agar plates at 37°C, unless indicated otherwise. Isolates were selected by screening on increasing concentrations of 31G12 in nutrient broth (TZNB). *S. aureus* TZNP was previously isolated from 31G12 nutrient agar plates from an unknown reference strain. Parental reference strain *S. aureus* 55/2053 genome was publicly available from NCBI.

DNA Extraction and Sequencing. *S. aureus* strains were cultured in tryptic soy broth (Bacto) at 37°C with shaking overnight. Chromosomal DNA purification methods were adapted from those provided by Dr. Horswill, University of Colorado School of Medicine (Aurora, CO), using the Qiagen PureGene Yeast/Bact. Kit B. Lysostaphin from *Staphylococcus simulans* was purchased from Sigma-Aldrich. Genomic DNA from WT and TZNB was sent to Washington State University Laboratory of Biotechnology and Bioanalysis (Pullman, WA) for library preparation, sequencing and assembly, using 60x coverage with a single SMRTCell by PacBio.

S. aureus TZNP was sent to University of Montana Genomics Core for library preparation (Nextera DNA library prep kit, Illumina) and Illumina MiSeq sequencing using 60x coverage.

Genome Assembly and Annotation. “Meta-service” comprehensive genome analysis service including assembly and annotation was done using the PATRIC Bacterial Bioinformatics Resource Center as follows. BayesHammer was run on *S. aureus* WT and TZNB reads and assembled using MiniASM. ARAST was used to sort assemblies and calculate quality score reads. BayesHammer was run on *S. aureus* TZNP and the sequence was assembled using Velvet, IDBA and Spades after which assemblies were sorted and scored using ARAST. All genome annotations were done using RASTtk.

Variation Analysis. Single-nucleotide polymorphism (SNP) calling was done using the PATRIC Bacterial Bioinformatics Resource Center as follows. Paired read libraries (FASTQ files) were used to align to a reference genome using BWA-mem and SNPs were called using FreeBayes.

Bacterial strains and plasmids. Strains and plasmids used in this work are listed in Appendix A Table 1. *Escherichia coli* was grown in Luria-Bertani broth or on Luria agar plates and supplemented with ampicillin (100 µg/mL) for the maintenance of plasmids and *S. aureus* was grown in TSB or on TSA and supplemented with chloramphenicol (7 µg/mL) for the maintenance of plasmids. pCM29 was provided by Dr. Alexander Horswill (Department of Immunology and Microbiology, University of Colorado School of Medicine, Aurora, CO, USA). Bacteria were grown overnight at 37°C with shaking at 225 rpm.

Mutant library constructs. Each of the high-quality variants was amplified using primers generated from sequencing data of *S. aureus* TZNB and joined by overlap PCR extension using genomic DNA from *S. aureus* TZNB as a template. PCR products were ligated with T4 DNA

ligase (Invitrogen) into pCM29 at the SacI and KpnI sites and electroporated into chemically competent TOP10F' *E. coli* and screened for plasmids via colony PCR. Plasmid DNA was purified from these strains using the Qiagen Plasmid Kit-tip 20 (Qiagen), and then introduced by electroporation into *S. aureus* RN4220. Plasmid DNA from *S. aureus* RN4220 strains was purified using the Qiagen Plasmid Kit-tip 20 and sequenced for mutation confirmation (Genewiz). A list of primers, strains and a map of pCM29 used in this study are listed in Appendix A, Table 2 and Figure 3.

31G12 resistance assay. *S. aureus* strains were grown overnight in TSB at 37°C with shaking at 225 rpm. Those with pCM29 were supplemented with 7 µg/mL chloramphenicol to maintain the plasmid. Cultures were plated in triplicate in 96-well microtiter plates at 1×10^5 cfu/100 µL in the presence of 31G12 and incubated at 37°C for 18 h. Plates were visualized at 600 nm on a SpectraMax M5 microplate reader to determine turbidity.

Results

Whole-genome sequencing and annotation statistics.

To identify genes that might contribute to 31G12 resistance, we sequenced and annotated the genomes of the susceptible parental strain *S. aureus* 13709 (WT), and two drug-resistant clones TZNB and TZNP. Parental strain *S. aureus* 55/2053 for TZNP was publicly available via NCBI. The whole-genome sequence statistics of the two drug-resistant clones compared to the parental strains are shown in Table 4.1. The sequencing depth was 60x, and read mapping results indicated nearly complete genome coverage for TZNB (96.90%) with only 159 (0.005%) of bases with zero coverage and good genome coverage for TZNP (91.96%) with 327847 (10.925%) bases with zero coverage. This suggested that the genomes of drug-resistant strains were closely related to their parental strains and could be used in further bioinformatic analysis to determine SNPs that may contribute to resistance.

Table 4.1: Statistics for whole-genome sequencing of the 31G12-resistant strains TZNB and TZNP compared their respective parent strains *S. aureus* 13709 WT and 55/2053.

Genome Statistics	TZNB	TZNP
Parent Strain	WT 13709	55/2053
Total Reads	119356	10908694
Properly Mapped Read	115661 (96.90%)	10032000 (91.96%)
Total reference bases	3000992	2756919
Median base coverage	143	472
Mean base coverage	140.5	487.7
Bases with zero coverage	159 (0.005%)	327847 (10.925%)
Bases with ≤ 10 coverage	21662 (0.722%), in 5614 contiguous regions	343314 (11.440%), in 3206 contiguous regions

Proteome Comparisons

In order to directly compare the proteomes of drug-resistant strains compared to parental strains, proteomic profiling was done using Sequence-based Comparison tool that was part of RAST. The circle plot shows the whole-genome schematic colored by BLAST similarity between compared strains (Figure 4.2 A and B). The changes in similarity relative to the reference genome goes from blue representing the highest protein sequence similarity to red representing the lowest. Analysis of the data table (data not shown) from the proteome profiling showed that 22 proteins from TZNB shared less than 100% identity when compared to the

reference genome WT 13709, resulting in 0.75% changes in conservation and 85 proteins from TZNP share less than 100% identity when compared to the reference genome 55/2053, resulting in 3.24% changes in conservation.

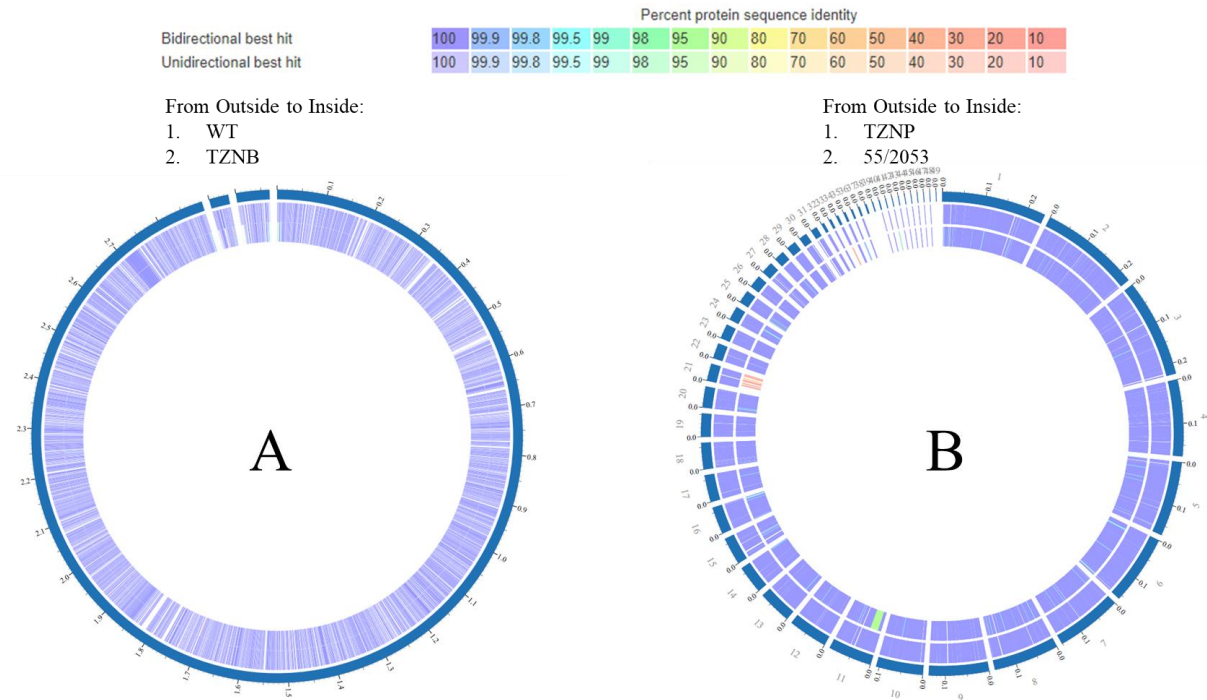


Figure 4.2: Proteomic profiling comparisons between parental strains and drug-resistant strains; WT and TZNB (A) and TZNP and 55/2053 (B).

Identification of high-quality SNPs reported in PATRIC variation analysis.

To identify genetic variants that may be involved in drug resistance, the variation analysis using BWA-mem and FreeBayes in PATRIC was used and yielded multiple SNPs between the parental strains and drug-resistant strains. The high-quality SNP variants for each comparative analysis between the four different genomes are presented in Figure 4.3.

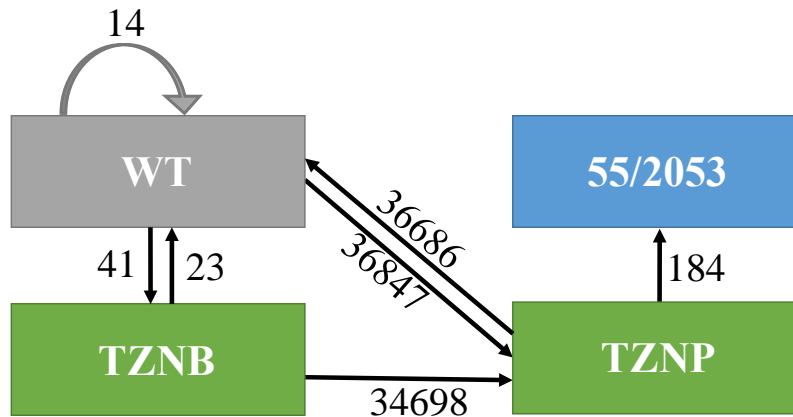


Figure 4.3: The high-quality SNP variants reported using PATRIC variation analysis. The tails of the arrow represent the input files and the heads represent the reference genome for each analysis. The number over the arrow represents the number of SNP variants called between that analysis.

As a reference point for probability scores reported by PATRIC in the variation analysis, the WT genome was assembled using two different assembly algorithms, PacBio’s Hierarchical Genome Assembly Process (HGAP) and PATRIC’s BWA assembly, and used with FreeBayes variant analysis. By using two different assemblers there were 14 SNPs called between genomes with scoring between 11.03-15.61. The probability scores indicate the likelihood that the SNP has occurred within the genome, and therefore these low scores indicated that the SNP is not likely to occur.

Identifying six potential proteins that confer resistance to 31G12.

To generate a list of possible protein targets from the variation analysis, the parental strain WT and drug-resistant strain TZNB were used to narrow down potential proteins of interest. From the 1971 raw FreeBayes variants called between TZNP and parent strain WT only 23 high-quality variants were reported (Table 4.2). The SNPs called were 1 synonymous, 20

non-homologous and 2 unidentified. From the remaining non-homologous SNPs, all proteins annotated as phage, hypothetical proteins or less than 20 kDa were removed. This filtered the 23 high-quality variants to six high-quality variants and therefore six possible target proteins that confer resistance, hereafter referred to as the six potential proteins (Table 4.3).

Table 4.2: The 23 high-quality variants in *S. aureus* TZNB compared to reference genome *S. aureus* WT.

Genome position	Putative gene product and function	Amino Acid change		Polymorphism
		<i>S. aureus</i> WT	<i>S. aureus</i> TZNB	
568				Deletion
1207	Phage-associated homing endonuclease	Q	*	Nonsyn
1819	Phage protein	G		Deletion
2234	Phage protein	DY	D	Deletion
3116				Insertion
3167	hypothetical protein	QN	HE	Insertion
3490				
3643	Ribosomal protein L11 methyltransferase (EC 2.1.1.-)	GV	GC	Insertion
13384	Replication protein	EKN	EK	Deletion
14388				Deletion
14610				Deletion
15318	hypothetical protein	FY	F	Deletion
16555	Transcriptional regulator, LysR family	GS	G	Deletion
62291	Lead, cadmium, zinc and mercury transporting ATPase (EC 3.6.3.3) (EC 3.6.3.5)	GKNI	GKKY	Insertion
63292	Multicopper oxidase	PKKI	PKKD	Insertion
64310	Multicopper oxidase	QF	QF	Insertion
65122	Transposase, IS4 family	IK	I-	Insertion
66535				
885721	DNA-directed RNA polymerase alpha subunit (EC 2.7.7.6)	L	*	Nonsyn
1450988	Phosphoserine phosphatase (EC 3.1.3.3)	QKI	QK*	Insertion
1823787	ABC-type dipeptide/oligopeptide/nickel transport system, ATP-binding protein	T	T	Synon
2225863	FIG00002411: Thioredoxin-fold protein	S	F	Nonsyn
2621562	DNA-directed RNA polymerase beta subunit (EC 2.7.7.6)	PK	QK	Nonsyn
2894249	Phage protein	NKNN	NKKQ	Insertion
2898237	Structural protein, phage associated	QW	H	Deletion

*, truncation

-, insertion.

Table 4.3: Six potential proteins filtered from the 23 high-quality variants in *S. aureus* TZNB compared to reference genome *S. aureus* WT 13709. Predicted protein size was generated using amino acid sequences obtained from PATRIC in ExPASy.

Genome position	Putative gene product and function	Amino acid change		Polymorphism	Predicted Protein Size (kD)	PATRIC Score
		<i>S. aureus</i> WT	TZNB			
3643	Ribosomal protein L11 methyltransferase	GV	GC	Insertion	35.54	13.28
16555	Transcriptional regulator, LysR family	GS	G	Deletion	33.79	20.06
62291	Lead, cadmium, zinc and mercury transporting ATPase	GKNI	GKKY	Insertion	86.7	14.22
885721	DNA-directed RNA polymerase alpha subunit	L	*	Nonsyn	34.37	927.80
1450988	Phosphoserine phosphatase	QKI	QK*	Insertion	38.26	180.65
2225863	Thioredoxin-fold protein	S	F	Nonsyn	31.31	880.34

*, truncation.

Identification of synonymous proteins in the comparative variation analysis of the resistant strains compared to the sensitive strain.

A comparison of SNP variants called between drug-resistant strains and parental strains was used to identify synonymous proteins identified in the variation analysis to determine the protein(s) potentially responsible for resistance to 31G12. These six potential proteins, and reported SNPs, were used to cross-reference all other high-quality variants called in independent variation analysis to look for a homologous SNP or protein.

The reverse variation analysis of TZNB and parental strain WT (i.e. WT was compared to the reference strains TZNB) reported 41 high-quality variants (Figure 4.3). From these 41 high-quality variants three proteins, thioredoxin-fold protein, DNA-directed RNA polymerase alpha subunit, and phosphoserine phosphatase, were all reported with the same SNPs as that of the six potential proteins.

In the variation analysis between TZNP and reference genome WT there were 36,686 high-quality variants reported (Figure 4.3). From these variants, the six potential proteins were reported with both synonymous and non-synonymous SNPs, but there was not an identical SNP

reported. From the 184 high-quality variants reported between TZNP and parental strain 55/2053, none of the six potential proteins was reported (Figure 4.3). However, the DNA-directed RNA polymerase beta subunit was reported to have a non-synonymous SNP. This protein is part of the DNA-directed RNA polymerase called in the six potential proteins, but the SNP was reported in a different subunit.

Protein alignments indicated presence or absence of SNPs in the six potential proteins.

The six potential proteins had amino acid changes based on the protein alignment of drug-resistant strains TZNB and TZNP compared to WT 13709 strain (Table 4.4). These predicted results suggest the likelihood that the non-synonymous SNPs called in the variation analysis may be present or absent in the genomes of drug-resistant TNZB and TZNP. The full protein alignments are available in Appendix A Figure 2.

Table 4.4: Predicted amino acid changes in the six potential proteins from drug-resistant TZNB and TZNP compared to WT 13709 strain.

Gene Product	TZNB	TZNP
Ribosomal protein L11 methyltransferase	-	D36Y, M71L, Q94H, H192Y, E257D
Transcriptional regulatory, LysR family Lead, cadmium, zinc and mercury transporting ATPase(1)	-	P181S, T241K, D244N, S270N K144R, I315V, N317D, R504C, V577M, S648N, A676T
Lead, cadmium, zinc and mercury transporting ATPase(2)	-	(No homologue)
DNA-directed RNA polymerase alpha subunit	L310*	-
Phosphoserine phosphatase	I334*	Q107R, K109E, L122I, I156T, T165N, Y295N, N298K, L376*
Thioredoxin-fold protein	F30S	V95L
DNA-directed RNA polymerase beta subunit	-	E355D, P614Q, Y737F

*, indicates truncation.

-, indicates no mutation observed.

Confirmation of SNPs in six potential proteins of TZNB in gene clones.

To test whether the potential SNPs identified by the variation analysis actually occurred and conferred resistance to 31G12, each high-quality variant from TZNB was cloned into vector pCM29 and expressed in sensitive strain RN4220. The expression system was validated in the selected transformants by PCR and sequencing. Sequence analysis of the transformants confirmed that only two of the predicted SNPs occurred in drug-resistant strain TZNB. The phosphoserine phosphatase was prematurely truncated due to experimental error and resulted in truncation of 36 amino acids (Table 4.5).

Table 4.5: Confirmed amino acid mutations of TZNB compared to parental strain WT 13709.

Gene Product	TZNB
DNA-directed RNA polymerase alpha subunit	L310*
Phosphoserine phosphatase	T341*
Thioredoxin-fold protein	F30S

*, indicates truncation.

Susceptibility of the TZNB mutants to 31G12.

The susceptibility of the generated TZNB mutants to 31G12 was assessed based on dose response inhibition. Although only two proteins had confirmed mutations, all variants were cloned into vector pCM29 under control of the *sarA* promoter to produce high expression levels when transformed into host strain RN4220. The EC_{50} , which is the concentration of 31G12 that gives half-maximal response, was determined for each mutant and compared to RN4220 (host), vector alone and TZNB (Table 4.6). The drug-resistant TZNB had an EC_{50} of $23 \pm 3.1 \mu\text{M}$, which was a two-fold increase in EC_{50} compared to the host (11.2 ± 2.3), vector control (9.276 ± 1.8) and WT (9.644 ± 1.4). All mutants fell within the range of the controls and exhibited sensitivity to 31G12 (Table 4.6). The EC_{50} from the growth inhibition of each transformed mutant did not exhibit resistance to 31G12 compared to that of WT, host, vector control and TZNB.

Table 4.6: Sensitivity of *S. aureus* 31G12 sensitive strains (WT, Host, Vector Only), drug-resistant strain TZNB and mutants to 31G12.

Strain or mutant	EC₅₀ (μM)
WT 13709	9.644 ± 1.4
TZNB	23.07 ± 3.1
Host (RN4220)	11.2 ± 2.3
Vector Control	9.276 ± 1.8
Phosphoserine Phosphatase	10.73 ± 1.8
DNA-Directed RNA Polymerase alpha subunit	10.21 ± 1.5
DNA-Directed RNA Polymerase beta subunit	10.41 ± 2.3
Lead, Cadmium, Zinc and Mercury ATPase (1)	10.64 ± 1.6
Lead, Cadmium, Zinc and Mercury ATPase (2)	9.519 ± 2.1
Transcriptional Regulator, LysR	8.818 ± 1.6
Ribosomal Protein L11 Methyltransferase	11.58 ± 1.5
Thioredoxin-fold Protein	11.28 ± 1.8

The percent maximum growth for the thioredoxin-fold protein mutant was found to be higher than that of the percent maximum growth of the host and vector control between 31G12 concentrations 2-16 μM (log₁₀ μM range 0.301-1.004) and the L11 methyltransferase was found to be higher than controls at 8μM (Figure 4.4). All other mutants exhibited maximum growth at or below the levels of host and vector controls (Figure 4.4). These results suggest that the high expression levels of the thioredoxin-fold protein and L11 methyltransferase may provide a fitness advantage at sub-inhibitory concentrations of 31G12.

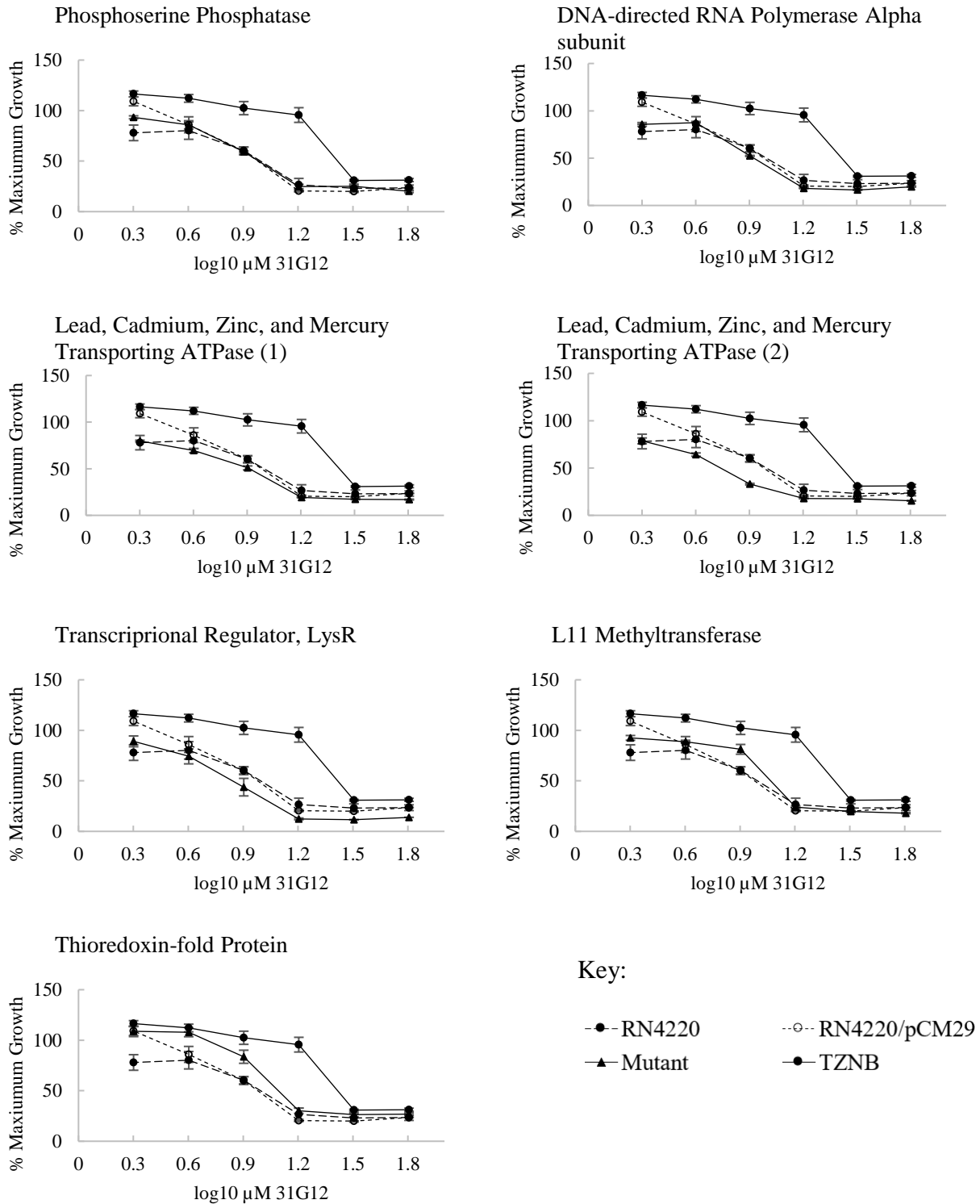


Figure 4.4: Dose response curves of each transformed mutant compared to drug-resistant TZNB and sensitive strains RN4220 (host) and RN4220/pCM29 (vector control) with error bars representing the standard error of the mean (SEM) of triplicate samples.

Discussion

To identify genetic markers of drug resistance to 31G12, we performed whole-genome sequencing of *S. aureus* WT, TZB, TZNP. These genomes and publicly available genomes were used in PATRIC for variation analysis to identify SNPs that could contribute to resistance.

Unlike other bioinformatics software, PATRIC does not require that the user have prior computer programming experience. However, additional background information on the algorithms implemented in each program does contribute to a better understanding of the probability scoring and evaluations of high-quality variants reported.

Selection of a proper alignment algorithm to be used in the variation analysis is important when using long reads, such as those produced by PacBio sequencing, or if the reads contain indels. The Burrows-Wheeler Alignment (BWA) is a sequence alignment package that is based on the backward search with Burrows-Wheeler Transform for mapping low-divergent sequences against a large reference genome.⁸² This algorithm allows for gapped alignment for single-end reads, supports paired-end mapping, generates mapping quality and gives multiple hits if required.⁸² For the variation analysis the BWA-mem aligner was selected because it can be used for mapping short reads, such as those from the TZNP Illumina sequencing, or long query sequences obtained from the PacBio sequencing of WT 13709 and TZNB (Figure 4.5). To use this algorithm in PATRIC, the user inputs the raw FASTQ files from sequencing to be

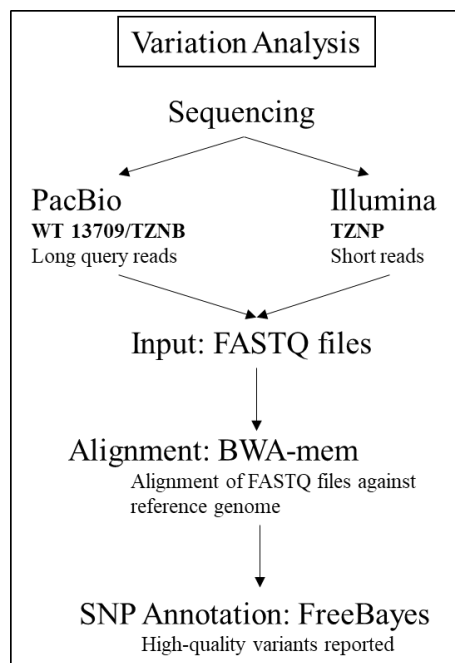


Figure 4.5: The workflow for variation analysis to determine genetic SNPs.

compared against a fully assembled reference genome, to generate an output alignment file in a SAM format, which can be used in other downstream analysis.

These SAM file alignments are then used in FreeBayes to detect genomic variants within the alignment (Figure 4.5). FreeBayes indicates the number of raw read variants determined from the variation analysis and use a Bayesian model to further refine the results to report only the high-quality variants. The variation summary indicates how well each of the input FASTQ files are properly mapped to the reference genome and the coverage of bases. Drug-resistant strain TZNB was derived from WT 13709, and as expected we see a high percentage of properly mapped reads (96.9%) with only 0.005% of bases with zero coverage. This indicates that the two are closely related and a good match when looking for variations called between the two genomes.

As previously mentioned, the original parent strain of TZNP was unknown and therefore when TZNP is compared to the WT strain there is a much lower percentage of properly mapped reads (89.58%) and a higher percent of bases with zero coverage (10.925%). This is not ideal when trying to identify SNPs that could contribute to resistance because of the low match between the two genomes. To find a more similar parental strain to use as a reference genome for variations analysis of TZNP, the whole genome was imported into BLASTn. *S. aureus* 55/2053 was selected for analysis in this study as a new reference genome for TZNP because it had the highest percent match (100%) and lowest e score (0.0) reported in BLASTn. When using 55/2053 as a reference genome for TZNP, the properly mapped reads increased to 91.96%, however there was still 10.925% of bases with zero coverage, which could be due to sequencing errors. This indicated that the genomes of 55/2053 and TZNP are more closely related and a better match for determining SNP variants that could confer resistance to 31G12.

This high similarity between genomes in drug-resistant strains and their respective parent genomes was also illustrated in the high protein sequence identity determined in the proteome profiling. This again illustrates the low changes in conservation of the genomes and suggest that they are good matches for SNP variant analysis.

By using the variation analysis of WT 13709 when compared to itself, a reference point for the scoring of likelihood variants reported was established. The fourteen SNPs reported were due to the use of two different assemblers to create a reference genome for the variation analysis. As expected, the likelihood scores reported are low (11.03-15.61) because the input genome was the same as the reference genome, except for the use of two different assemblers. Therefore, in other variation analyses a likelihood score reported that is close to that of the reference point scoring can be expected to occur less likely in the genome.

The list of six potential proteins was used to search for similar proteins in the other variation analysis because TZNB was derived from WT 13709 and therefore provided the best comparison between genomes to identify SNPs that could contribute to drug-resistance of 31G12. When filtering the non-homologous SNPs reported between TZNB and WT 13709, we applied a 20 kDa protein size cutoff based on our previous work to elucidate the target protein through a 31G12-based photoaffinity assay. The western blots indicated that no proteins below 20 kDa were being labeled. However, in applying this filter, three proteins were removed from the list of potential proteins, but the likelihood scores were in the same range as the reference point scores and therefore disregarded. It was very unlikely that 31G12 target protein was a phage protein and therefore we removed four of these proteins from our potential list and those proteins reported as hypothetical or no function were also disregarded due to the low likelihood that these could theoretically be our target and mode of action.

The next objective was to conduct a comparative analysis using the six potential proteins to search for a protein that is shared between TZNB and TZNP from all the variation analysis that could be identified as the target protein and mode of action for 31G12. It is not surprising that the thioredoxin-fold protein, RNA-dependent DNA polymerase alpha subunit and phosphoserine phosphatase was reported in the reverse variation analysis between TZNB and WT 13709 due to their large likelihood scores. From the 36,686 SNPs reported in the variation analysis between TZNP and WT 13709, it was also not surprising that five of the six potential proteins, apart from the lead, cadmium, zinc and mercury ATPase (2), were reported with various synonymous and non-synonymous SNPs because the two strains are not very similar to one another. Although TZNB and TZNP share five similar proteins with variants reported it was surprising that there was not an identical SNP reported within these five proteins. By using 55/2053 as a reference genome for TZNP instead of WT 13709, it decreased the number of high-quality variants reported from 36,686 to 184. This was expected due to the high similarity between the two genomes, however it was unexpected that none of the six potential proteins was reported. One explanation for these results is that 31G12 is targeting two different proteins causing two separate SNPs or are there different SNPs within the same protein conferring resistance. Another alternative explanation is that the drug is being extruded from the cell by way of an efflux pump and did not select for a SNP, which is why no mutation would be found conferring resistance through the bioinformatics approach of target elucidation.

Although our bioinformatics results did not produce a single protein with an identical SNP, each of the six potential proteins from TZNB was screened for resistance against 31G12. The *sarA* promoter in pCM29 produces high expression levels of the cloned gene when transformed into host RN4220. However, the host gene product is still being produced by the

cells. This approach of cloning by exploitation of gene dosage effects has been widely used based on the principle that by increasing the number of copies of a given gene can lead to increased synthesis of the products of that gene.⁸⁴ The transformed *S. aureus* mutants exhibited a different phenotype than that of TZNB, host, and vector control. When the transformed clones were grown in broth media the cells were observed to settle to the bottom of the culture tubes but were easily resuspended. One hypothesis is that the gene products were being over expressed in the cells causing this observed difference in phenotype. Future experiments should be done to determine if the gene products are actually being over expressed by *sarA* in pCM29, such as qPCR.

To explore the significance of each strain's resistance, growth inhibition was compared between host, vector control, and TZNB. Sequencing of the gene within the pCM29 construct confirmed the presence or absence of the *in silico* predicted SNP variants. Looking at the likelihood scores reported, it is again not surprising that the DNA-directed RNA polymerase alpha subunit and the thioredoxin-fold protein had confirmed mutations. The phosphoserine phosphatase was predicted to be truncated by forty-three amino acids, but the mutation was not confirmed and therefore the whole gene would have been transcribed in TZNB. However, due to the primer design based on this predicted mutation, the protein was accidentally truncated by thirty-six amino acids. The EC₅₀ of drug-resistant TZNB was determined to be two-fold greater than the host, vector control and WT 13709, which can be confirmed as drug-resistant. All of the transformed mutants' EC₅₀ values were determined to be less than that of the TZNB and closer to the EC₅₀ values for host and vector controls, which demonstrates that none of the predicted SNPs variants confirm resistance to 31G12 when expressed in the RN4220/pCM29 system. Closer examination of the dose-response curves shows that L11 methyltransferase and the thioredoxin-

fold protein exhibit increased maximum growth at sub-inhibitory concentrations of 31G12. It is possible that these mutations and over expression of these genes results in increased fitness at sub-inhibitory concentrations of 31G12 but currently does not confirm that either of these proteins is the target for 31G12 and the mode of action.

In summary, our whole-genome sequencing approach revealed multiple mutations in *S. aureus* drug-resistant strains TZNB and TZNP. The results suggest that the use of the bioinformatic system PATRIC was a good approach for determining genetic variation among different strains. Although the mode of action for 31G12 has not been confirmed, the results yielded six potential proteins; two of which are good candidates for further studies. Future research should examine the levels of gene expression using the RN4220/pCM29 system and plasmid stability studies of pCM29 to ensure that the plasmid is not being lost from the clones during the drug inhibition studies. Another alternative for drug inhibition studies and conferring resistance to 31G12 is use of a new system RN4220/pTet15. The significance of finding the mode of action for 31G12 in *S. aureus* is for future studies involving crystallization of the target protein for a target-based drug development approach for new antibiotics.

CHAPTER V. CONCLUSIONS

Staphylococcus aureus is a Gram-positive bacterial pathogen responsible for nosocomial and community-acquired infections. Its ability to quickly acquire antibiotic resistance has made it practically resistant to all known antibiotics. Here, we have identified a novel triazole antimicrobial 31G12 based on the natural product core of nonactin. We have demonstrated that this novel antimicrobial is active against multiple Gram-positive bacteria as well as antibiotic-resistant MRSA and VRE. The synthesis and characterization of 31G12 indicated it exists as a mixture of two rotamers and was used to select for *S. aureus* resistant mutants TZNB and TZNP for target elucidation studies to determine the mode of action. It was also determined that 31G12 is a bacteriostatic antimicrobial against *S. aureus* with moderate mammalian cell toxicity.

We have currently revealed potential protein targets of 31G12 in *S. aureus* by a chemical proteomic strategy that utilized 31G12 based photoaffinity-cross-linking probe JH-7-088. It was established that probe JH-7-088 and biotin-azide tag JH-7-022 binds to a protein at approximately 110 kDa when visualized via western blot. The probe was competitively displaced with 31G12 and displayed a strong dose-response with increasing concentrations. Preliminary results using azide-fluor 545 instead of the biotin-streptavidin tag also suggest that a protein at ~110 kDa is being labeled via in-gel scans. This evidence suggest that the protein of interest and potential target for antimicrobial 31G12 is a protein(s) with a molecular weight of ~110 kDa, but further experiments are needed to verify these results.

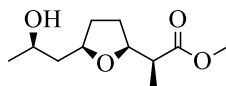
Using whole-genome sequencing and a bioinformatic approach to target elucidation of 31G12 revealed multiple mutations in *S. aureus* drug resistant-strains TZNB and TZNP. The bioinformatic system PATRIC was a good approach for determining genetic variations among the different strains and yielded six potential protein targets of 31G12. Two of these proteins,

thioredoxin-fold protein and L11 methyltransferase, were determined to be good candidates based on dose-response curves. Future studies could be done to verify if either of these proteins contributes to resistance against 31G12 in *S. aureus* and therefore reveal the mode of action.

Although the mode of action for novel antimicrobial 31G12 has not been established we are confident that we are close to finding it. More broadly, this work highlights the use of an interdisciplinary approach to elucidate the target of a novel antimicrobial thereby providing a rational framework for expanding efficacy. To expand this efficacy, future structure-based drugs designed on the mode of action for antimicrobial 31G12 could be investigated to produce a more potent antimicrobial against Gram-positive bacteria with lowered toxicity to mammalian cells.

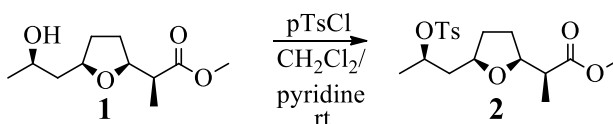
CHAPTER VI. SYNTHESIS EXPERIMENTALS

Synthesis of 31G12



Methyl Nonactate

Methyl nonactate was purified from a mixture of methyl nonactate and methyl homononactate by column chromatography and eluted with EtOAc/Hexanes (10%-90%). $^1\text{H NMR}$ (400 MHz, CDCl_3 -*d*) δ ppm 1.06 (d, $J=7.03$ Hz, 3H), 1.13 (d, $J=6.27$ Hz, 3H), 1.49-1.69 (m, 4H), 1.88-1.99 (m, 2H), 2.42-2.53(m, 1H), 3.02 (s, 1H), 3.62 (s, 3H), 3.89-3.99 (m, 3H).



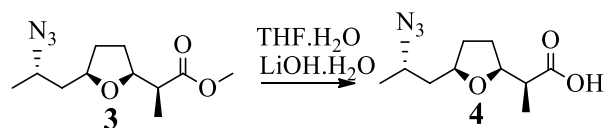
Methyl (*S*)-2-((2*S*,5*R*)-5-((*R*)-2-(tosyloxy)propyl)tetrahydrofuran-2-yl)propanoate⁸⁵

Methyl nonactate **1** (1.015 g, 4.62 mmol) was dissolved in CHCl_2 (10 mL). Pyridine (1.2 mL, 13.9 mmol) and *p*TsCl (1.375 g, 6.93 mmol) were added and reaction was stirred at room temperature for 18 h. The reaction mixture was diluted with EtOAc, washed with aq. CuSO_4 (3 x 10 mL), and aq. NH_4Cl (10 mL) and then dried over anhyd. NaSO_4 . The solvent was removed by evaporation *in vacuo*. The crude product was purified by column chromatography and eluted with EtOAc/Hexanes (1:9) to yield **2** (0.725 g, 75%). $^1\text{H NMR}$ (400 MHz, CDCl_3 -*d*) δ ppm 1.07 (d, $J=7.03$ Hz, 3H), 1.32 (d, $J=6.27$ Hz, 3H), 1.47-1.69 (m, 2H), 1.79-1.93 (m, 3H), 2.42-2.48 (m, 4H), 3.54-3.62 (m, 1H), 3.69 (s, 3H), 3.73-3.80 (m, 1H), 4.73-4.81 (m, 1H), 7.33 (d, $J=8.03$ Hz, 2H), 7.78 (d, $J=7.69$ Hz, 2H).



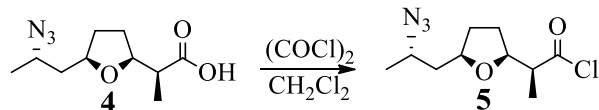
Methyl (S)-2-((2S,5R)-5-((S)-2-azidopropyl)tetrahydrofuran-2-yl)propanoate⁸⁵

Sodium azide (2.6470 g, 40.7 mmol) was dissolved in DMSO (8.5 mL) and added to a solution of **2** (0.7272 g, 3.24 mmol) in DMSO (15 mL). The mixture heated at reflux for 18 h. The reaction mixture was diluted with H₂O and extracted with EtOAc (2 x 15 mL). The organic phase was washed with aq. NaHCO₃ (2 x 10 mL), and brine (10 mL), and then dried over anhyd. Na₂SO₄. The solvent was removed by evaporation *in vacuo* to yield **3** (0.634 g, 92%). ¹H NMR (400 MHz, CDCl₃-*d*) δ ppm 1.12 (d, *J*=7.03 Hz, 3H), 1.28 (d, *J*=6.53 Hz, 3H), 1.49-1.72 (m, 3H), 1.80-1.89 (m, 1H), 1.93-2.09 (m, 2H), 2.53 (dd, *J*=7.91, 7.15 Hz, 1H), 3.51-3.62 (m, 1H), 3.70 (s, 3H), 3.90-3.99 (m, 1H), 4.03 (d, *J*=8.03 Hz, 1H).



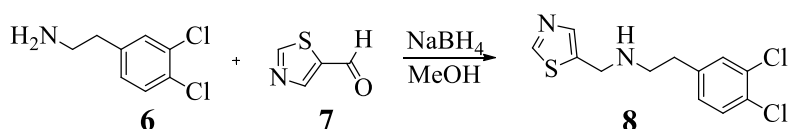
(S)-2-((2S,5R)-5-((S)-2-Azidopropyl)tetrahydrofuran-2-yl)propanoic acid⁸⁵

Compound **3** (0.7272 g, 3.24 mmol) was dissolved in THF (14.5 mL) to which H₂O (7.3 mL) was added. LiOH (0.7858 g, 32.4 mmol) was added to the solution which was stirred at room temperature for 18 h. The reaction was diluted with EtOAc and washed with aq. 1% (w/v) NaOH (3 x 20 mL). The aqueous layers were combined and cooled to 0 °C and then acidified with aq. 1 M HCl, and washed with EtOAc (2 x 10 mL). The combined organic phases were washed brine (2 x 10 mL), dried over anhyd. Na₂SO₄. The solvent was removed by evaporation *in vacuo* to yield **4** (0.558 g, 81%). ¹H NMR (400 MHz, DMSO-*d*₆) δ ppm 1.00 (d, *J*=7.03 Hz, 3H), 1.22 (d, *J*=6.53 Hz, 3H), 1.44-1.65 (m, 3H), 1.71 (dt, *J*=13.74, 7.06 Hz, 1H), 1.84-2.02 (m, 2H), 2.31-2.41 (m, 1H), 3.54-3.65 (m, 1H), 3.80-3.95 (m, 2H), 12.06 (br s, 1H).



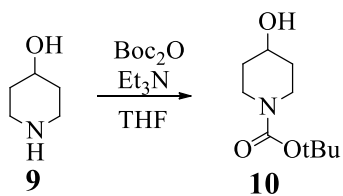
(S)-2-((2S,5R)-5-((S)-2-Azidopropyl)tetrahydrofuran-2-yl)propanoyl chloride

Compound **4** (0.266 g, 1.17 mmol) was dissolved in CHCl_2 (6 mL) and cooled to 0 °C, after which oxalyl chloride (0.41 mL, 4.7 mmol) and two drops of DMF were added. The mixture was stirred for 18 h. The reaction mixture was concentrated by evaporation *in vacuo* yielding **5** (.288 g, 100%).



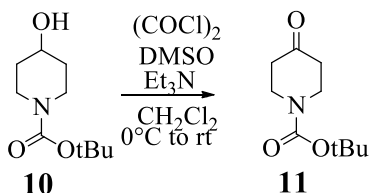
2-(3,4-Dichlorophenyl)-N-(thiazol-5-ylmethyl)ethanamine⁸⁶

Thiazole-5-carbaldehyde **7** (0.55 mL, 6.35 mmol) and NaBH_4 (0.3844 g, 8.46 mmol) were added to MeOH (6 mL), and then 3,4-dichlorophenethylamine **6** (0.6 mL, 4.23 mmol) was added and stirred for 1 h at room temperature. The reaction was diluted with water and acidified with aq. 1 M HCl to pH 1 and washed with CH_2Cl_2 (3 x 20 mL). The aqueous phases were adjusted to pH 10 with 10% NaOH and extracted with CH_2Cl_2 (3 x 15 mL), and washed with brine, and then dried over anhyd. Na_2SO_4 . The solution was concentrated *in vacuo* yielding **8** (0.8101 g, 70.5%). ^1H NMR (400 MHz, $\text{DMSO}-d_6$) δ ppm 2.34 (br s, 1H), 2.67-2.85 (m, 5H), 3.93 (s, 2H), 7.20 (dd, $J=8.19, 2.08$ Hz, 1H), 7.46-7.56 (m, 2H), 7.73 (s, 1H), 8.95 (s, 1H). ^{13}C NMR (CDCl_3 -d, 100 MHz) δ 152.8, 140.8, 140.0, 138.4, 132.3, 130.6, 130.3, 130.2, 128.1, 49.6, 45.4, and 35.4



tert-Butyl 4-hydroxypiperidine-1-carboxylate⁸⁷

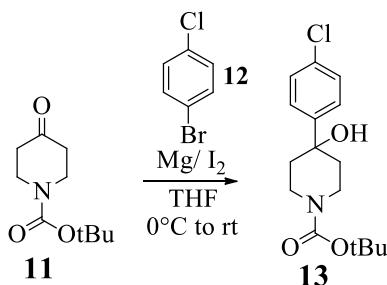
4-hydroxypiperidine **9** (2.0095 g, 19.7 mmol) and trimethylamine (TEA) (6.3 mL, 39.5 mmol) were dissolved in THF (18 mL) and Boc_2O (5.5 mL, 39.5 mmol) was added then stirred at room temperature for 18 h. THF was removed by evaporation *in vacuo* and the product was dissolved in EtOAc (10 mL) and washed with brine (2 x 10 mL), and dried over anhyd. Na_2SO_4 and then solvent removed by evaporation *in vacuo*. The crude product was purified by column chromatography and eluted in EtOAc/Hexanes (10-75%) to yield **10** (2.371 g, 59%). ^1H NMR (400 MHz, $\text{DMSO}-d_6$) δ ppm 1.14-1.31 (m, 2H), 1.33-1.44 (s, 9H), 1.59-1.72 (m, 2H), 2.94 (br s, 2H), 3.55-3.85 (m, 3H), 4.69 (d, $J=4.27$ Hz, 1H).



tert-Butyl 4-oxopiperidine-1-carboxylate⁸⁸

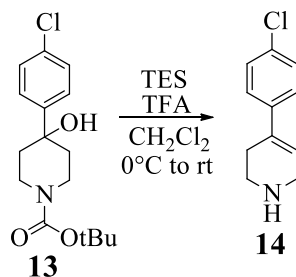
Oxalyl chloride (1.872 g, 15.2 mmol) was dissolved in CH_2Cl_2 (15 mL) and cooled to -78°C . DMSO (2.1 mL, 29.5 mmol) in CH_2Cl_2 (6 mL) was added to the reaction mixture and stirred for 15 min. Compound **10** (2.3394 g, 11.8 mmol) was dissolved in CH_2Cl_2 (6 mL) and added to the reaction mixture and stirred for 1 h before the addition of Et_3N (4.9 mL, 35.1 mmol) and then stirred for an additional 20 minutes. The reaction was allowed to come to room temperature over 18 h. The reaction was washed with H_2O (2 x 20 mL) and dried over anhyd. Na_2SO_4 and then the solvent was removed by evaporation *in vacuo*. The crude product was purified by column

chromatography and eluted in EtOAc/Hexanes (1:4) to yield **11** (1.357 g, 73%). $^1\text{H NMR}$ (400 MHz, CDCl_3 -*d*) δ ppm 1.42 (s, 9H), 2.37 (t, 4H), 3.65 (t, 4H).



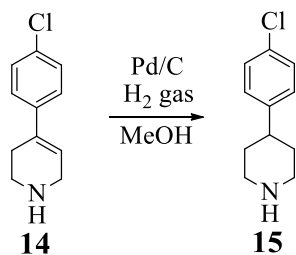
***tert*-Butyl 4-(4-chlorophenyl)-4-hydroxypiperidine-1-carboxylate⁸⁹**

Magnesium turnings (0.43 g, 16.6 mmol), THF (10 mL) and a crystal of iodine were added to a dry 3 neck flask equipped with an addition funnel and reflux condenser. 1-Bromo-4-chlorobenzene **12** (3.178 g, 16.6 mmol) in THF (10 mL) was added to the addition funnel and slowly added to the reaction mixture. The solution was stirred and heated at reflux for an hour before being cooled to 0 °C in an ice bath. A solution of **11** (0.661 g, 3.3 mmol) in THF (10 mL) was added dropwise via the addition funnel to the reaction solution and heated at reflux for 1 h. After reaching room temperature, the reaction was quenched with NH_4Cl and extracted with EtOAc (3 x 20 mL), and then dried over anhyd. Na_2SO_4 and the solvent was removed by evaporation *in vacuo*. The crude product was purified by column chromatography and eluted with EtOAc/Hexanes (5-30%) to yield **13** (0.187 g, 27%). $^1\text{H NMR}$ (400 MHz, CDCl_3 -*d*) δ ppm 1.26 (t, $J=7.09$ Hz, 1H), 1.48 (s, 9H), 1.96 (td, $J=13.20, 4.89$ Hz, 2H), 2.05 (s, 1H), 3.22 (td, $J=13.02, 2.81$ Hz, 2H), 3.99-4.09 (m, 2H), 4.12 (q, $J=7.09$ Hz, 1H), 7.30-7.37 (m, 2H), 7.39-7.45 (m, 2H).



4-(4-Chlorophenyl)-1,2,3,6-tetrahydropyridine⁹⁰

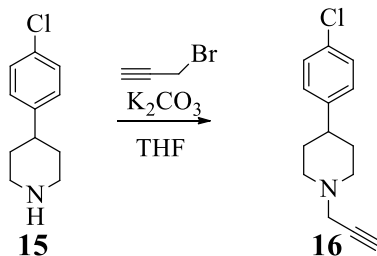
Compound **13** (3.627 g, 11.7 mmol) was dissolved in CH₂Cl₂ (55 mL) and triethylsilane (9.2 mL, 58.5 mmol) was added and then cooled to 0 °C. Trifluoroacetic acid (TFA) (21.5 mL, 280.8 mmol) was slowly added to the mixture and stirred for 24 h. 1 M NaOH (25 mL) was added to the reaction mixture and stirred for 20 min before being washed with CH₂Cl₂ (2 x 30 mL). The organic phases were combined and washed with aq. Brine (2 x 10 mL) and then dried over anhyd. Na₂SO₄. The solvent was removed by evaporation *in vacuo* to yield **14** (1.484, 65%). ¹H NMR (400 MHz, CD₃OD-*d*₄) δ ppm 2.68-2.76 (m, 2H), 3.56 (s, 3H), 3.72 (br d, *J*=2.93 Hz, 2H), 6.43 (br s, 1H), 7.55 (d, *J*=8.56 Hz, 2H), 7.65 (d, *J*=8.56 Hz, 2H).



4-(4-Chlorophenyl)piperidine⁹¹

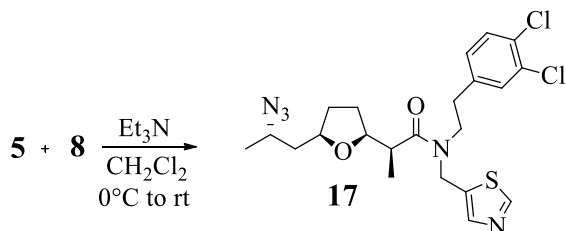
Compound **14** (2.26 g, 11.67 mmol) was dissolved in MeOH (58 mL) and Pd/C (0.6224 g, 5.83 mmol) was added. The solution was stirred vigorously under a H₂ pressurized balloon for 6 h at room temperature. The reaction was filtered through a MeOH celite slurry and then the solvent was removed by evaporation *in vacuo*. The crude product was dissolved in EtOAc and washed with 1 M NaOH (2 x 25 mL), NaOH/brine (1:1, 2 x 25 mL), and then dried over anhyd. Na₂SO₄.

The solvent was removed by evaporation *in vacuo* to yield **15** (1.972, 86%).



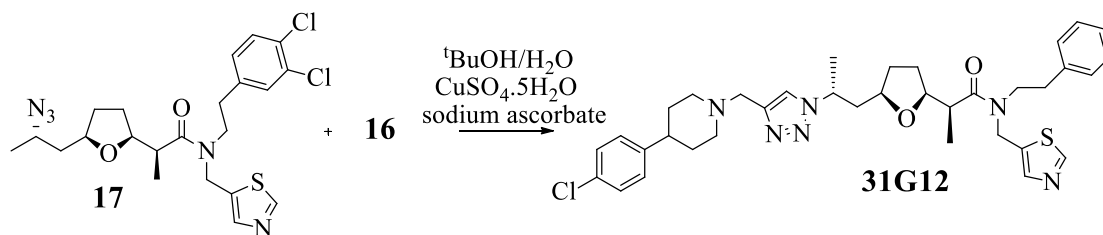
4-(4-chlorophenyl)-1-(prop-2-yn-1-yl)piperidine⁹²

Compound **15** (0.7624 g, 3.9 mmol) was dissolved in THF (4 mL) and added to a solution of propargyl bromide (0.46 mL, 4.09 mmol) in THF (1 mL). The reaction was wrapped in tin foil and stirred for 7 min before the addition of K_2CO_3 (1.0920 g, 7.79 mmol) and reacted at room temperature for 18 hr. The reaction mixture was diluted with EtOAc and washed with aq. 1 M NaOH (2 x 5 mL), aq. 1 M NaOH/brine (1:1, 10 mL), and then dried over anhyd. Na_2SO_4 . The solvent was removed by evaporation *in vacuo*. The crude product was purified by column chromatography and eluted with EtOAc/Hexanes (1:4) to yield **16** (0.469, 51%).



(S)-2-((2S,5R)-5-((S)-2-Azidopropyl)tetrahydrofuran-2-yl)-N-(3,4-dichlorophenethyl)-N-(thiazol-5-ylmethyl)propanamide

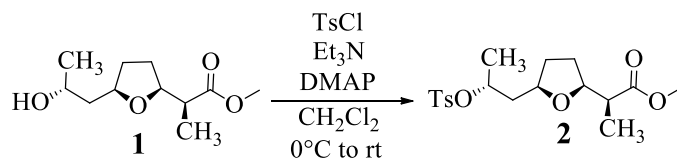
Compound **8** (0.396g, 1.44 mmol) was dissolved in CH_2Cl_2 (2 mL) and cooled to 0 °C, after which Et_3N (0.22 mL, 1.51 mmol) was added to the solution. Compound **5** (0.439g, 1.38 mmol) was dissolved in CH_2Cl_2 (2.5 mL) and slowly added to the reaction mixture and then stirred for 18 h. The reaction was diluted with aq. Na_2CO_3 and then stirred for five min, before extraction with EtOAc (10 mL) and washed with H_2O (1 x 10 mL) to yield crude **17** (0.387 g, 48%).



2-(5-(2-(4-((4-(4-Chlorophenyl)piperidin-1-yl)methyl)-1H-1,2,3-triazol-1-yl)propyl)tetrahydrofuran-2-yl)-N-(3,4-dichlorophenethyl)-N-(thiazol-5-ylmethyl)propanamide⁹³

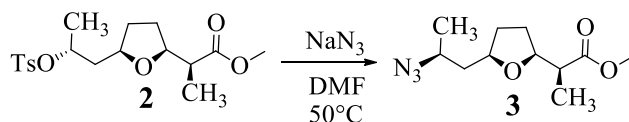
Crude **17** (0.387, 0.78 mmol) and **16** (0.197 g, 0.79 mmol) were dissolved in *t*-BuOH (1.4 mL) and then H₂O (1.4 mL) was added. CuSO₄·5H₂O (0.00214 g, 0.078 mmol) was added immediately followed by sodium ascorbate (0.0323 g, 0.16 mmol) and then stirred at room temperature 18 h. The reaction was diluted with EtOAc and washed with H₂O (2 x 5 mL), then aq. brine (10 mL) and the solvent was removed by evaporation *in vacuo*. The crude product was purified by column chromatography and eluted with EtOAc/Hexanes (1:4) (0.052 g, 21%). ¹H NMR (400 MHz, CDCl₃-*d*) δ ppm 0.91-1.15 (m, 3H), 1.42-1.61 (m, 5H), 1.68-2.23 (m, 10H), 2.43-2.79 (m, 2H), 2.80-2.92 (m, 2H), 3.01-3.11 (m, 2H), 3.44-3.62 (m, 1H), 3.62-3.86 (m, 4H), 3.90-4.06 (m, 1H), 4.53-4.94 (m, 3H), 6.97-7.10 (m, 1H), 7.11-7.19 (br d, *J*=7.95 Hz, 2H), 7.22-7.53 (m, 5H), 7.72-7.78 (m, 1H), 8.71-8.79 (m, 1H). ¹³C NMR (CHLOROFORM-*d*, 100 MHz) δ 175.2, 175.0, 154.1, 153.5, 144.7, 144.6, 142.2, 141.4, 139.2, 138.3, 134.6, 132.7, 131.7, 131.0, 130.8, 130.8, 130.7, 130.4, 128.5, 128.3, 128.2, 128.2, 120.0, 119.9, 82.0, 81.9, 77.2, 75.5, 75.3, 54.5, 54.4, 54.1, 53.8, 53.7, 48.4, 48.1, 44.9, 43.9, 43.5, 42.3, 42.1, 41.8, 41.7, 34.8, 33.3, 33.0, 30.9, 29.1, 20.6, 20.5, 14.7, and 14.2.

Synthesis of Photoaffinity Probe JH-7-088



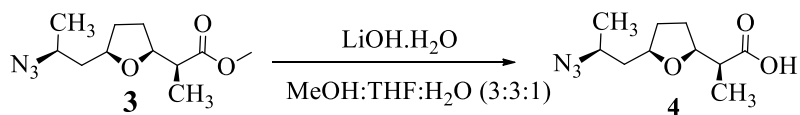
Methyl (S)-2-((2S,5R)-5-((R)-2-(tosyloxy)propyl)tetrahydrofuran-2-yl)propanoate⁹⁴

Methyl nonactate (**1**) (5.4 g, 25 mmol) was dissolved in CH₂Cl₂ (37 mL). Et₃N (7.6 mL, 54.9 mmol) was added to the reaction mixture and cooled to 0 °C, after which *p*-TsCl (10.1 g, 52.4 mmol) and a catalytic amount of DMAP (0.003 g, 0.025 mmol) were added. The solution was stirred for 22 h and allowed to come to room temperature. The reaction mixture was diluted with CH₂Cl₂ (10 mL) and washed with aq. Brine (2 x 20 mL). The organic layer was dried over anhyd. Na₂SO₄ and the solvent was removed by evaporation *in vacuo*. A yellow oil was obtained and purified with column chromatography and eluted with EtOAc/Hexanes (5%-60%) yielding **2** (6.82 g, 74%).



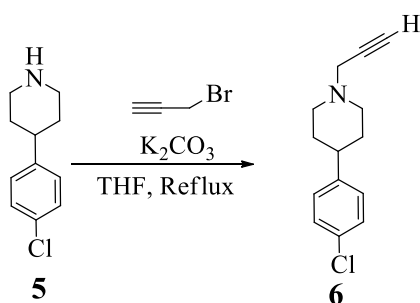
Methyl (S)-2-((2S,5R)-5-((S)-2-azidopropyl)tetrahydrofuran-2-yl)propanoate⁹⁵

Compound **2** (6.8 g, 18.4 mmol) was dissolved in DMF (175 mL) and NaN₃ (6.4, 92.0 mmol) was added to the solution. The reaction was heated at reflux for three h before cooling to room temperature. The reaction mixture was extracted with EtOAc and quenched with H₂O. The organic layer was collected, and the solvent was removed by evaporation *in vacuo* to yield **3** a yellow oil (4.40 g, 99%).



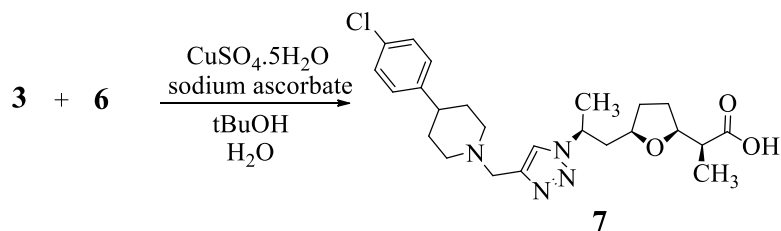
(S)-2-((2S,5R)-5-((S)-2-Azidopropyl)tetrahydrofuran-2-yl)propanoic acid⁸⁵

Crude **4** (2.2 g, 9.1 mmol) was diluted in Et_2N (11 mL) and MeOH (11 mL) to which H_2O (3.8 mL) was added along with $\text{LiOH}\cdot\text{H}_2\text{O}$ (2.1 g, 47.9 mmol) and stirred for 24 h. The reaction mixture was extracted with EtOAc and acidified with aq. 2 M HCl. The organic layer was washed with HCl (aq. 0.5 M, 20 mL) and acidified brine (20 mL) before collected and then dried over anhyd. Na_2SO_4 and the solvent was removed by evaporation *in vacuo* to yield **4** a yellow oil (1.97 g, 95%).



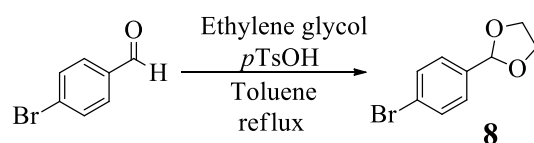
4-(4-Chlorophenyl)-1-(prop-2-yn-1-yl)piperidine⁹²

4-(4-Chlorophenyl)piperidine **5** (0.4 g, 2.0 mmol) was dissolved in THF (20 mL) to which propargyl bromide (80% wt. in toluene, 0.30 mL, 2.6 mmol) was then added. The mixture was wrapped in tin foil and stirred for seven min before the addition of potassium carbonate (0.6 g, 4.1 mmol) and then stirred at room temperature for 2.5 h. The reaction mixture was extracted with EtOAc (20 mL) and washed with aq. 0.5 M NaOH (2 x 10 mL), basified brine (2 x 10 mL), dried over anhyd. Na_2SO_4 and the solvent was removed by evaporation *in vacuo* to yield **6** an orange solid (0.5 g, 18%).



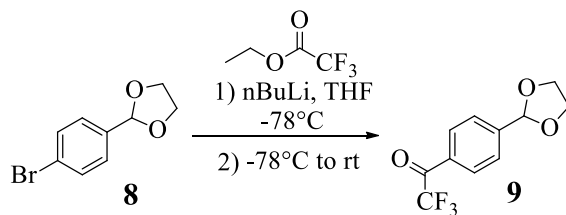
(S)-2-((2S,5R)-5-((S)-2-(4-((4-(4-Chlorophenyl)piperidin-1-yl)methyl)-1H-1,2,3-triazol-1-yl)propyl)tetrahydrofuran-2-yl)propanoic acid⁶

Compound **3** (0.2 g, 0.9 mmol) was dissolved in *t*-BuOH (0.7 mL). Compound **6** (0.2 g, 0.9 mmol) was dissolved in *t*-BuOH (1 mL) and both **3** and **6** were added to a round bottom flask. To the mixture was added H₂O (1.7 mL), CuSO₄·5H₂O (0.03 g, 0.09 mmol) and sodium ascorbate (0.09 g, 0.4 mmol) and the mixture was heated at 40 °C for 23 h. The reaction mixture was diluted with EtOAc (3 mL), then washed with brine (2 x 0 mL) and organic layer was dried over anhyd. Na₂SO₄ and the solvent was removed by evaporation *in vacuo* to yield **7** an orange brown solid. Crude product was purified by reverse phase LC with MeOH/H₂O, to yield a white solid (0.7 g, 18 %).



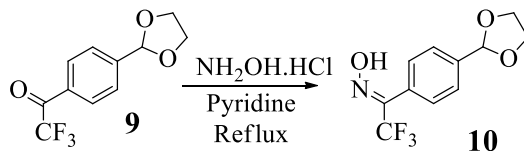
2-(4-Bromophenyl)-1,3-dioxolane⁹⁷

4-Bromobenzaldehyde (24.9 g, 135.1 mmol) was dissolved in toluene (155 mL) to which ethylene glycol (11.5 mL, 202.7 mmol) and *p*-TsOH (0.1747, 0.5 mmol) were added to the reaction mixture and heated at reflux for 30 h. The reaction was quenched with saturated aq. NaHCO₃, washed with brine (2 x 50 mL), then dried over anhyd. Na₂SO₄ and the solvent was removed by evaporation *in vacuo* to yield **8**, a clear oil (30.60 g, 99%). ¹H NMR (400 MHz, CDCl₃-d) δ ppm 4.00-4.16 (m, 4H), 5.78 (s, 1H), 7.36 (d, *J*=8.31 Hz, 2H), 7.52 (d, *J*=8.44 Hz, 2H).



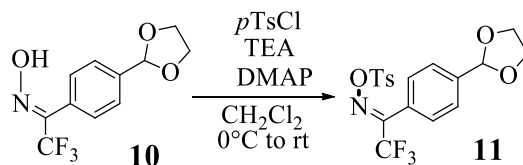
1-(4-(1,3-Dioxolan-2-yl)phenyl)-2,2,2-trifluoroethanone⁹⁷

Compound **8** (4.4 g, 19.3 mmol) was dissolved in THF (90 mL) and cooled to -78°C before *n*-BuLi (2.5 M in hexanes, 9.3 mL, 23.1 mmol) was added and then stirred for 1.5 h. Ethyl trifluoroacetate (3 mL, 25.1 mmol) in THF (5 mL) was added to the mixture and then stirred for 18 h at room temperature. The reaction mixture was quenched with aq. NH_4Cl and diluted with EtOAc (50 mL), washed with water (2 x 25 mL) and brine (2 x 25 mL). The organic layer was dried over anhyd. NaSO_4 and the solvent was removed by evaporation *in vacuo* to yield **9**, a yellow oil (4.7 g, 78%). Compound **9** was used in subsequent step without further purification. ^1H NMR (400 MHz, DMSO-d_6) δ ppm 3.93-4.10 (m, 4H), 5.88 (s, 1H), 7.72 (d, $J=8.31$ Hz, 2H), 8.08 (d, $J=7.95$ Hz, 2H)



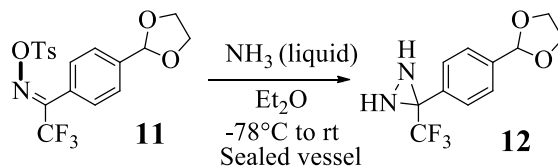
1-(4-(1,3-Dioxolan-2-yl)phenyl)-2,2,2-trifluoroethanone oxime⁹⁸

Compound **9** (4.7 g, 19.3 mmol) was dissolved in pyridine (39 mL), to which hydroxylamine (4.7 g, 57.8 mmol) was added and heated at reflux for two h. The solvent was removed by evaporation *in vacuo* to yield **10**, a crude yellow oil (6.39 g).



1-(4-(1,3-Dioxolan-2-yl)phenyl)-2,2,2-trifluoroethanone *O*-tosyl oxime⁹⁴

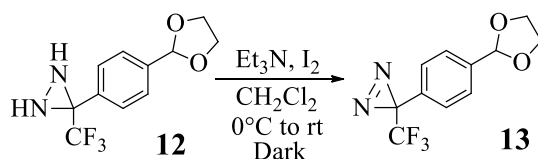
Compound **10** (4.9 g, 18.9 mmol) was dissolved in CH₂Cl₂ (35 mL) and Et₃N (8 mL, 56.7 mmol) was added to the mixture before being cooled to 0 °C. *p*TsCl (7.4 g, 37.8 mmol) and a catalytic amount of DMAP (0.002 g, 0.0025 mmol) were added to the mixture and after 1.5 h the reaction mixture was concentration by evaporation *in vacuo* to near dryness and diluted with EtOAc and washed with H₂O (25 mL), aq. brine (25 mL) and the organic layer was dried over anhyd. Na₂SO₄ and then concentrated again by evaporation *in vacuo*. The crude reaction was purified by column chromatography and eluted with EtOAc/Hexanes (2.5%-10%) to yield **11**, a yellow solid (3.7 g, 47%). ¹H NMR (400 MHz, CDCl₃-d) δ ppm 2.45-2.56 (m, 3H), 4.01-4.20 (m, 4H), 5.79-5.90 (m, 1H), 7.30-8.03 (m, 8H)



3-(4-(1,3-dioxolan-2-yl)phenyl)-3-(trifluoromethyl)diaziridine⁹⁹

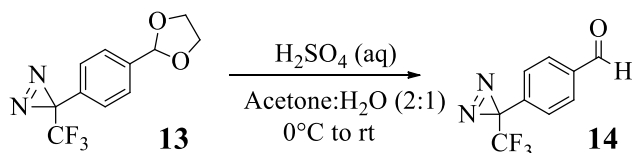
Compound **11** (2.7 g, 8.8 mmol) was dissolved in Et₂O (10 mL) and cooled to -78 °C. Liquid ammonia (30 mL) was added to the flask and then stirred for 30 m at -78 °C, 1.5 h at 0 °C and cooled back to -78 °C. The flask was then opened to allow the ammonia to slowly evaporate. The mixture was diluted with Et₂O (10 mL) and H₂O (10 mL), then washed with H₂O (10 mL), aq. brine (10 mL) and the organic layer was dried over anhyd. NaSO₄ and then the solvent was removed by evaporation *in vacuo* to yield **12**, a yellow orange powder (1.7 g, 74% yield). ¹H

NMR (500 MHz, CDCl₃-d) δ ppm 2.19-2.25 (d, $J=8.80$ Hz, 1H), 2.78-2.84 (d, $J=8.31$ Hz, 1H), 4.03-4.16 (m, 4H), 5.85 (s, 1H), 7.51-7.60 (d, $J=8.31$ Hz, 2H), 7.62-7.73 (d, $J=8.31$ Hz, 2H).



3-(4-(1,3-Dioxolan-2-yl)phenyl)-3-(trifluoromethyl)-3H-diazirine⁹⁹

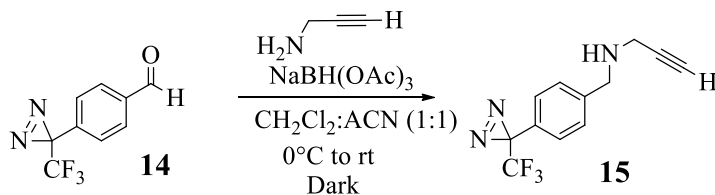
Compound **12** (0.8 g, 2.9 mmol) was diluted in CH₂Cl₂ (8 mL) with Et₃N (0.9 mL, 5.8 mmol), wrapped in tin foil and cooled to 0 °C. Iodine (0.9 g, 3.2 mol) was added to the reaction and then stirred for ten min before being brought to room temperature and allowed to react for 24 h. The reaction was quenched with aq. NaHCO₃ and extracted into CH₂Cl₂. The organic layer was washed with CH₂Cl₂ (10 mL), aq. 1 M NaOH (10 mL), H₂O (10 mL) and brine (10 mL) before being dried over anhyd. Na₂SO₄ and the solvent was removed by evaporation *in vacuo* to yield a yellow powder. The crude product was purified with column chromatography and eluted with EtOAc/Hexanes (5%-20%) to yield **13** (0.778 g). ¹H NMR (500 MHz, CDCl₃-d) δ ppm 4.02-4.14 (m, 4H), 5.83 (s, 1H), 7.19-7.28 (d, $J=7.83$ Hz, 2H), 7.53 (d, $J=8.31$ Hz, 2H). ¹³C NMR (CDCl₃-d, 100 MHz) δ 139.7, 129.9, 126.9, 126.5, 123.4, 120.7, 102.8, and 65.3



4-(3-(trifluoromethyl)-3H-diazirin-3-yl)benzaldehyde¹⁰⁰

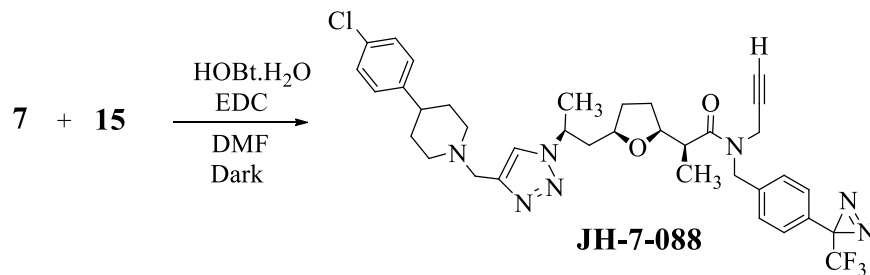
Compound **14** (0.8 g, 3.0 mmol) was dissolved in acetone (24 mL) and H₂O (12 mL) and then cooled to 0 °C, to which aq. sulfuric acid (0.5 M, 30 mL) was added slowly, brought to room temperature and stirred for 18 h in the dark. The reaction was quenched with saturated NaHCO₃ and extracted with CH₂Cl₂. The organic layer was washed with brine (20 mL) and dried over

anhyd. Na₂SO₄. The solvent was removed by evaporation *in vacuo* to yield **14**, a yellow oil (0.36 g, 80%). ¹H NMR (500 MHz, CDCl₃-d) δ ppm 7.34-7.38 (d, *J*=8.31 Hz, 2H), 7.90-7.95 (d, *J*=8.31 Hz, 2H), 10.05 (s, 1H).



N-(4-(3-(Trifluoromethyl)-3H-diazirin-3-yl)benzyl)prop-2-yn-1-amine ¹⁰¹

Compound **14** (0.2 g, 0.9 mmol) was dissolved in CH₂Cl₂ (0.95 mL) and acetonitrile (0.95 mL). Propargylamine (0.18 g, 2.8 mmol) was added to the mixture and cooled to 0 °C and then stirred for 15 min before NaB(OAc)₃ (0.6 g, 2.8 mmol) was added. The mixture was stirred for 24 h in the dark before being diluted with EtOAc (5 mL) and quenched with H₂O (5 mL). The organic layer was washed with H₂O (2 x 5 mL), saturated NaHCO₃ (2 x 5 mL), brine (5 mL) and then dried over anhyd. Na₂SO₄ and then concentrated by evaporation *in vacuo*. The crude product was purified with column chromatography and eluted with EtOAc/Hexanes (5%-25%) to yield **15**, a yellow oil (0.12 g, 51%). ¹H NMR (500 MHz, CDCl₃-d) δ ppm 2.27 (t, *J*=2.45 Hz, 1H), 3.41 (d, *J*=2.45 Hz, 2H), 3.91 (s, 2H), 7.17 (d, *J*=8.31 Hz, 2H), 7.36-7.44 (d, *J*=8.80 Hz, 2H).

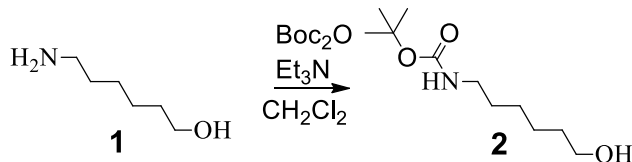


(S)-2-((2S,5R)-5-((S)-2-(4-((4-(4-Chlorophenyl)piperidin-1-yl)methyl)-1H-1,2,3-triazol-1-yl)propyl)tetrahydrofuran-2-yl)-N-(prop-2-yn-1-yl)-N-(4-(3-(trifluoromethyl)-3H-diazirin-3-yl)benzyl)propanamide ¹⁰²

Compound **7** (0.07 g, 0.12 mmol) was dissolved in DMF (0.4 mL) and cooled to 0 °C, after which HOBt hydrate (0.033 g, 0.18 mmol) and EDC (0.04 g, 0.18 mmol) were added.

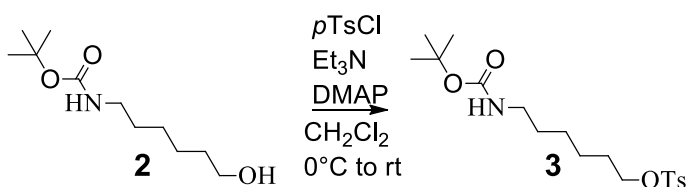
Compound **15** (0.04 g, 0.14 mmol) was dissolved in DMF (0.3 mL) and added to the reaction and then stirred for 18 h in the dark. The reaction was diluted with EtOAc (10 mL) and quenched with H₂O (2 mL). The organic layer was washed with H₂O (2 x 10 mL), brine (10 mL), and then dried over anhyd. Na₂SO₄ and the solvent was removed by evaporation *in vacuo*. The crude product was purified by column chromatography and eluted with EtOAc/Hexanes (25%-100%) to yield **JH-7-088**, white crystals (0.23 g, 22 %). ¹H NMR (400 MHz, CDCl₃-d) δ ppm 0.77-1.21 (m, 5H), 1.22-1.32 (br s, 2H), 1.41-1.65 (m, 5H), 1.74-1.86 (br s, 3H), 1.88-2.35 (m, 6H), 2.43-2.56 (br s, 1H), 2.60-2.97 (m, 1H), 3.04-3.17 (m, 2H), 3.70-3.87 (m, 3H), 3.96-4.07 (m, 1H), 4.18-4.33 (m, 1H), 4.35-4.43 (br d, *J*=16.26 Hz, 1H), 4.62-5.15 (m, 2H), 7.08-7.22 (m, 4H), 7.23-7.29 (m, 2H), 7.29-7.37 (m, 2H). ¹³C NMR (CDCl₃-d, 100 MHz) δ 175.2, 144.5, 139.2, 138.7, 131.8, 128.5, 128.5, 128.5, 128.2, 128.1, 127.1, 126.9, 126.6, 123.5, 120.7, 120.2, 82.3, 81.9, 78.8, 78.7, 75.4, 75.4, 72.9, 72.2, 54.6, 54.4, 54.0, 53.9, 53.6, 49.6, 48.4, 43.8, 43.6, 41.9, 41.7, 37.0, 34.7, 33.1, 31.0, 30.9, 29.7, 29.2, 29.0, 28.9, 28.5, 28.1, 27.7, 20.7, 20.2, 14.5, and 14.4

Synthesis of Tag



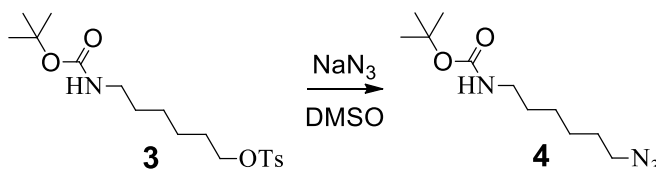
6-Hydroxyhexyl tert-butylcarbamate⁹⁸

6-Amino-1-hexanol **1** (2 g, 17 mmol) was dissolved in CH₂Cl₂ (30 mL). Boc₂O anhydride (3.9 g, 17 mmol) was dissolved in CH₂Cl₂ (20 mL) and Et₃N (2.6 mL, 18.9 mmol) were then added to the reaction mixture and reacted for 3 h. The mixture was concentration *in vacuo* to yield **2** a brown oil (3.7 g, 99%).



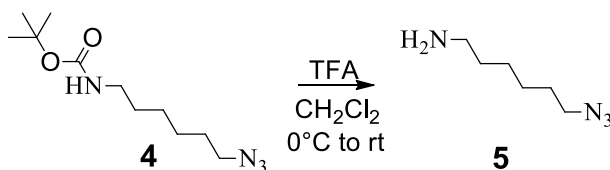
6-((tert-Butoxycarbonyl)amino)hexyl 4-methylbenzenesulfonate⁹⁴

Crude **2** (3.7 g, 17.1 mmol) was dissolved in CH₂Cl₂ (25 mL), and Et₃N (3.1 mL, 25.6 mmol) at 0 °C, then *p*-TsCl (4 g, 20.5 mmol) and a crystal DMAP were added to the solution. After stirring for 18 h at room temperature, the reaction was diluted with CH₂Cl₂ and washed by brine (25 mL), and then extracted with CH₂Cl₂ (25 mL) and washed once more with brine (25 mL) before the organic layer was dried over anhyd. Na₂SO₄ and the solvent was removed by evaporation *in vacuo* to yield **3** a brown oil (6.41 g, 100%).



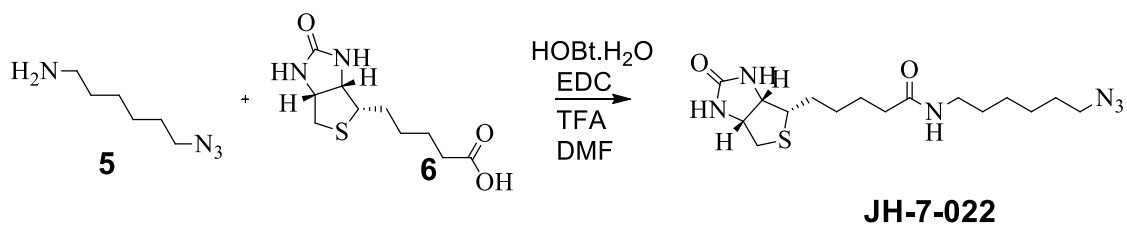
***tert*-Butyl (6-azidoxyhexyl)carbamate**⁹⁵

Compound **3** (6.3 g, 17.1 mmol) was dissolved in DMSO (150 mL), then NaN₃ (5.9 g, 85.3 mmol) was added and then stirred for 3 h. The reaction mixture was diluted with EtOAc, washed with water (3 x 50 mL), brine (50 mL), and then dried over anhyd. NaSO₄. The solvent was removed by evaporation *in vacuo*. The crude product was purified by column chromatography and eluted with EtOAc/Hexanes (10%-50%) to yield **4** a clear oil (0.77 g, 19%).
¹H NMR (400 MHz, CDCl₃-d) δ ppm 1.31-1.54 (m, 15H), 1.56-1.65 (quin, *J*=7.00 Hz, 2H), 3.07-3.17 (br t, *J*=6.05 Hz, 2H), 3.23-3.31 (t, *J*=6.91 Hz, 2H), 4.39-4.66 (br s, 1H).



6-Azidohexan-1-amine¹⁰³

Compound **4** (0.76 g, 3.1 mmol) was dissolved in CH₂Cl₂ and cooled to 0 °C, and then TFA (1.5 mL) was added and brought to room temperature and finally stirred for an additional hour. The reaction mixture was diluted with CH₂Cl₂ and then quenched with aq. 1 M NaOH to yield **5** a light brown oil (0.4 g, 89%).
¹H NMR (400 MHz, CDCl₃-d) δ ppm 1.20-1.52 (m, 8H), 1.54-1.67 (quin, *J*=6.85 Hz, 2H), 2.65-2.75 (t, *J*=6.85 Hz, 2H), 3.23-3.31 (t, *J*=6.85 Hz, 2H).



***N*-(6-Azidoethyl)-5-((3a*S*,4*S*,6a*R*)-2-oxohexahydro-1*H*-thieno[3,4-*d*]imidazol-4-yl)pentanamide**¹⁰⁴

Biotin **6** (0.3 g, 1.22 mmol) was dissolved in DMF (2mL), then HOBt·H₂O (0.24 g, 1.22 mmol) and EDC (0.29 g, 1.47 mmol) were added and stirred for 5 min before the addition of **5** (0.23 g, 1.6 mmol) and stirred for an additional 24 h. The reaction was diluted with EtOAc and H₂O and washed with H₂O (10 mL), brine (10 mL) and then dried over anhyd. NaSO₄. The solvent was removed by evaporation *in vacuo* and the crude product was purified with column chromatography and eluted with EtOAc/Hexanes (25%-100%) to yield **JH-7-022** a white solid (.025 g, 5.5%). ¹H NMR (400 MHz, CDCl₃-*d*) δ ppm 1.28-1.86 (m, 15H), 2.18-2.37 (t, *J*=7.27 Hz, 2H), 2.74-2.83 (d, *J*=12.84 Hz, 1H), 2.88-2.97 (dd, *J*=4.65, 12.84 Hz, 1H), 3.12-3.35 (m, 5H), 4.24-4.42 (m, 1H), 4.50-4.64 (m, 1H), 5.48-5.92 (br s, 1H), 6.34-6.73 (br s, 1H). ¹³C NMR (CDCl₃-*d*, 100 MHz) δ 173.6, 163.9, 61.9, 60.4, 55.5, 51.3, 40.5, 39.6, 35.7, 29.4, 28.7, 28.0, 28.0, 26.5, 26.4, and 25.7

Appendix A: Supplementary Information

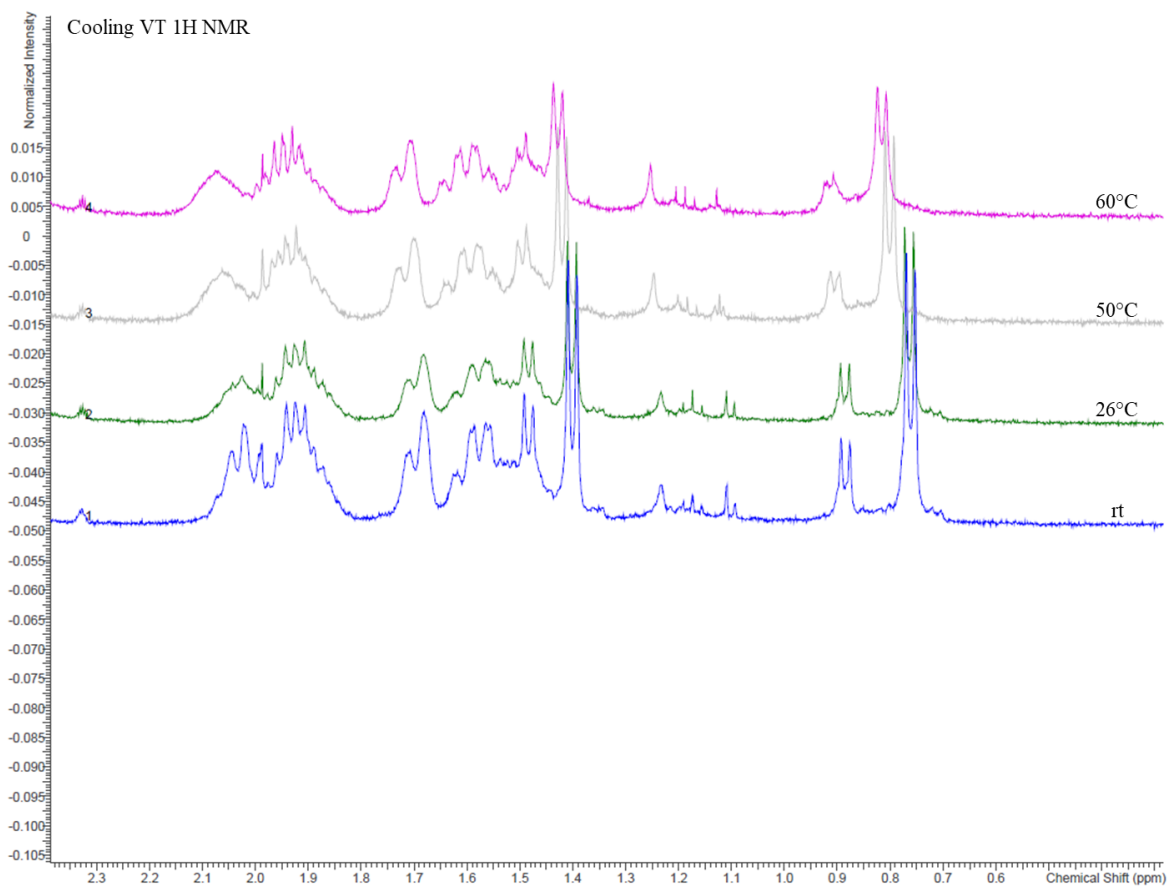


Figure 1: Observed cooling of 31G12 variable temperature ^1H NMR in DMSO-d_6 .

Figure 2: Multiple sequence alignment using CLUSTAL O (1.2.4) of *S.aureus* 13709 WT and drug -resistant strains TNZB and TZNP for all transformed mutants with indicated amino acid changes.

CLUSTAL O(1.2.4) multiple sequence alignment

Ribosomal Protein L11 Methyltransferase

```

WT      MNWTELSIIINHEAVELATNILENHGSNGVVIEDSDDLINQPEDKYGEIYALKKEDYDPK  60
TZNB    MNWTELSIIINHEAVELATNILENHGSNGVVIEDSDDLINQPEDKYGEIYALKKEDYDPK  60
TZNP    MNWTELSIIINHEAVELATNILENHGSNGVVIEDSYDLINQPEDKYGEIYALKKEDYDPK  60
*****

WT      GVRLKAYFNEMTYDDKLRQRIKDELLNLDDELQQNVQFSEQIIAETDWENEWKNYFHPFR  120
TZNB    GVRLKAYFNEMTYDDKLRQRIKDELLNLDDELQQNVQFSEQIIAETDWENEWKNYFHPFR  120
TZNP    GVRLKAYFNELTYDDKLRQRIKDELLNLDDELQHNQVQFSEQIIAETDWENEWKNYFHPFR  120
*****

WT      ASKKFTIVPSWETYAKEADEELCIELDPGMAFGTGDHPTTSMCLKAIETYVLPQHVIDV  180
TZNB    ASKKFTIVPSWETYAKEADEELCIELDPGMAFGTGDHPTTSMCLKAIETYVLPQHVIDV  180
TZNP    ASKKFTIVPSWETYAKEADEELCIELDPGMAFGTGDHPTTSMCLKAIETYVLPQHVIDV  180
*****

WT      GTGSGILSIASHLIGVKRIKALDIDEMAVSVAKENFRRNHCETLIEAVPGNLLKDETEKF  240
TZNB    GTGSGILSIASHLIGVKRIKALDIDEMAVSVAKENFRRNHCETLIEAVPGNLLKDETEKF  240
TZNP    GTGSGILSIASYLIGVKRIKALDIDEMAVSVAKENFRRNHCETLIEAVPGNLLKDETEKF  240
*****

WT      DIVIANILAHIIDEMIEDAYNTLNIEGGYFITSGIIKEKYEGIQSHMERVGFKIISEQHDN  300
TZNB    DIVIANILAHIIDEMIEDAYNTLNIEGGYFITSGIIKEKYEGIQSHMERVGFKIISEQHDN  300
TZNP    DIVIANILAHIIDEMIDDAYNTLNIEGGYFITSGIIKEKYEGIQSHMERVGFKIISEQHDN  300
*****

WT      GWVCLVGQKVSE  312
TZNB    GWVCLVGQKVSE  312
TZNP    GWVCLVGQKVSE  312
*****

```

TZNB – no mutations

TZNP – D36Y, M71L, Q94H, H193Y, E257D

CLUSTAL O(1.2.4) multiple sequence alignment

Transcriptional regulator, LysR family

```
WT      MNLDWYYTFVILAKTLNRYLASEEINLTIPSIHKQIKNLEQHLNVKLFETYKNQIILTED 60
TZNB    MNLDWYYTFVILAKTLNRYLASEEINLTIPSIHKQIKNLEQHLNVKLFETYKNQIILTED 60
TZNP    MNLDWYYTFVILAKTLNRYLASEEINLTIPSIHKQIKNLEQHLNVKLFETYKNQIILTED 60
        *****

WT      GHTFLPIAQSFIEQYESGIKHIQLKKTMFQSKLNVVSSYIATFIMPKFLKSFFNEHPFI 120
TZNB    GHTFLPIAQSFIEQYESGIKHIQLKKTMFQSKLNVVSSYIATFIMPKFLKSFFNEHPFI 120
TZNP    GHTFLPIAQSFIEQYESGIKHIQLKKTMFQSKLNVVSSYIATFIMPKFLKSFFNEHPFI 120
        *****

WT      DVSLHVKNENIEKDINNHTYDIGISRNQPKLREHVHSEKVCEGKIVLIAPNKENNHLLEA 180
TZNB    DVSLHVKNENIEKDINNHTYDIGISRNQPKLREHVHSEKVCEGKIVLIAPNKENNHLLEA 180
TZNP    DVSLHVKNENIEKDINNHTYDIGISRNQPKLREHVHSEKVCEGKIVLIAPNKENNHLLEA 180
        *****

WT      PLFEKYKIIISDNHPEYWSSLKNNILNIYEKAQFLSINDVHTSIKLIEMNQGISFLPIYIT 240
TZNB    PLFEKYKIIISDNHPEYWSSLKNNILNIYEKAQFLSINDVHTSIKLIEMNQGISFLPIYIT 240
TZNP    SLFEKYKIIISDNHPEYWSSLKNNILNIYEKAQFLSINDVHTSIKLIEMNQGISFLPIYIT 240
        *****

WT      TNSDYNISVINTKILQAPISFTYIYSKKESPEILAFIKSFKKYIANEQL 289
TZNB    TNSDYNISVINTKILQAPISFTYIYSKKESPEILAFIKSFKKYIANEQL 289
TZNP    KNSNYNISVINTKILQAPISFTYIYSKKENPEILAFIKSFKKYIANEQL 289
        .**.:*****.*****.
```

TZNB – none

TZNP – P181S, T241K, D244N, S270N

Transcriptional regulator, LysR family

CLUSTAL O(1.2.4) multiple sequence alignment

```
WT   MDSLKVLTEVVKTSFTKAAENLYTSQPSISRDIKRLELEYDVKIFEFRHSKMSLTS DGE 60
TZNB MDSLKVLTEVVKTSFTKAAENLYTSQPSISRDIKRLELEYDVKIFEFRHSKMSLTS DGE 60
*****

WT   KLFQYALQRRERLEQNLRHDLKMQPDIISGDLTIGSSYTYGEYRLSQHLADLAKNYPELYI 120
TZNB KLFQYALQRRERLEQNLRHDLKMQPDIISGDLTIGSSYTYGEYRLSQHLADLAKNYPELYI 120
*****

WT   HVYLNNSDTVLQHIKNNNTIDLGIIEKEVQSNIH SRRIAQDEIVLIRKKSSSSNK SICFI 180
TZNB HVYLNNSDTVLQHIKNNNTIDLGIIEKEVQSNIH SRRIAQDEIVLIRKKSSSSNK SICFI 180
*****

WT   RERGS GTRVYQENALSQMTSSSYLVEINNTNLIK NMVHADKGF SIVSKSTLTPYDLEKLE 240
TZNB RERGS GTRVYQENALSQMTSSSYLVEINNTNLIK NMVHADKGF SIVSKSTLTPYDLEKLE 240
*****

WT   VTNLDIKRYFYLVIHKDKYIDTKLNEVIK N LIS 273
TZNB VTNLDIKRYFYLVIHKDKYIDTKLNEVIK N LIS 273
*****
```

TZNB – no mutations

Lead, cadmium, zinc and mercury transporting ATPase (1)

WT MANTKKTTLDITGMTCAACSNRIEKKLNKLDVNAQVNLTTTEKATVEYNPDQHDVQEFIN 60
TZNB MANTKKTTLDITGMTCAACSNRIEKKLNKLDVNAQVNLTTTEKATVEYNPDQHDVQEFIN 60
TZNP MANTKKTTLDITGMTCAACSNRIEKKLNKLDVNAQVNLTTTEKATVEYNPDQHDVQEFIN 60

WT TIQHLGYGVAVETVELDITGMTCAACSSRIEKVLNKMMDGVQONATVNLTTTEQAKVDYYPEE 120
TZNB TIQHLGYGVAVETVELDITGMTCAACSSRIEKVLNKMMDGVQONATVNLTTTEQAKVDYYPEE 120
TZNP TIQHLGYGVAVETVELDITGMTCAACSSRIEKVLNKMMDGVQONATVNLTTTEQAKVDYYPEE 120

WT TDADKLVTRIQLKGYDASIKDNNKDQTSRKAALQHKLIKLIISAVLSLPLLMLMFVHLF 180
TZNB TDADKLVTRIQLKGYDASIKDNNKDQTSRKAALQHKLIKLIISAVLSLPLLMLMFVHLF 180
TZNP TDADKLVTRIQLKGYDASIKDNNRDQTSRKAALQHKLIKLIISAVLSLPLLMLMFVHLF 180
*****:*****

WT NMHIPALFTNPWFQFILATPVQFIIGWQFYVYGAYKNLRNGGANMDVLA VGTSAAYFYSI 240
TZNB NMHIPALFTNPWFQFILATPVQFIIGWQFYVYGAYKNLRNGGANMDVLA VGTSAAYFYSI 240
TZNP NMHIPALFTNPWFQFILATPVQFIIGWQFYVYGAYKNLRNGGANMDVLA VGTSAAYFYSI 240

WT YEMVRWLNSTTQPHLYFETSAVLITLILFGKYLEARAKSQTTNALGELLSSLQAKEARIL 300
TZNB YEMVRWLNSTTQPHLYFETSAVLITLILFGKYLEARAKSQTTNALGELLSSLQAKEARIL 300
TZNP YEMVRWLNSTTQPHLYFETSAVLITLILFGKYLEARAKSQTTNALGELLSSLQAKEARIL 300

WT KDGNEVMIPLNEVHIGNTLIVKPGEKIPVDGKI IKGMTAIDESMLTGESIPVEKNVDDTV 360
TZNB KDGNEVMIPLNEVHIGNTLIVKPGEKIPVDGKI IKGMTAIDESMLTGESIPVEKNVDDTV 360
TZNP KDGNEVMIPLNEVHVGDTLIVKPGEKIPVDGKI IKGMTAIDESMLTGESIPVEKNVDDTV 360
*****:*****

WT IGSTMNKNGTITMTATKVGDTALANI I KVVVEEAQSSKAPIQRLADIISGYFVPIVVGIA 420
TZNB IGSTMNKNGTITMTATKVGDTALANI I KVVVEEAQSSKAPIQRLADIISGYFVPIVVGIA 420
TZNP IGSTMNKNGTITMTATKVGDTALANI I KVVVEEAQSSKAPIQRLADIISGYFVPIVVGIA 420

WT LLTFIVWITLVTPGTFEPALVASISVLVIACPCALGLATPTSIMVGTGRAAENGILFKGG 480
TZNB LLTFIVWITLVTPGTFEPALVASISVLVIACPCALGLATPTSIMVGTGRAAENGILFKGG 480
TZNP LLTFIVWITLVTPGTFEPALVASISVLVIACPCALGLATPTSIMVGTGRAAENGILFKGG 480

WT EFVERTHQIDTIVLDKGTITNGRPVVTDYHGDDQTLQLLATAEKDSEHPLAEAI VNYAK 540
TZNB EFVERTHQIDTIVLDKGTITNGRPVVTDYHGDDQTLQLLATAEKDSEHPLAEAI VNYAK 540
TZNP EFVERTHQIDTIVLDKGTITNGCPVVTDYHGDDQTLQLLATAEKDSEHPLAEAI VNYAK 540

WT EKQLTLTETTTFKAVPGHGIEATIDHHHILVGNRKL VADNDISLPKHISDDLTHYERD GK 600
TZNB EKQLTLTETTTFKAVPGHGIEATIDHHHILVGNRKL VADNDISLPKHISDDLTHYERD GK 600
TZNP EKQLTLTETTTFKAVPGHGIEATIDHHHILVGNRKL M ADNDISLPKHISDDLTHYERD GK 600
*****:*****

WT TAMLIAVNYSLTGIIAVADTVKD HAKDAIKQLHDMGIEVAMLTGDNKSTAQAIAKQV GID 660
TZNB TAMLIAVNYSLTGIIAVADTVKD HAKDAIKQLHDMGIEVAMLTGDNKSTAQAIAKQV GID 660
TZNP TAMLIAVNYSLTGIIAVADTVKD HAKDAIKQLHDMGIEVAMLTGDNKNTAQAIAKQV GID 660
*****.*****

WT TVIADILPEEKAAQIAKLQQQGKKVAMVGDGVNDAPALVKADIGIAIGTGTEVAIEAADI 720
TZNB TVIADILPEEKAAQIAKLQQQGKKVAMVGDGVNDAPALVKADIGIAIGTGTEVAIEAADI 720
TZNP TVIADILPEEKAAQITKLQQQGKKVAMVGDGVNDAPALVKADIGIAIGTGTEVAIEAADI 720
*****:*****

WT TILGGDLMLIPKAIYASKATIRNIRQNLFWAFGYNIAGIPIAALGLLAPWVAGAAMALSS 780
TZNB TILGGDLMLIPKAIYASKATIRNIRQNLFWAFGYNIAGIPIAALGLLAPWVAGAAMALSS 780
TZNP TILGGDLMLIPKAIYASKATIRNIRQNLFWAFGYNIAGIPIAALGLLAPWVAGAAMALSS 780

WT VSVVTNALRLKMRLEPRRKDA 802
TZNB VSVVTNALRLKMRLEPRRKDA 802
TZNP VSVVTNALRLKMRLEPRRKDA 802

TZNB – no mutation
TZNP – K144R, I315V, N317D, R504C, V577M, S648N, A676T

Lead, cadmium, zinc and mercury transporting ATPase (2)

WT MSNNKKHQHEHHSHQEHEHNTSHGNHEHHHHGNGFKSKFFISLIFAIPIIILSPMMGVKL 60
TZNB MSNNKKHQHEHHSHQEHEHNTSHGNHEHHHHGNGFKSKFFISLIFAIPIIILSPMMGVKL 60

WT PFQISFTGSDWIVLILATILFFYGGKPFSLGAKDEISTKKPGMMLVALGISVAYIISLY 120
TZNB PFQISFTGSDWIVLILATILFFYGGKPFSLGAKDEISTKKPGMMLVALGISVAYIISLY 120

WT AFYMNNSFGSSSTHTMDFWELATLILIMLLGHWIEMNAVGNAGNALKKMAELLNPNTAVKL 180
TZNB AFYMNNSFGSSSTHTMDFWELATLILIMLLGHWIEMNAVGNAGNALKKMAELLNPNTAVKL 180

WT IDNNQREEVKISDIHIDDIVEVRAGESIPTDGIIVQGETSIDESLVTGESKVKVHKTHND 240
TZNB IDNNQREEVKISDIHIDDIVEVRAGESIPTDGIIVQGETSIDESLVTGESKVKVHKTHND 240

WT VIGGSINGSGTVQVKVTATGENGYLSQVMGLVNAQNDKSKAELLSDKVAGYLFYFAVSI 300
TZNB VIGGSINGSGTVQVKVTATGENGYLSQVMGLVNAQNDKSKAELLSDKVAGYLFYFAVSI 300

WT GLISFIVWMLIQNNVDFALERLVTVLVIACPHALGLAIPLVSTARSTSIGAHNGLIIKNRE 360
TZNB GLISFIVWMLIQNNVDFALERLVTVLVIACPHALGLAIPLVSTARSTSIGAHNGLIIKNRE 360

WT SVEIAQHIDYIMMDKTGTLTEGNFSVNHYESFTDELNNEEILSLFASLESNSNHPLATGI 420
TZNB SVEIAQHIDYIMMDKTGTLTEGNFSVNHYESFTDELNNEEILSLFASLESNSNHPLATGI 420

WT VDFAKGKNISYATPQEVNIPGVGLEGTVDNKKLKIVNVSYLDKSNFDYNKEQFTNLAQQ 480
TZNB VDFAKGKNISYATPQEVNIPGVGLEGTVDNKKLKIVNVSYLDKSNFDYNKEQFTNLAQQ 480

WT GNSISYLIHDRQVIGIIAQGDKIKESSQMVSDDLRSNITPVMLTGDNKEVAQTVAEELG 540
TZNB GNSISYLIHDRQVIGIIAQGDKIKESSQMVSDDLRSNITPVMLTGDNKEVAQTVAEELG 540

WT ISDVHAQLMPEDKESIIQDYQSNQSKIMMVG DGINDAPSLIRADIGMAIGAGTDVAIESG 600
TZNB ISDVHAQLMPEDKESIIQDYQSNQSKIMMVG DGINDAPSLIRADIGMAIGAGTDVAIESG 600

WT DVILVKSNSPDIINFLSLSKNTMCKMVQNLWWGAGYNVIAVPLAAGILASIGLILSPAVG 660
TZNB DVILVKSNSPDIINFLSLSKNTMCKMVQNLWWGAGYNVIAVPLAAGILASIGLILSPAVG 660

WT AILMSLSTIIIVAINAFTLKLK 681
TZNB AILMSLSTIIIVAINAFTLKLK 681

TZNB – no mutation

Phosphoserine phosphatase (based on bioinformatics)

WT MKKILFDVDGVFLSEERCFDVSALTVYELLMDKCYLGLHSHIDWETLTDNDIQDIRNRIF 60
TZNB MKKILFDVDGVFLSEERCFDVSALTVYELLMDKCYLGLHSHIDWETLTDNDIQDIRNRIF 60
TZNP MKKILFDVDGVFLSEERCFDVSALTVYELLMDKCYLGLHSHIDWETLTDNDIQDIRNRIF 60

WT QKDKILNKLSLGLNSNWDMLFIVFSIHLIDILKKLSDHDEIEAFMYQDKPVELKLNIST 120
TZNB QKDKILNKLSLGLNSNWDMLFIVFSIHLIDILKKLSDHDEIEAFMYQDKPVELKLNIST 120
TZNP QKDKILNKLSLGLNSNWDMLFIVFSIHLIDILKKLSDHDEIEAFMYRDEPVELKLNIST 120
*****:*.*****

WT NLADRFNLNEQLPLQFLDNVKGKNNIYAALAEFAITELHVSDATLFLSLKGALWTLAQEV 180
TZNB NLADRFNLNEQLPLQFLDNVKGKNNIYAALAEFAITELHVSDATLFLSLKGALWTLAQEV 180
TZNP NIADRFNLNEQLPLQFLDNVKGKNNIYAALAEFATTELHVSDANLFLSLKGALWTLAQEV 180
*:.*****.*****

WT YQEWYLGSKLYEEVEKKIARTTFKTYIYQEIILRPVDEVKVLNLDLKGAGFELGIATGR 240
TZNB YQEWYLGSKLYEEVEKKIARTTFKTYIYQEIILRPVDEVKVLNLDLKGAGFELGIATGR 240
TZNP YQEWYLGSKLYEEVEKKIARTTFKTYIYQEIILRPVDEVKVLNLDLKGAGFELGIATGR 240

WT PYTETVVPFENLGLLPYFEADFIATASDVLEAENMYPQARPLGKPNPFSYIAALYGNRND 300
TZNB PYTETVVPFENLGLLPYFEADFIATASDVLEAENMYPQARPLGKPNPFSYIAALYGNRND 300
TZNP PYTETVVPFENLGLLPYFEADFIATASDVLEAENMYPQARPLGKPNPFSYIAALNGNKRND 300
***** **:*

WT KYESYINKQDNIVNKDDVFIVGDSLADLLSAQKIGATFIGTTLTGLKGDAAASELEAHHAD 360
TZNB KYESYINKQDNIVNKDDVFIVGDSLADLLSAQK----- 333
TZNP KYESYINKQDNIVNKDDVFIVGDSLADLLSAQKIGATFIGTLSGLKGDAAAGELEAHHAD 360

WT YVINHLGELRGVLDNL 376
TZNB -----
TZNP YVINHLGELRGVLDN- 375

TZNB – I334*

TZNP – 107R, K109E, L122I, I156T, T165N, Y295N, N298K, L376*

Phosphoserine Phosphatase Clone Alignment

WT MKKILFDVDGVFLSEERCFDVSALTYEELLMDKCYLGLHSHIDWETLTDNDIQDIRNRIF 60
TZNB MKKILFDVDGVFLSEERCFDVSALTYEELLMDKCYLGLHSHIDWETLTDNDIQDIRNRIF 60

WT QKDKILNKLSLGLNSNWDMLFIVFSIHLIDILKKLSHDEIEAFMYQDKPVELKLQONIST 120
TZNB QKDKILNKLSLGLNSNWDMLFIVFSIHLIDILKKLSHDEIEAFMYQDKPVELKLQONIST 120

WT NLADRFNLNEQLPLQFLDNVKGKNNIYAALEEFATELHVSDATLFLSLK GALWTLAQEV 180
TZNB NLADRFNLNEQLPLQFLDNVKGKNNIYAALEEFATELHVSDATLFLSLK GALWTLAQEV 180

WT YQEWYLGSKLYEEVEKKIARTTFKTYIYQEIILRPVDEVKVLNNDLKGAGFELGIATGR 240
TZNB YQEWYLGSKLYEEVEKKIARTTFKTYIYQEIILRPVDEVKVLNNDLKGAGFELGIATGR 240

WT PYTETVVPFENLGLLPYFEADFIATASDVLEAENMYPQARPLGKPNPFSYIAALYGNRND 300
TZNB PYTETVVPFENLGLLPYFEADFIATASDVLEAENMYPQARPLGKPNPFSYIAALYGNRND 300

WT KYESYINKQDNIVNKDDVFIVGDSLADLLSAQKIGATFIGTLTGLKGKDAASELEAHHAD 360
TZNB KYESYINKQDNIVNKDDVFIVGDSLADLLSAQKIGATFIG----- 340

WT YVINHLGELRGVLDNL 376
TZNB -----

TZNB - T341*

DNA-directed RNA Polymerase alpha subunit

WT MIEIEKPRIETIEISEDAKFGKFFVEPLERGYGTTLGNSLRRILLSSLPAAVKYIEIEG 60
TZNB MIEIEKPRIETIEISEDAKFGKFFVEPLERGYGTTLGNSLRRILLSSLPAAVKYIEIEG 60
TZNP MIEIEKPRIETIEISEDAKFGKFFVEPLERGYGTTLGNSLRRILLSSLPAAVKYIEIEG 60

WT VLHEFSAVDNVVEDVSTIIMNIKQLALKIYSEEDKTLEIDVRDEGEVTASDITHSDVEI 120
TZNB VLHEFSAVDNVVEDVSTIIMNIKQLALKIYSEEDKTLEIDVRDEGEVTASDITHSDVEI 120
TZNP VLHEFSAVDNVVEDVSTIIMNIKQLALKIYSEEDKTLEIDVRDEGEVTASDITHSDVEI 120

WT LNPELKIATVSKGGHLKIRLVANKGRGYALAEQNNTSDLPIGVIPVDSLSPVERVNYTV 180
TZNB LNPELKIATVSKGGHLKIRLVANKGRGYALAEQNNTSDLPIGVIPVDSLSPVERVNYTV 180
TZNP LNPELKIATVSKGGHLKIRLVANKGRGYALAEQNNTSDLPIGVIPVDSLSPVERVNYTV 180

WT ENTRVGQSSDFDKLTLDVWTNGSITPQESVSLAAKIMTEHLNIFVGLTDEAQNAEIMIEK 240
TZNB ENTRVGQSSDFDKLTLDVWTNGSITPQESVSLAAKIMTEHLNIFVGLTDEAQNAEIMIEK 240
TZNP ENTRVGQSSDFDKLTLDVWTNGSITPQESVSLAAKIMTEHLNIFVGLTDEAQNAEIMIEK 240

WT EEDQKEKVLEMSIEELDLSVRSYNCLKRAGINSVQELADKSEADMMKVRNLGRKSLEEVK 300
TZNB EEDQKEKVLEMSIEELDLSVRSYNCLKRAGINSVQELADKSEADMMKVRNLGRKSLEEVK 300
TZNP EEDQKEKVLEMSIEELDLSVRSYNCLKRAGINSVQELADKSEADMMKVRNLGRKSLEEVK 300

WT YKLEDLGLGLRKED 314
TZNB YKLEDLGLG----- 309
TZNP YKLEDLGLGLRKED 314

TZNB – L310*

TZNP – no mutations

DNA-directed RNA Polymerase beta subunit

WT MAGQVVQYGRHRKRRNYARISEVLELPNLIEIQTKSYEWFLREGLIEMFRDISPIEDFTG 60
TZNB MAGQVVQYGRHRKRRNYARISEVLELPNLIEIQTKSYEWFLREGLIEMFRDISPIEDFTG 60
TZNP MAGQVVQYGRHRKRRNYARISEVLELPNLIEIQTKSYEWFLREGLIEMFRDISPIEDFTG 60

WT NLSLEFVDYRLGEPKYDLEESKNRDATYAAPLRVKVRLIIKETGEVKEQEVFMGDFPLMT 120
TZNB NLSLEFVDYRLGEPKYDLEESKNRDATYAAPLRVKVRLIIKETGEVKEQEVFMGDFPLMT 120
TZNP NLSLEFVDYRLGEPKYDLEESKNRDATYAAPLRVKVRLIIKETGEVKEQEVFMGDFPLMT 120

WT DTGTFVINGAERVIVSQLVRSVSVYFNEKIDKNGRENYDATIIPNRGAWLEYETDAKDVV 180
TZNB DTGTFVINGAERVIVSQLVRSVSVYFNEKIDKNGRENYDATIIPNRGAWLEYETDAKDVV 180
TZNP DTGTFVINGAERVIVSQLVRSVSVYFNEKIDKNGRENYDATIIPNRGAWLEYETDAKDVV 180

WT YVRIDRTRKPLPTVLLRALGFSSDQEIVDLLGDNEYLRNTLEKDGTEQALLEIYERL 240
TZNB YVRIDRTRKPLPTVLLRALGFSSDQEIVDLLGDNEYLRNTLEKDGTEQALLEIYERL 240
TZNP YVRIDRTRKPLPTVLLRALGFSSDQEIVDLLGDNEYLRNTLEKDGTEQALLEIYERL 240

WT RPGEPTVENAKSLLYSRFFDPKRYDLASVGRYKTNKKLHLKHRLFNQKLAEPVNTETG 300
TZNB RPGEPTVENAKSLLYSRFFDPKRYDLASVGRYKTNKKLHLKHRLFNQKLAEPVNTETG 300
TZNP RPGEPTVENAKSLLYSRFFDPKRYDLASVGRYKTNKKLHLKHRLFNQKLAEPVNTETG 300

WT EIVVEEGTVLDRRKIDEIMDVLESNANSEVFELHGSVIDEPVEIQSIKVYVPNDEEGRTT 360
TZNB EIVVEEGTVLDRRKIDEIMDVLESNANSEVFELHGSVIDEPVEIQSIKVYVPNDEEGRTT 360
TZNP EIVVEEGTVLDRRKIDEIMDVLESNANSEVFELHGSVIDEPVEIQSIKVYVPNDEEGRTT 360
***** :*****

WT TVIGNAFPDPSEVKCITPADIIASMSYFFNLLSGIGYTDDIDHLGNRRLRSVGELLQNQFR 420
TZNB TVIGNAFPDPSEVKCITPADIIASMSYFFNLLSGIGYTDDIDHLGNRRLRSVGELLQNQFR 420
TZNP TVIGNAFPDPSEVKCITPADIIASMSYFFNLLSGIGYTDDIDHLGNRRLRSVGELLQNQFR 420

WT IGLSRMERVVRRERMSIQDTESITPQQLINIRPVIASIKEFFGSSQLSQFMDQANPLAELT 480
TZNB IGLSRMERVVRRERMSIQDTESITPQQLINIRPVIASIKEFFGSSQLSQFMDQANPLAELT 480
TZNP IGLSRMERVVRRERMSIQDTESITPQQLINIRPVIASIKEFFGSSQLSQFMDQANPLAELT 480

WT HKRRLSALGPGGLTRERAQMEVRDVHSHYGRMCPIETPEGPNIGLINSLSYARVNEFG 540
TZNB HKRRLSALGPGGLTRERAQMEVRDVHSHYGRMCPIETPEGPNIGLINSLSYARVNEFG 540
TZNP HKRRLSALGPGGLTRERAQMEVRDVHSHYGRMCPIETPEGPNIGLINSLSYARVNEFG 540

WT FIETPYRKVDLDTHAITDQIDYLTADEEDSYVVAQANSKLDENGRFMDDEVVCRFRGNNT 600
TZNB FIETPYRKVDLDTHAITDQIDYLTADEEDSYVVAQANSKLDENGRFMDDEVVCRFRGNNT 600
TZNP FIETPYRKVDLDTHAITDQIDYLTADEEDSYVVAQANSKLDENGRFMDDEVVCRFRGNNT 600

WT VMAKEKMDYMDVSPKQVVSAAATACIPFLENDDSNRALMGANMQRQAVPLMNPEAPFVGTG 660
TZNB VMAKEKMDYMDVSPKQVVSAAATACIPFLENDDSNRALMGANMQRQAVPLMNPEAPFVGTG 660
TZNP VMAKEKMDYMDVSPKQVVSAAATACIPFLENDDSNRALMGANMQRQAVPLMNPEAPFVGTG 660

WT MEHVAARDSGAAITAKHRGRVEHVESNEILVRRLVEENGVEHEGELDRYPLAKFKRSNSG 720
TZNB MEHVAARDSGAAITAKHRGRVEHVESNEILVRRLVEENGVEHEGELDRYPLAKFKRSNSG 720
TZNP MEHVAARDSGAAITAKHRGRVEHVESNEILVRRLVEENGVEHEGELDRYPLAKFKRSNSG 720

WT TCYNQRPIVAVGDVVEYNEILADGPSMELGEMALGRNVVVGFMWTDGYNVEDAVIMSERL 780
TZNB TCYNQRPIVAVGDVVEYNEILADGPSMELGEMALGRNVVVGFMWTDGYNVEDAVIMSERL 780
TZNP TCYNQRPIVAVGDVVEFNEILADGPSMELGEMALGRNVVVGFMWTDGYNVEDAVIMSERL 780

WT VKDDVYTSIHIEEYSEARDTKLGPEEITRDIPNVSEALKNLDDRGIVYIGA EVKDGDI 840
TZNB VKDDVYTSIHIEEYSEARDTKLGPEEITRDIPNVSEALKNLDDRGIVYIGA EVKDGDI 840
TZNP VKDDVYTSIHIEEYSEARDTKLGPEEITRDIPNVSEALKNLDDRGIVYIGA EVKDGDI 840

WT LVGKVTPKGVTTELTAERLLHAI FGEKAREVRDTSLRVPHGAGGIVLDVKVFNREEGDDT 900
TZNB LVGKVTPKGVTTELTAERLLHAI FGEKAREVRDTSLRVPHGAGGIVLDVKVFNREEGDDT 900
TZNP LVGKVTPKGVTTELTAERLLHAI FGEKAREVRDTSLRVPHGAGGIVLDVKVFNREEGDDT 900

WT LSPGVNQLVRVYIVQKRKIHVGDKMCGRHGNKGVISKIVPEEDMPYLPDGRPIDIMLNPL 960
TZNB LSPGVNQLVRVYIVQKRKIHVGDKMCGRHGNKGVISKIVPEEDMPYLPDGRPIDIMLNPL 960
TZNP LSPGVNQLVRVYIVQKRKIHVGDKMCGRHGNKGVISKIVPEEDMPYLPDGRPIDIMLNPL 960

WT GVPSRMNIGQVLELHLGMAAKNLGIHVASPVFDGANDDVWSTIEEAGMARDGKT VLYDG 1020
TZNB GVPSRMNIGQVLELHLGMAAKNLGIHVASPVFDGANDDVWSTIEEAGMARDGKT VLYDG 1020
TZNP GVPSRMNIGQVLELHLGMAAKNLGIHVASPVFDGANDDVWSTIEEAGMARDGKT VLYDG 1020

WT RTGEPFDNRISVGVMYMLKLAHMVDDKLHARSTGPYSLVTQQPLGGKAQFGGQRF GEME V 1080
TZNB RTGEPFDNRISVGVMYMLKLAHMVDDKLHARSTGPYSLVTQQPLGGKAQFGGQRF GEME V 1080
TZNP RTGEPFDNRISVGVMYMLKLAHMVDDKLHARSTGPYSLVTQQPLGGKAQFGGQRF GEME V 1080

WT WALEAYGAAYTLQEILTYKSDDTVGRVKTYEAI VKGENISRPSVPESFRVLMKELQSLGL 1140
TZNB WALEAYGAAYTLQEILTYKSDDTVGRVKTYEAI VKGENISRPSVPESFRVLMKELQSLGL 1140
TZNP WALEAYGAAYTLQEILTYKSDDTVGRVKTYEAI VKGENISRPSVPESFRVLMKELQSLGL 1140

WT DVKVMDEQDNEIEMTDVDDDDVVERKVLDLQQNDAPETQKEVTD 1183
TZNB DVKVMDEQDNEIEMTDVDDDDVVERKVLDLQQNDAPETQKEVTD 1183
TZNP DVKVMDEQDNEIEMTDVDDDDVVERKVLDLQQNDAPETQKEVTD 1183

TZNB – no mutations
TZNP – E355D, P614Q, Y737F

Thioredoxin-fold Protein

WT MAGELRIMENKSREDINLSPVSKIEIYSFFDPFSSDCFKLSAILS SKLRIEYNQYIRIRHI 60
TZNB MAGELRIMENKSREDINLSPVSKIEIYSFSDPFSSDCFKLSAILS SKLRIEYNQYIRIRHI 60
TZNP MAGELRIMENKSREDINLSPVSKIEIYSFFDPFSSDCFKLSAILS SKLRIEYNQYIRIRHI 60

WT LNPSLKVLTKCQAQSTSNFDNIALAYKAAELQGRVRAERFIHLMQNEIIPKRDIITESMI 120
TZNB LNPSLKVLTKCQAQSTSNFDNIALAYKAAELQGRVRAERFIHLMQNEIIPKRDIITESMI 120
TZNP LNPSLKVLTKCQAQSTSNFDNIALAYKAAELQGRVRAERFIHLMQNEIIPKRDIITESMI 120
*****:*****

WT CDCIQNAGIDLEVFKDDLQKSKLTSLSKIDLHIAREMEIEQAPSLVFFSEDVHEEGLKVE 180
TZNB CDCIQNAGIDLEVFKDDLQKSKLTSLSKIDLHIAREMEIEQAPSLVFFSEDVHEEGLKVE 180
TZNP CDCIQNAGIDLEVFKDDLQKSKLTSLSKIDLHIAREMEIEQAPSLVFFSEDVHEEGLKVE 180

WT GLYPYHIYTYIINELMGKPIEKNLPPKLETYIQQQQQLVTMEELLTIYEWPEKLLNKELKK 240
TZNB GLYPYHIYTYIINELMGKPIEKNLPPKLETYIQQQQQLVTMEELLTIYEWPEKLLNKELKK 240
TZNP GLYPYHIYTYIINELMGKPIEKNLPPKLETYIQQQQQLVTMEELLTIYEWPEKLLNKELKK 240

WT LAIQQKIEKLYPDGDFWWSKMPKIKSK 268
TZNB LAIQQKIEKLYPDGDFWWSKMPKIKSK 268
TZNP LAIQQKIEKLYPDGDFWWSKMPKIKSK 268

TZNB – F30S
TZNP – V95L

Table 1: Strains and plasmids used in this study

Strain/plasmid	Genotype/properties	Reference
<i>E. coli</i>		
TOP10F ⁺	Cloning strain	Invitrogen
<i>S. aureus</i>		
RN4220	Restriction deficient cloning host	105
pCM29	sGFP expression vector, Cam ^R	106
RN4220/pCM29	Cloning host with pCM29	This study
RN4220/pCM29 variant	Cloning host with pCM29 and gene of interest	This study

Table 2: List of primers and their respective protein/gene in *S. aureus*

Primer	Sequence	Protein/Gene
CLM531	GGCTCATATTTGCTTTTTTAAAAGC	Sequencing Primer pCM29
CLM539	GGCTCGTATGTTGTGTGGAATTG	Sequencing Primer pCM29
Thio F	TAAGCAGGTACCATTAATTGTAGGT	Thioredoxin-fold protein
Thio R	TGCTTAGAGCTCACGAGGTCTTTAATTTATTTA	Thioredoxin-fold protein
L11 Meth F	TACACAGGTACCAGGGAGAATAAAGTATGAACT	Ribosomal protein L11 methyltransferase
L11 Meth R	TGCTTAGAGCTCATAACGTTGCACATTATTCAC	Ribosomal protein L11 methyltransferase
B Pol F	TAAGTAGGTACCTGAGGGGTGAATCTGTTTGG	DNA-directed RNA Polymerase beta subunit
B Pol R	TGCTTAGAGCTCCCTGTTTTGTAAATTGAGTA	DNA-directed RNA Polymerase beta subunit
Metal ATP F	TAAGTAGGTACCAATCACAGGGAGGCAATAAT	Lead, cadmium, zinc and mercury transporting ATPase
Metal ATP R	TGCTTAGAGCTCTCCTTCATTATTAAGGAATC	Lead, cadmium, zinc and mercury transporting ATPase
Phos F	TAAGCAGGTACCTCAGAAATGGAGTGGGGATT	Phosphoserine Phosphatase
Phos R	TGCTTAGAGCTCGTTCCAATAAACGTTGCACC	Phosphoserine Phosphatase
LysR F	TAAGCAGGTACCTTTTTGAAAGAGGTAAGTTC	Transcriptional regulator, LysR family
LysR R	TGCCGAGAGCTCTTTTTAGATTTGAAATTTAT	Transcriptional regulator, LysR family
A Pol F	TAAGCAGGTACCGTATATAAGGAGGATATTTAA	DNA-directed RNA Polymerase alpha subunit
A Pol R	TGCTTAGAGCTCTTTATCAATCTTCTTTCTTCA	DNA-directed RNA Polymerase alpha subunit

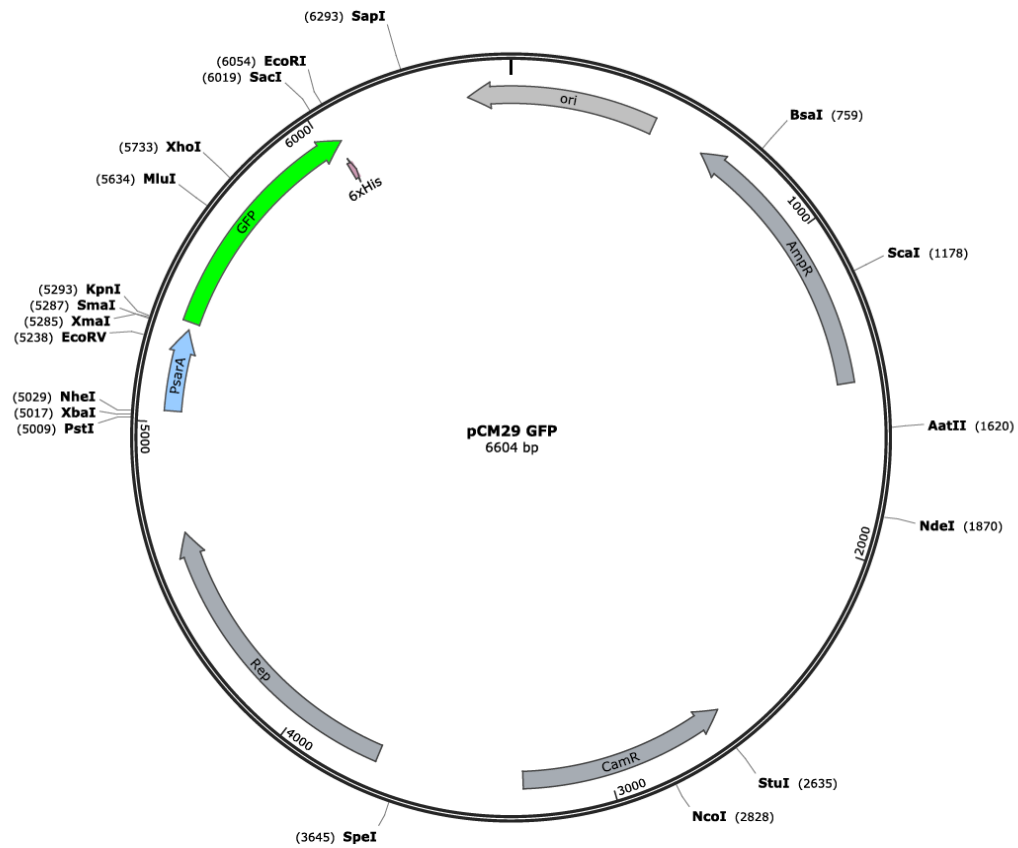
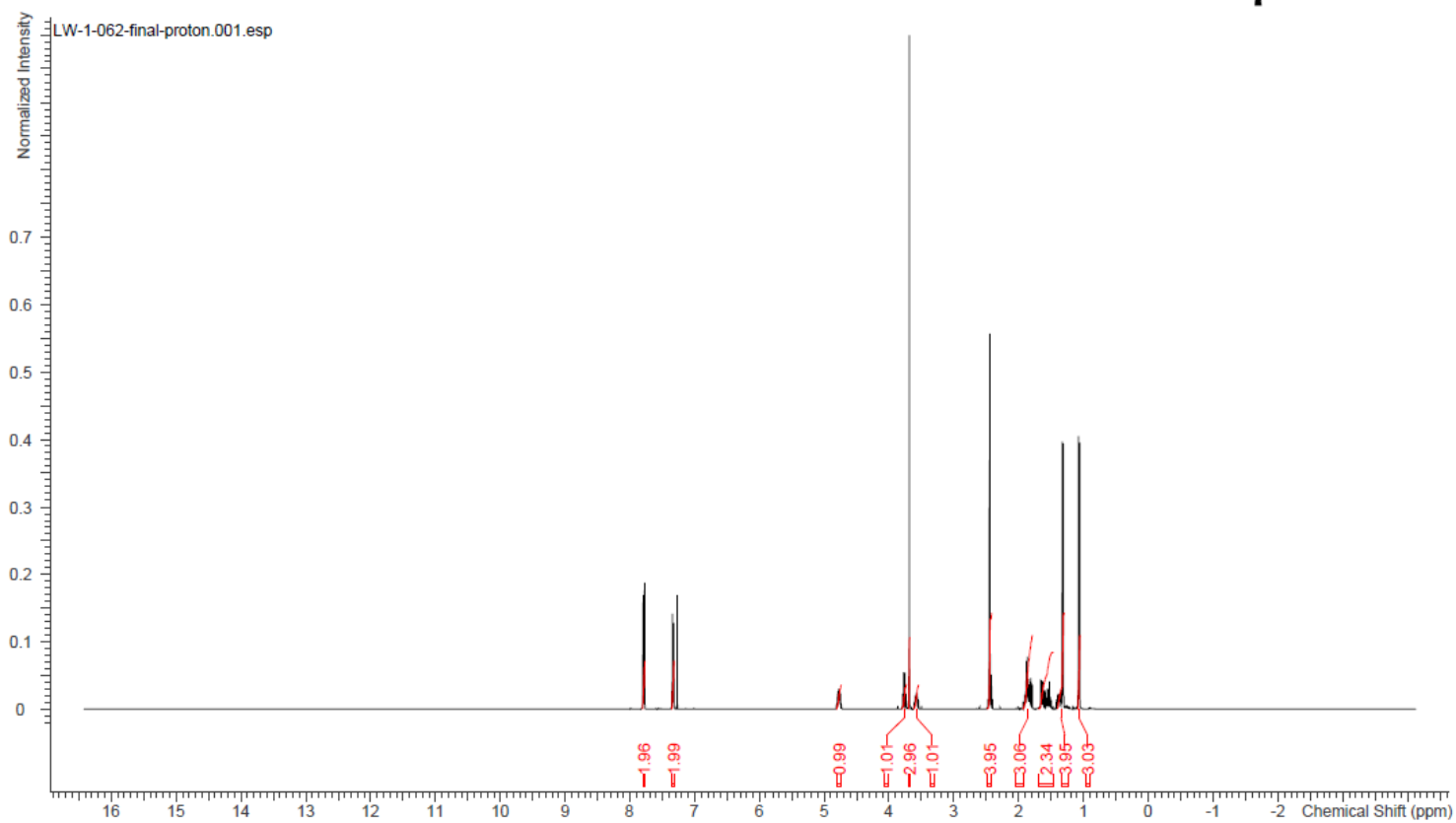
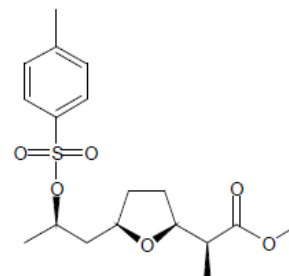
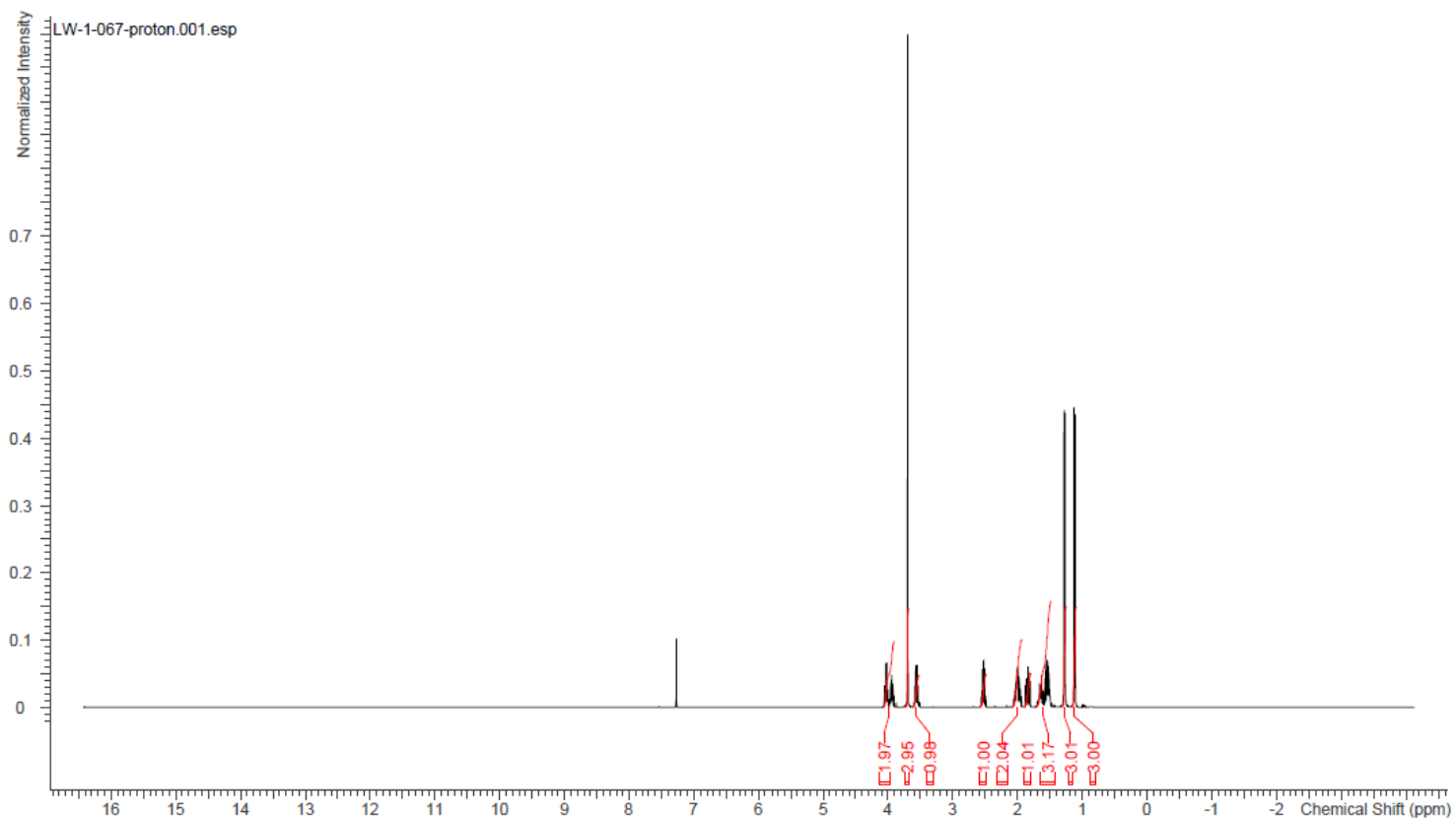
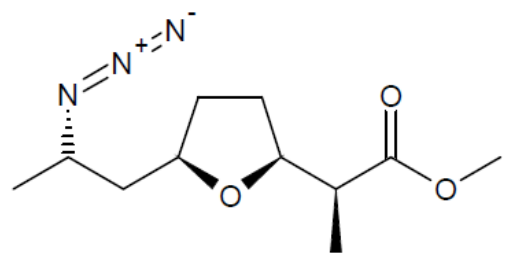
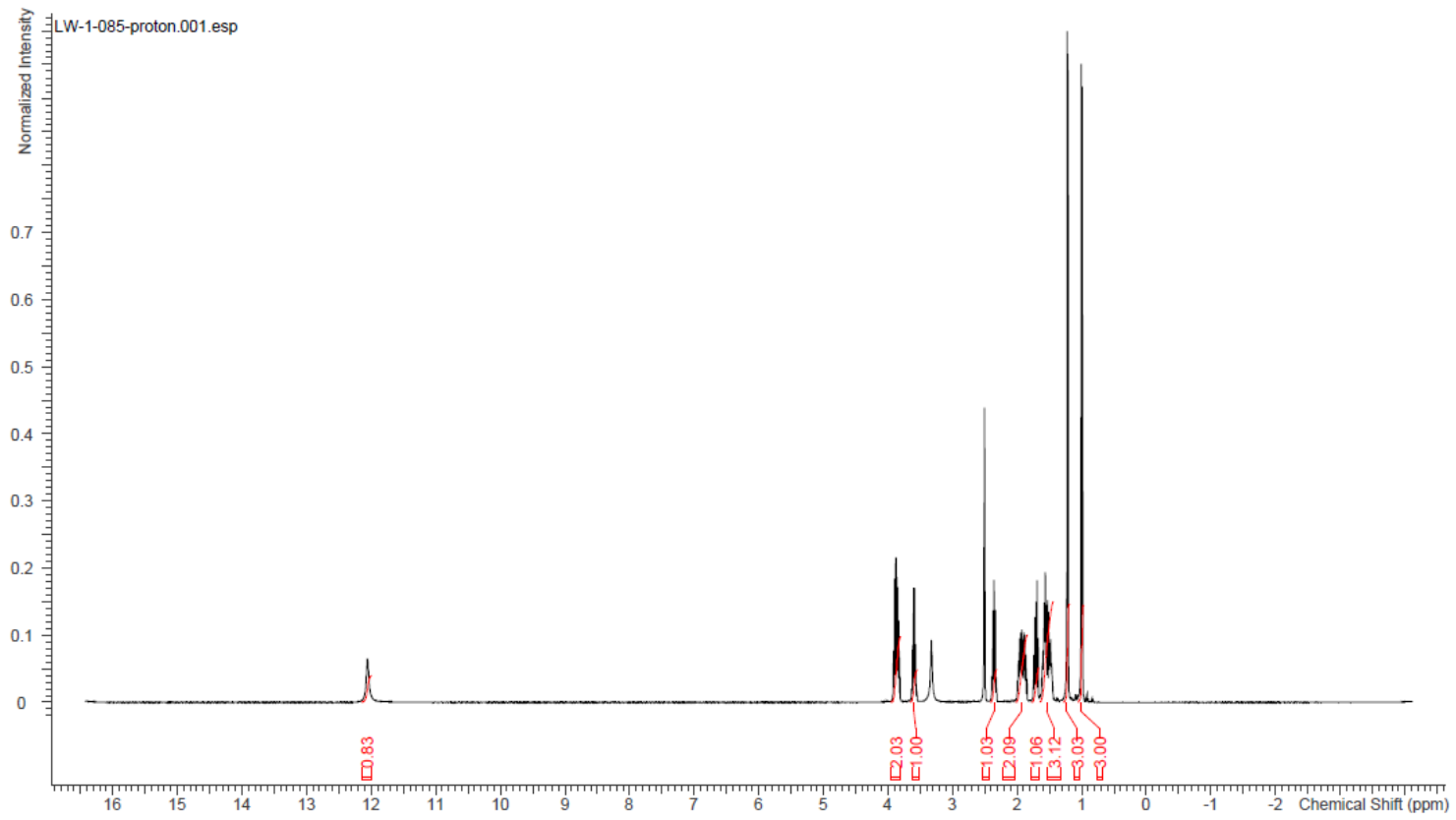
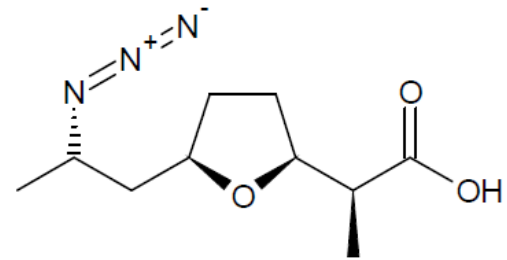


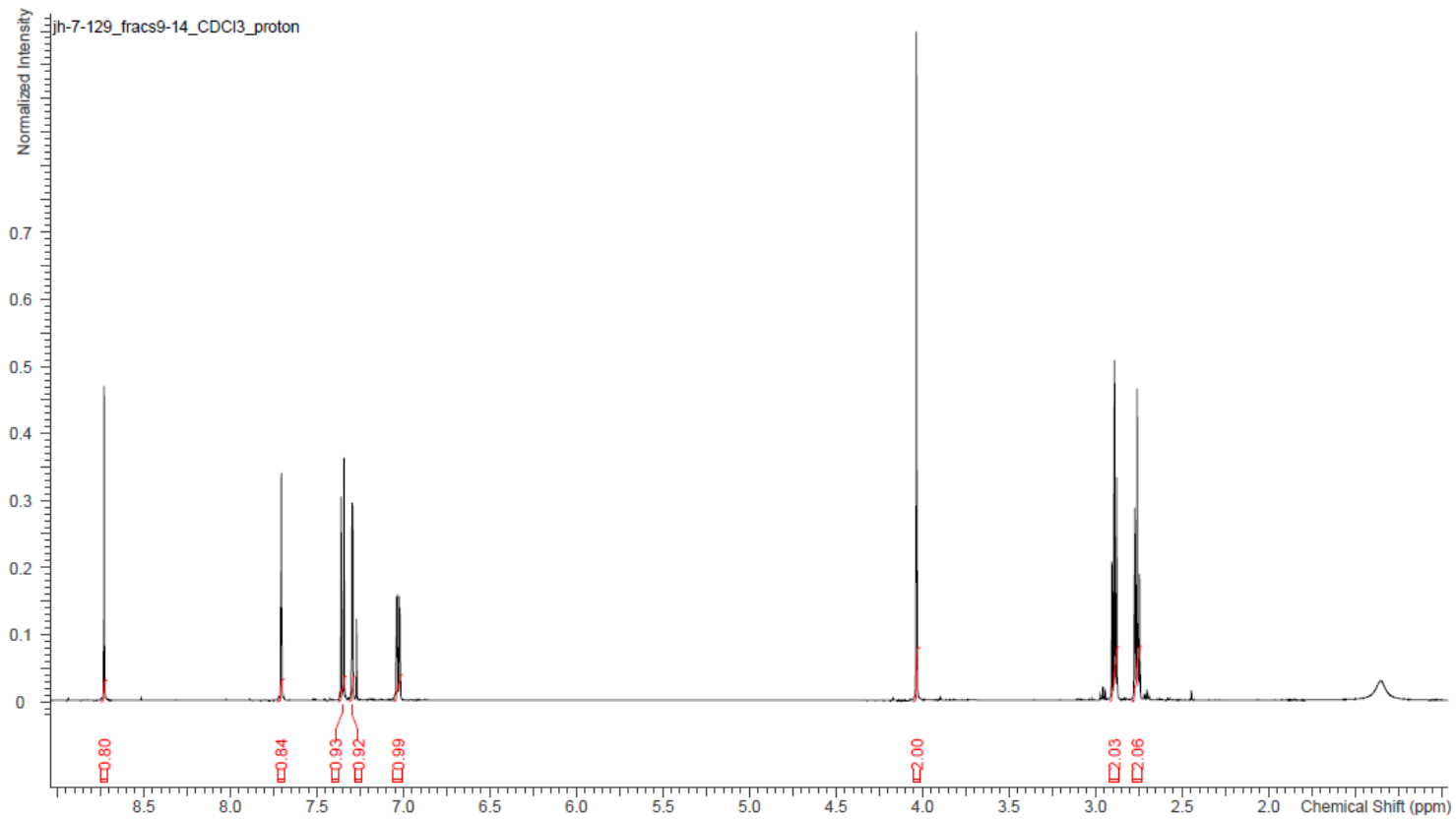
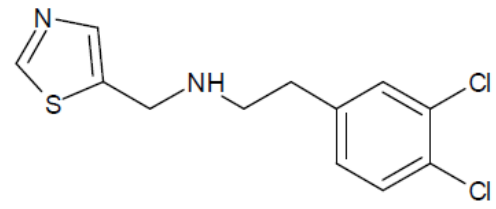
Figure 3: Map of pCM29 with the Amp^R and Cam^R genes indicated for selection in *E. coli* and *S. aureus*. Genes of interest were cloned in place of the GFP gene at restriction sites KpnI and SacI under control of the PsarA promoter.

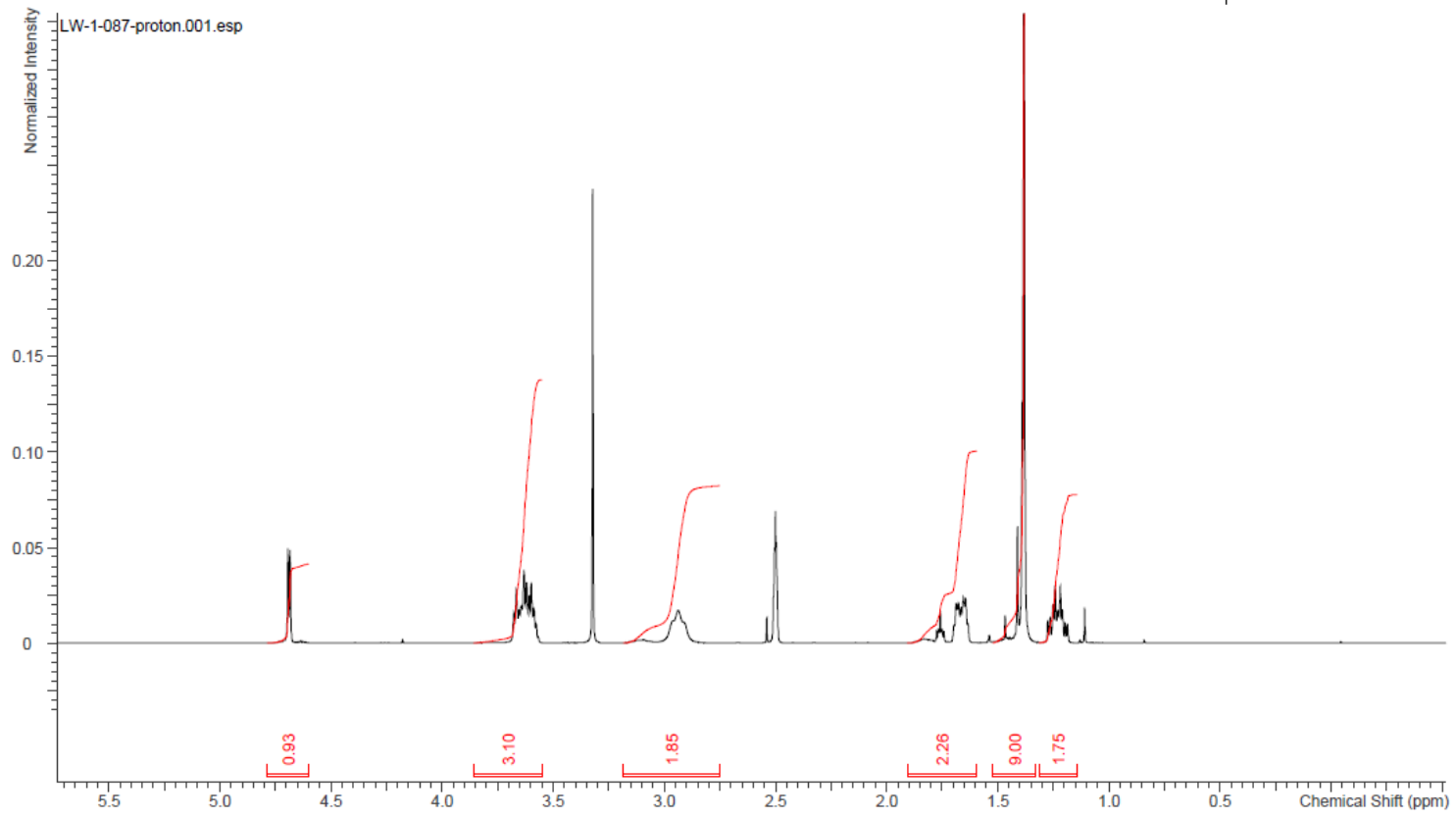
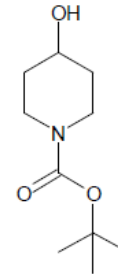
Appendix B: Selected NMR Spectra for Synthesized Compounds

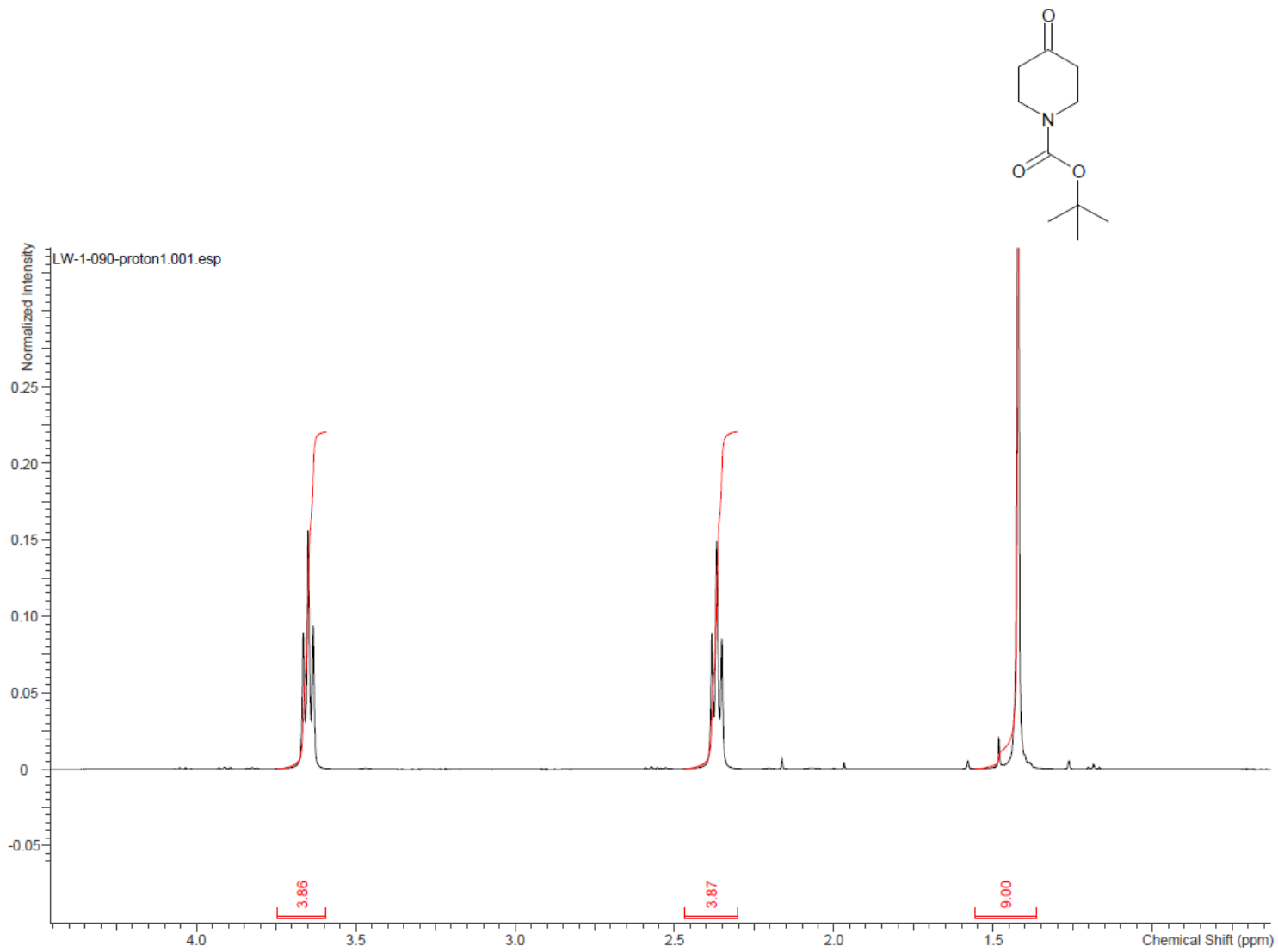


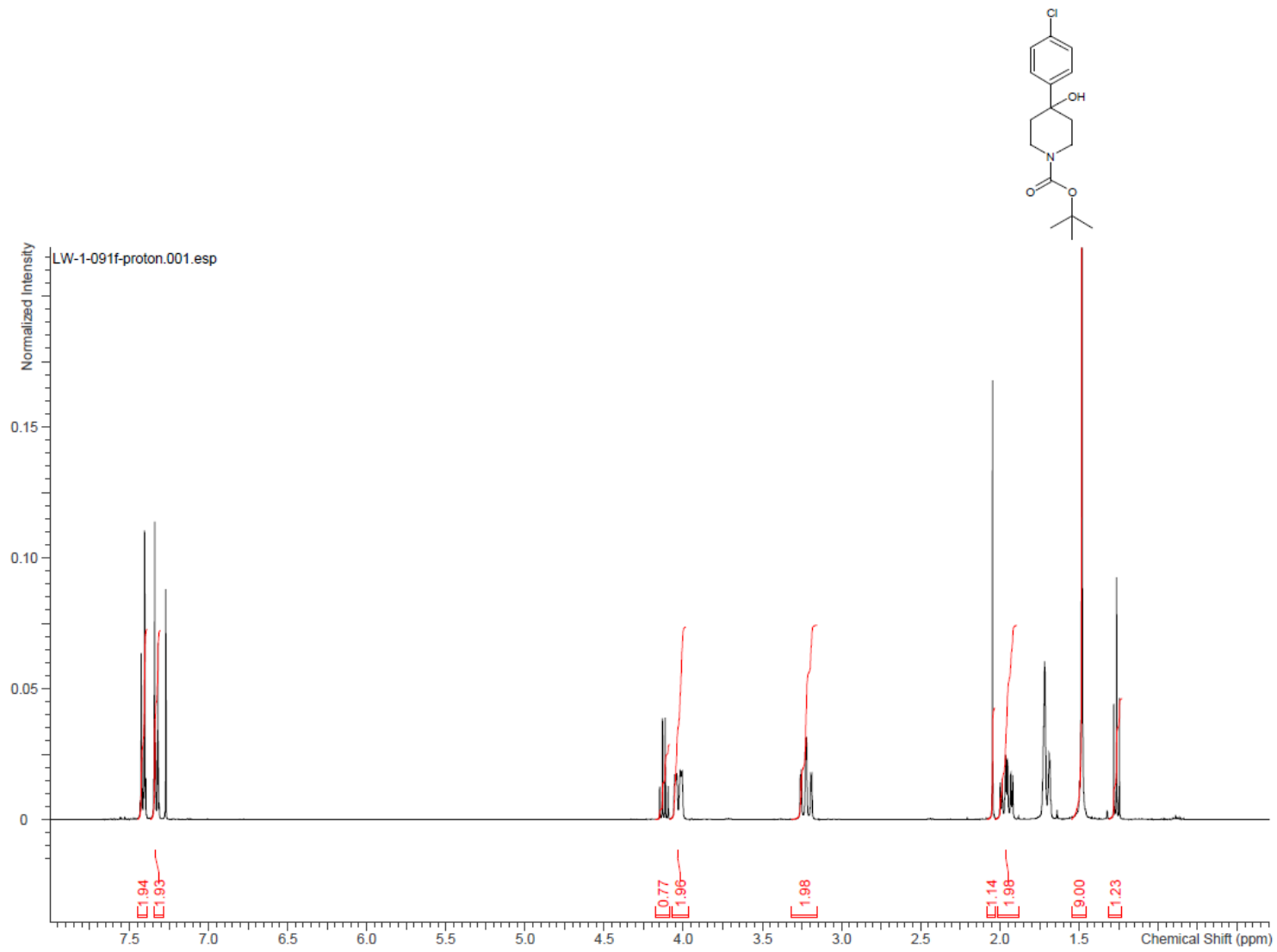


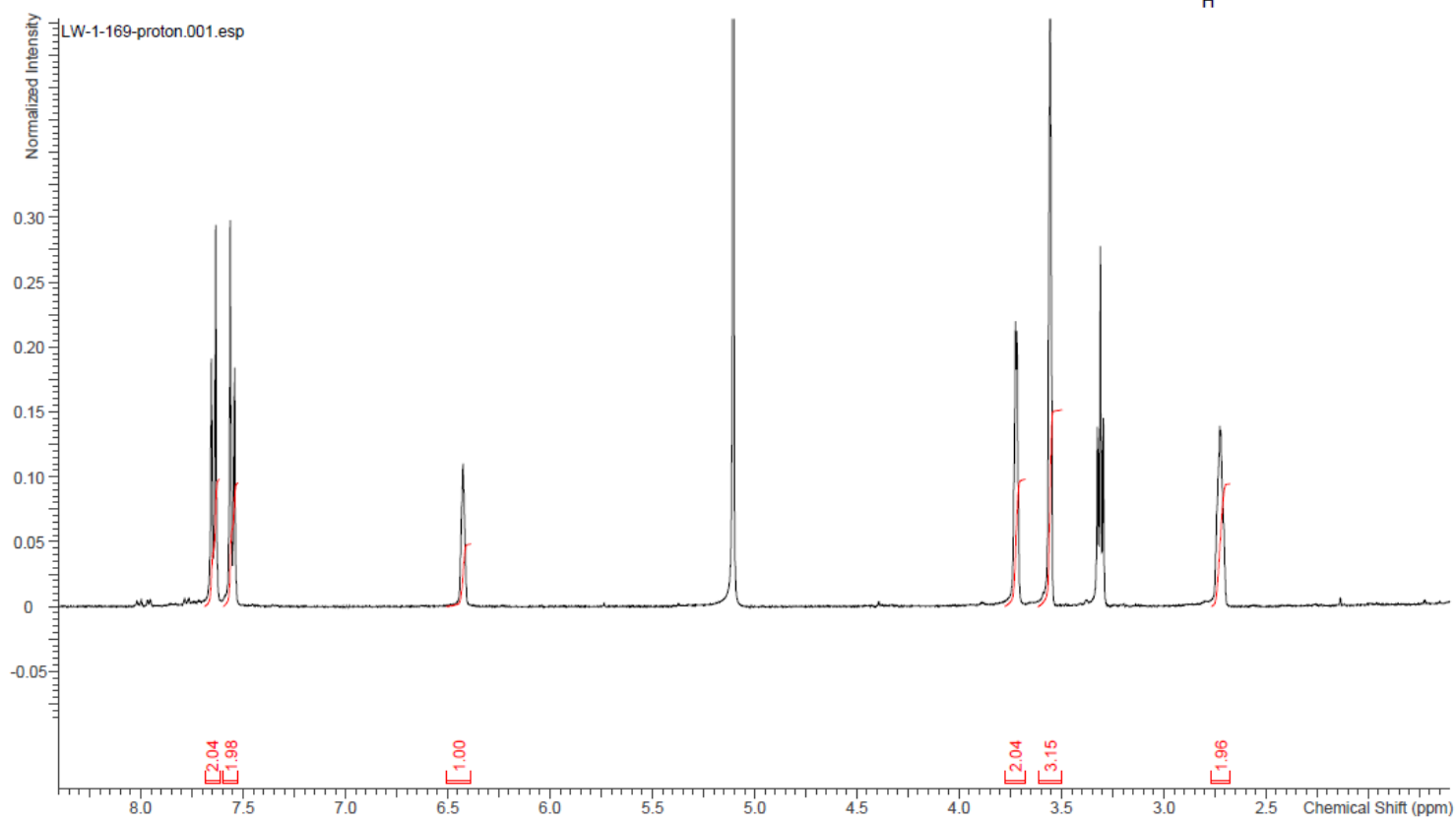
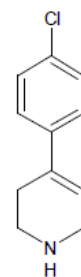


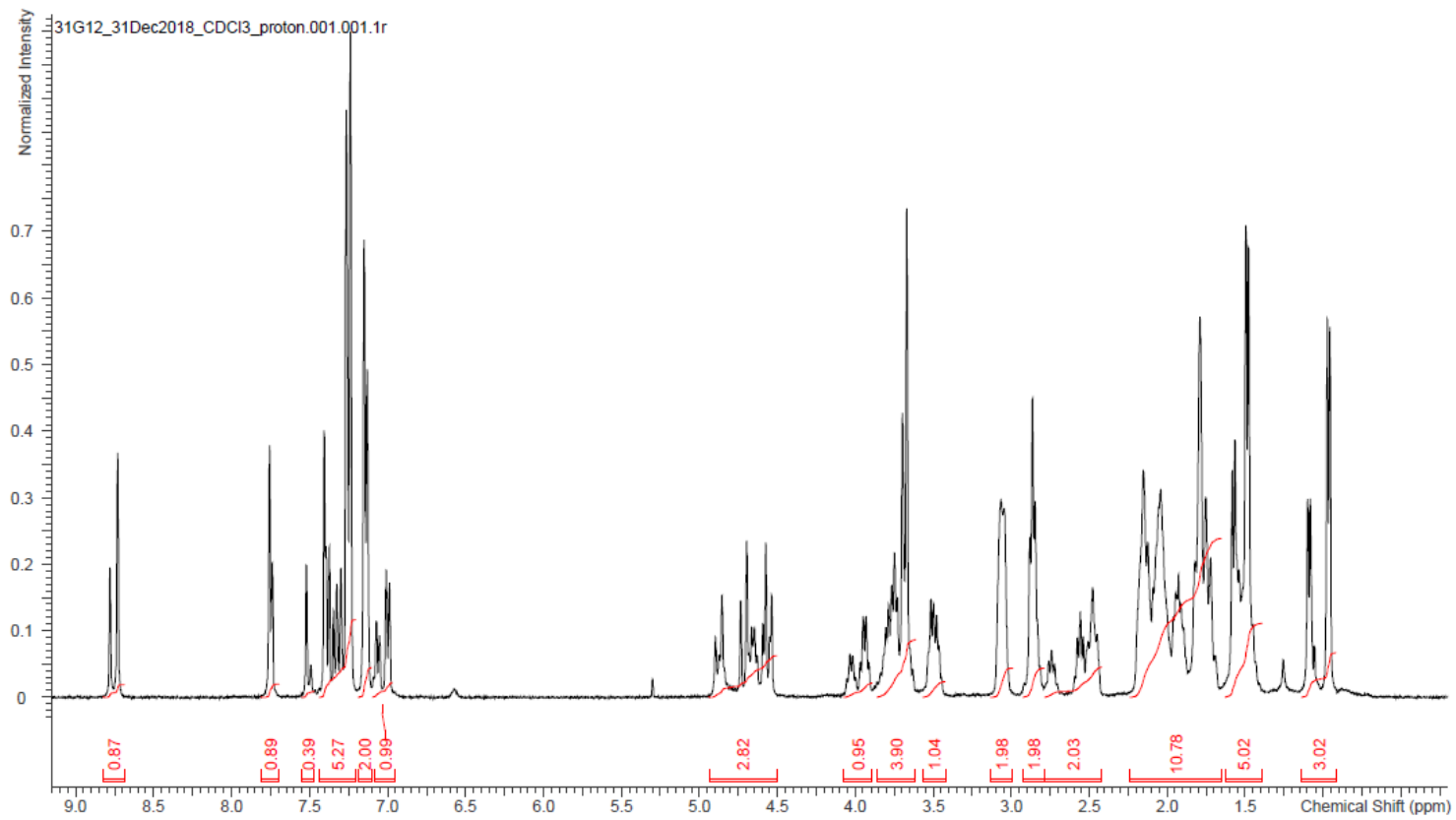
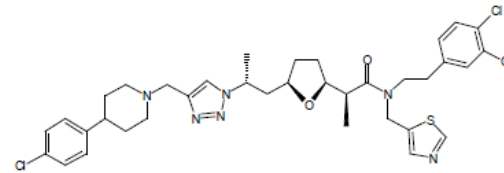


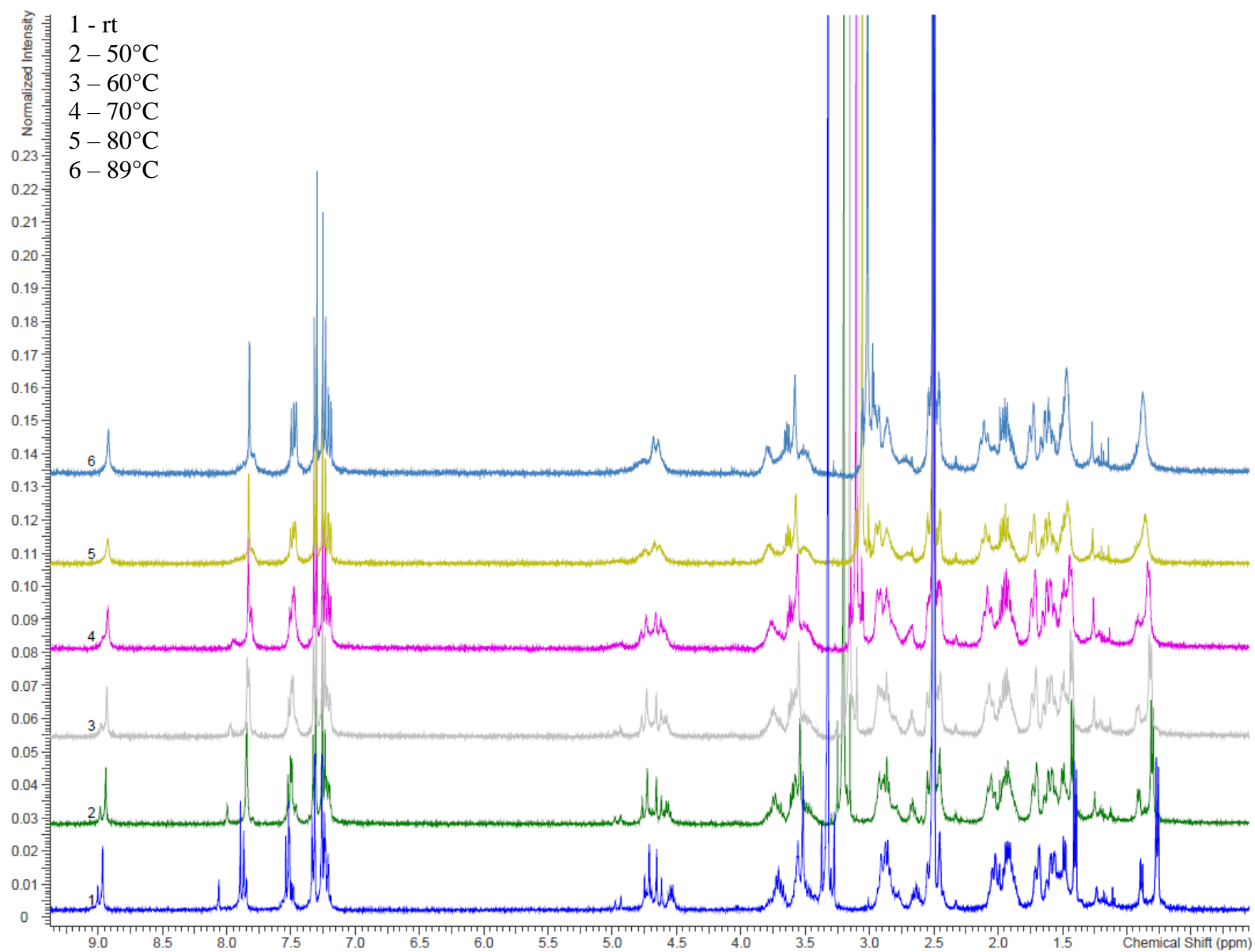


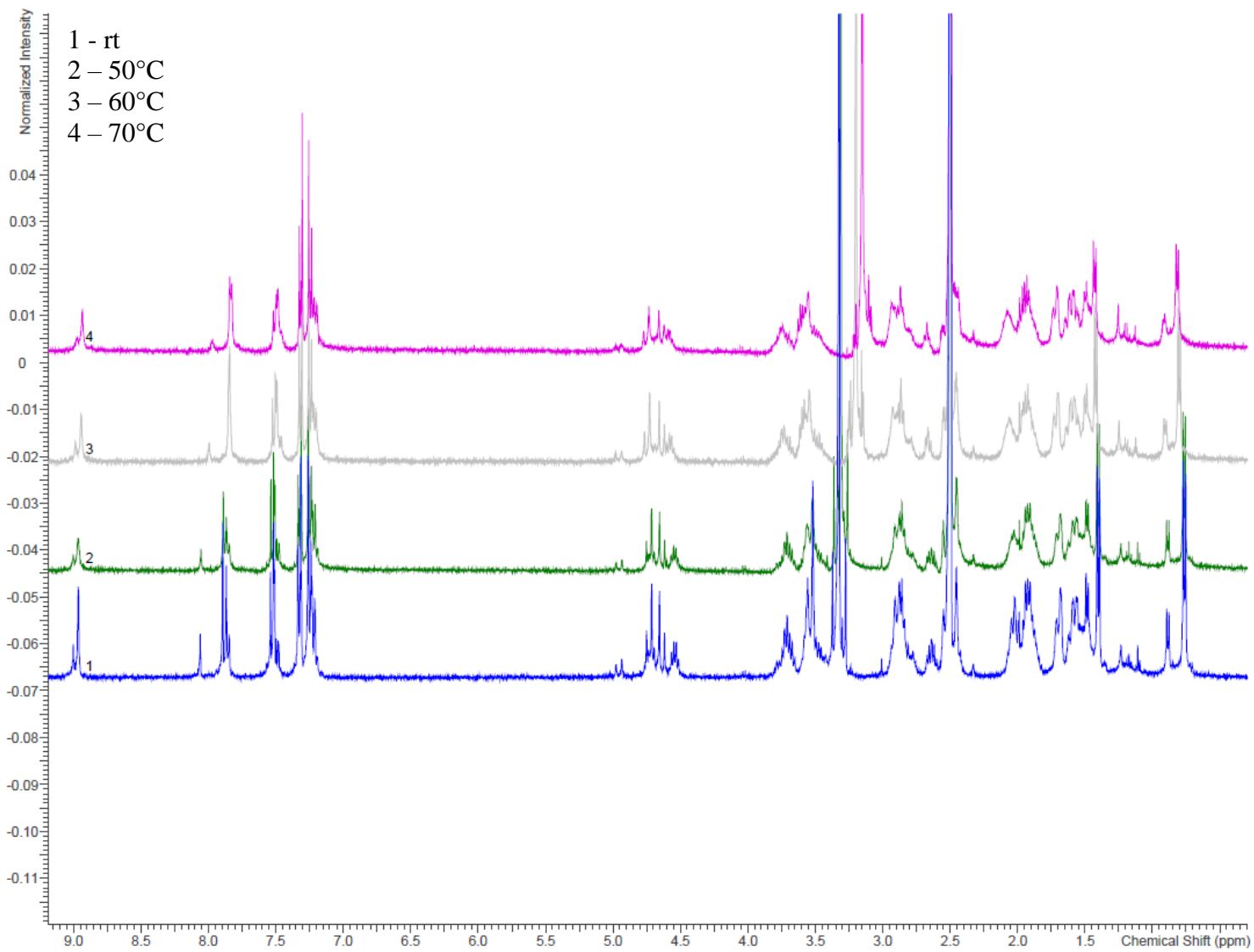


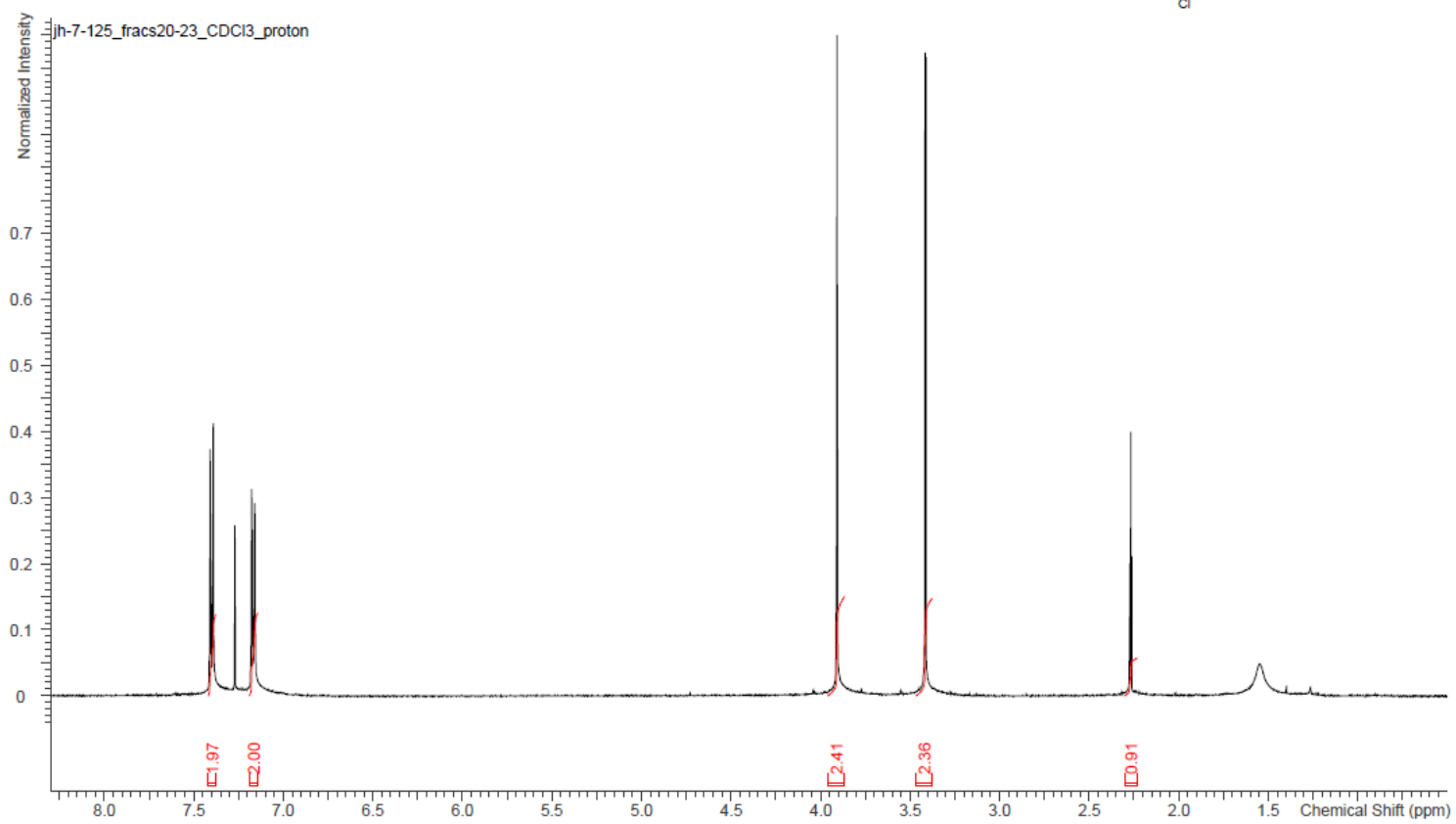
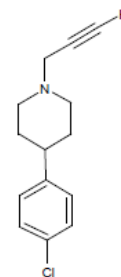


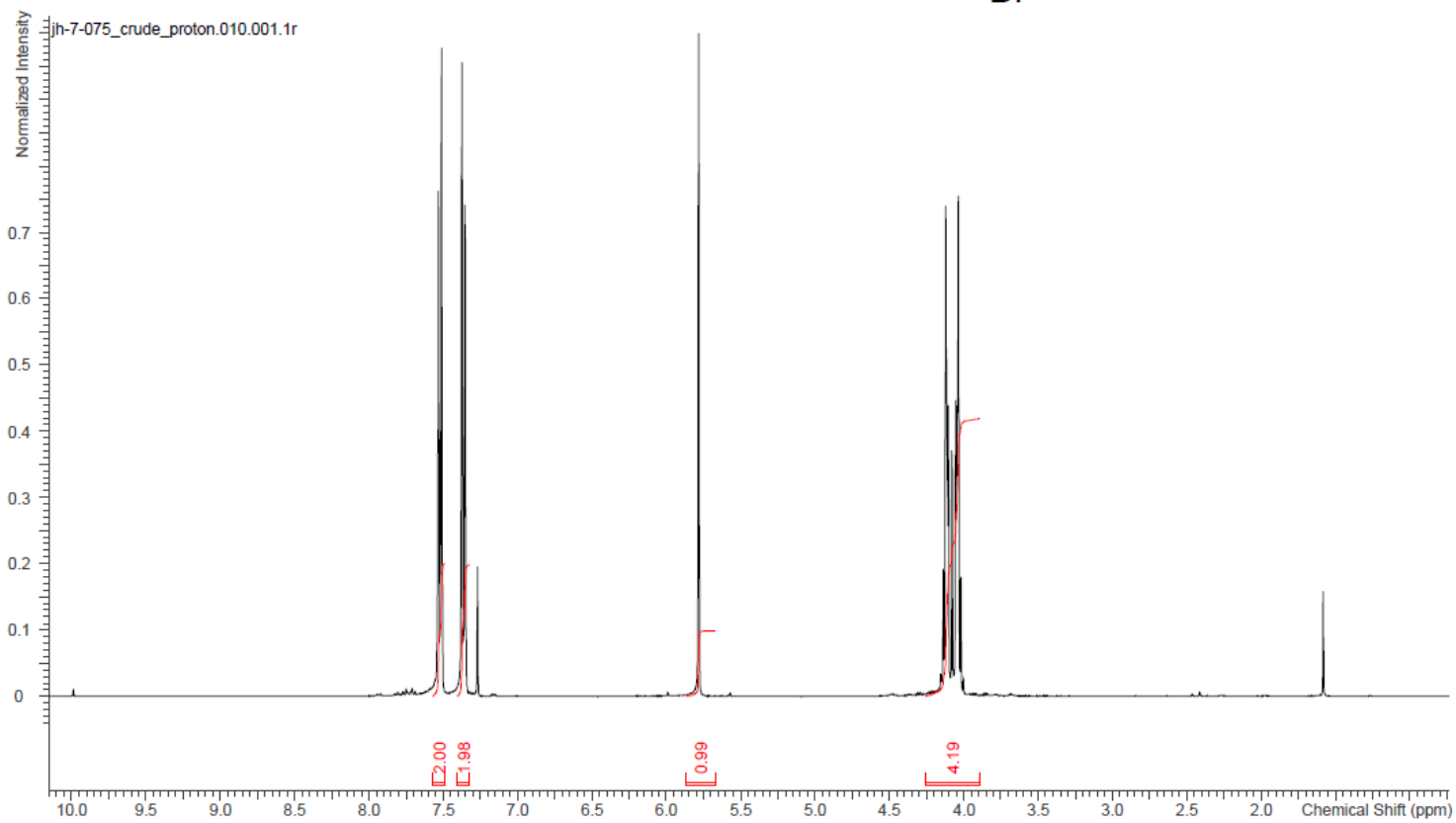
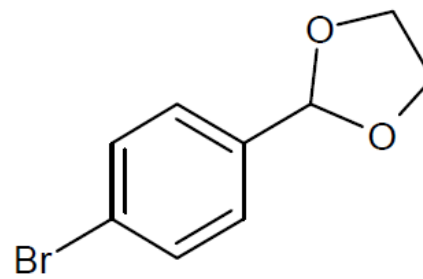


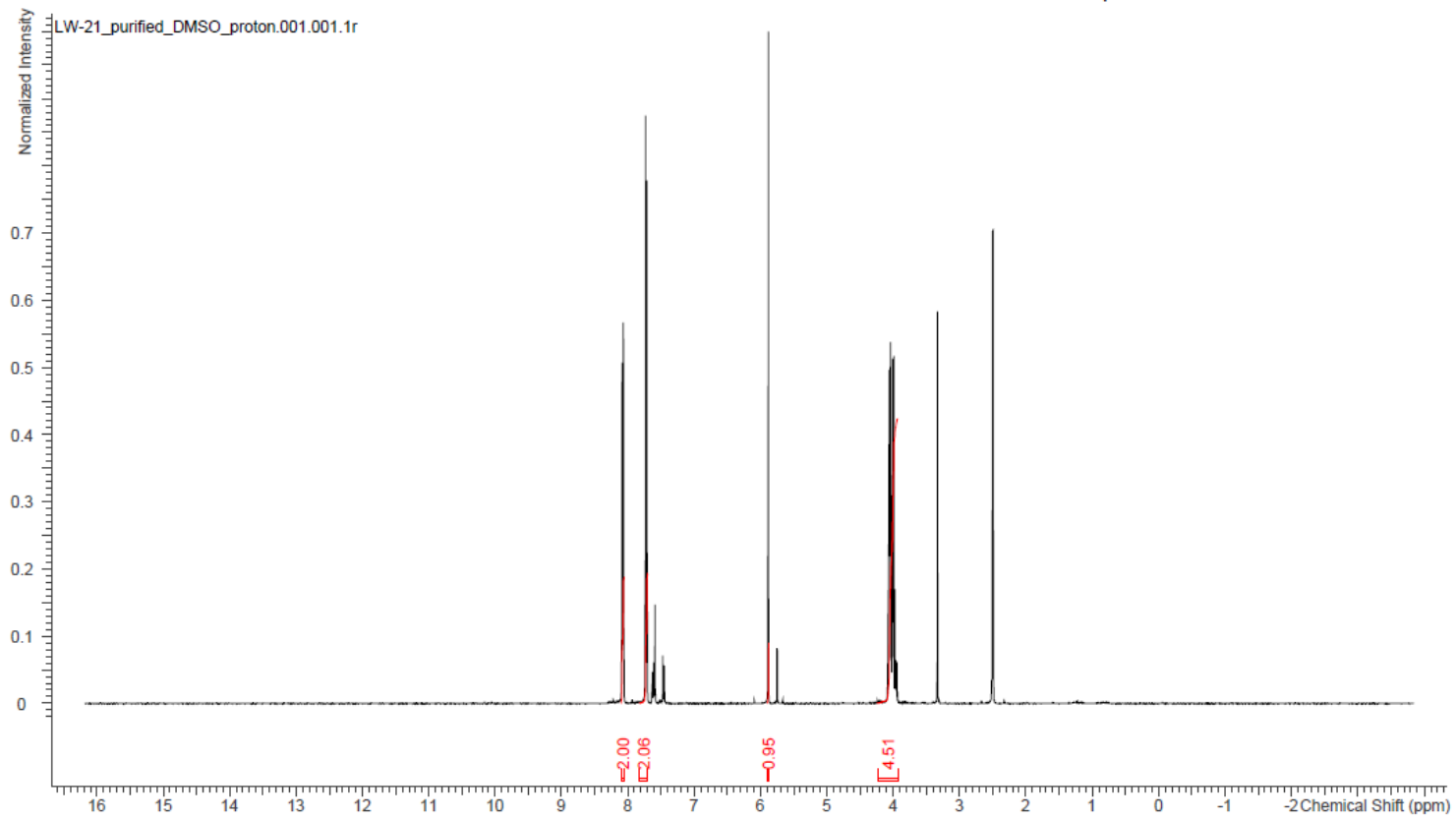
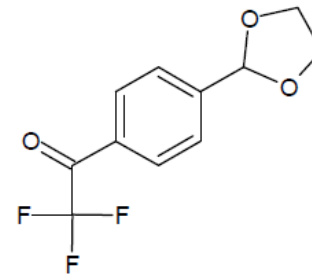


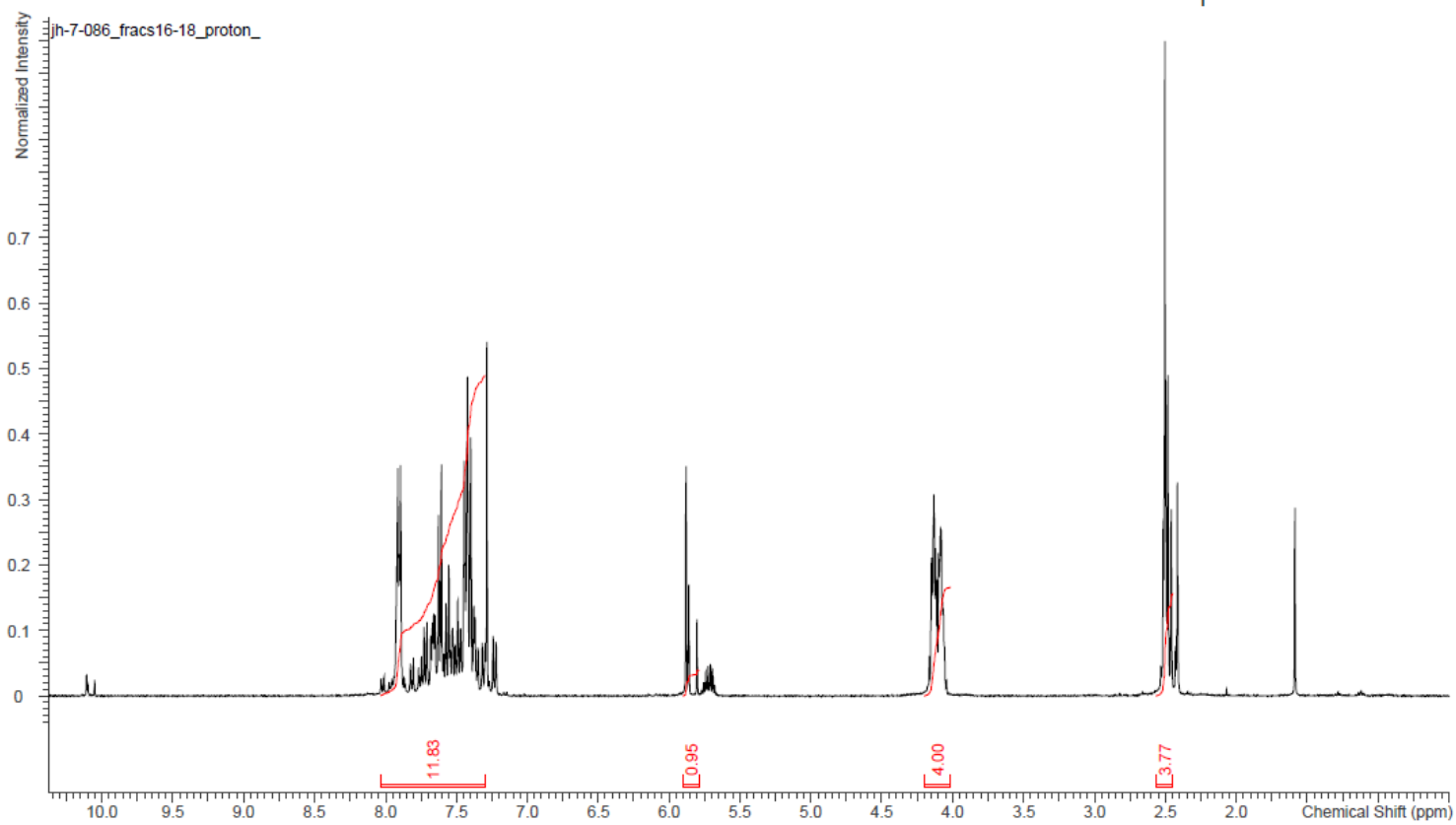
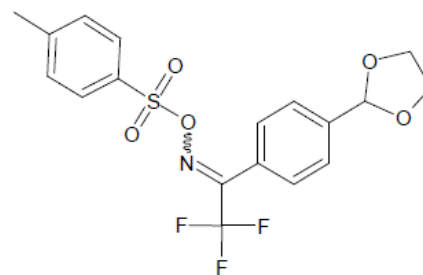


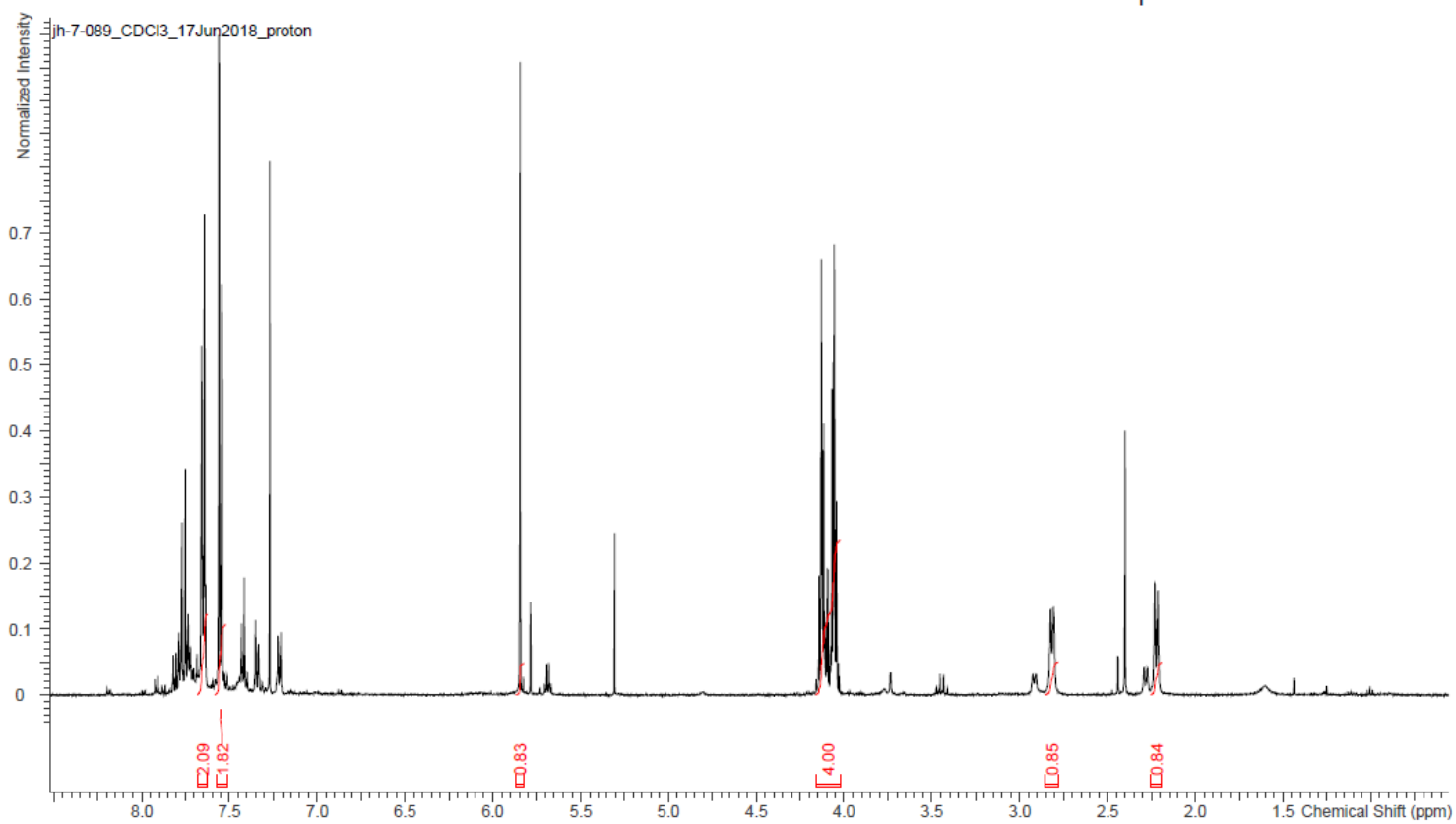
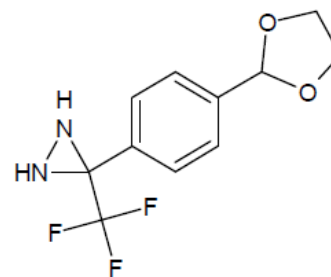


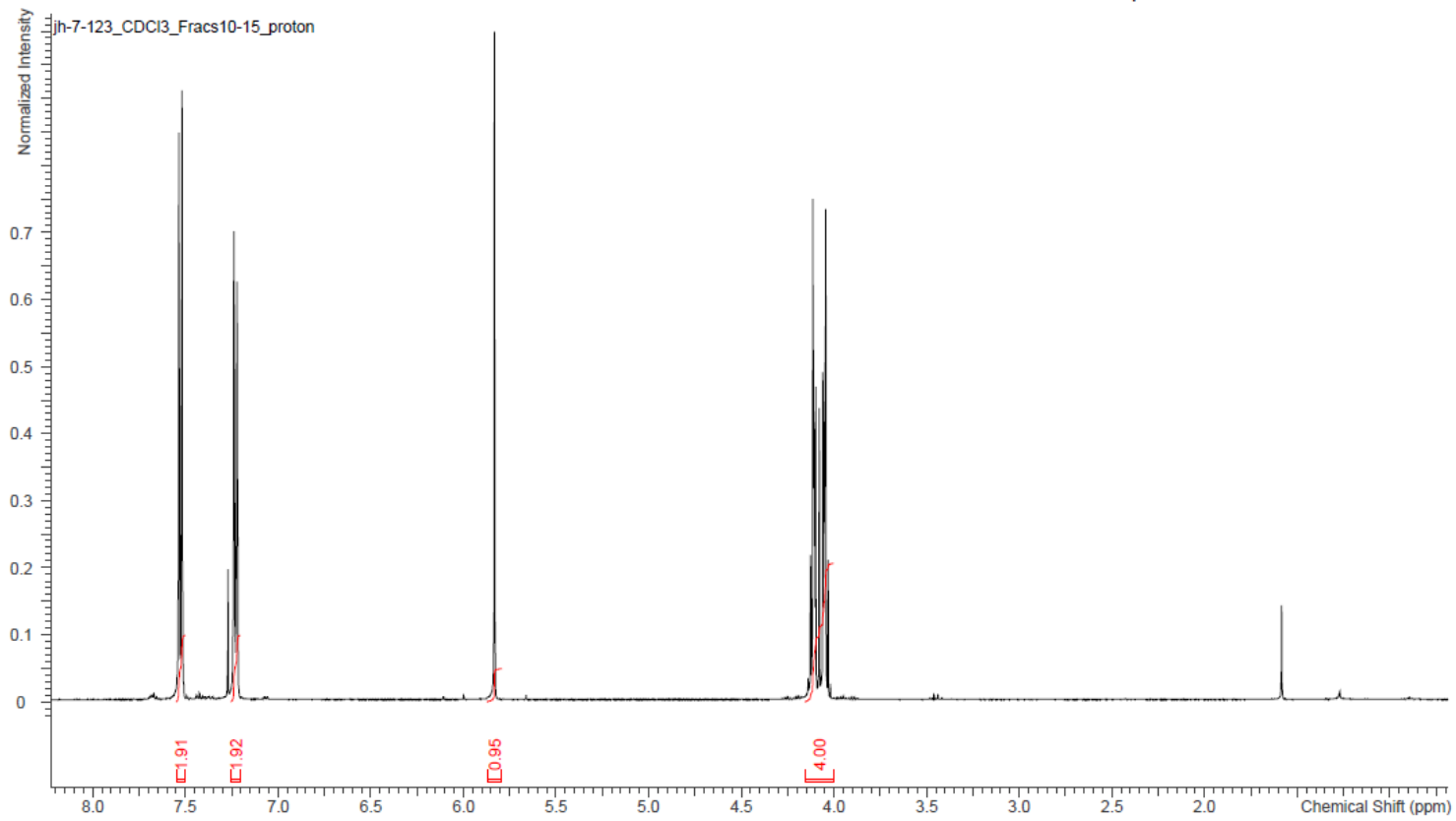
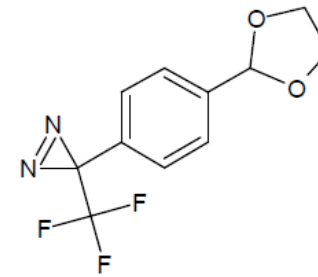


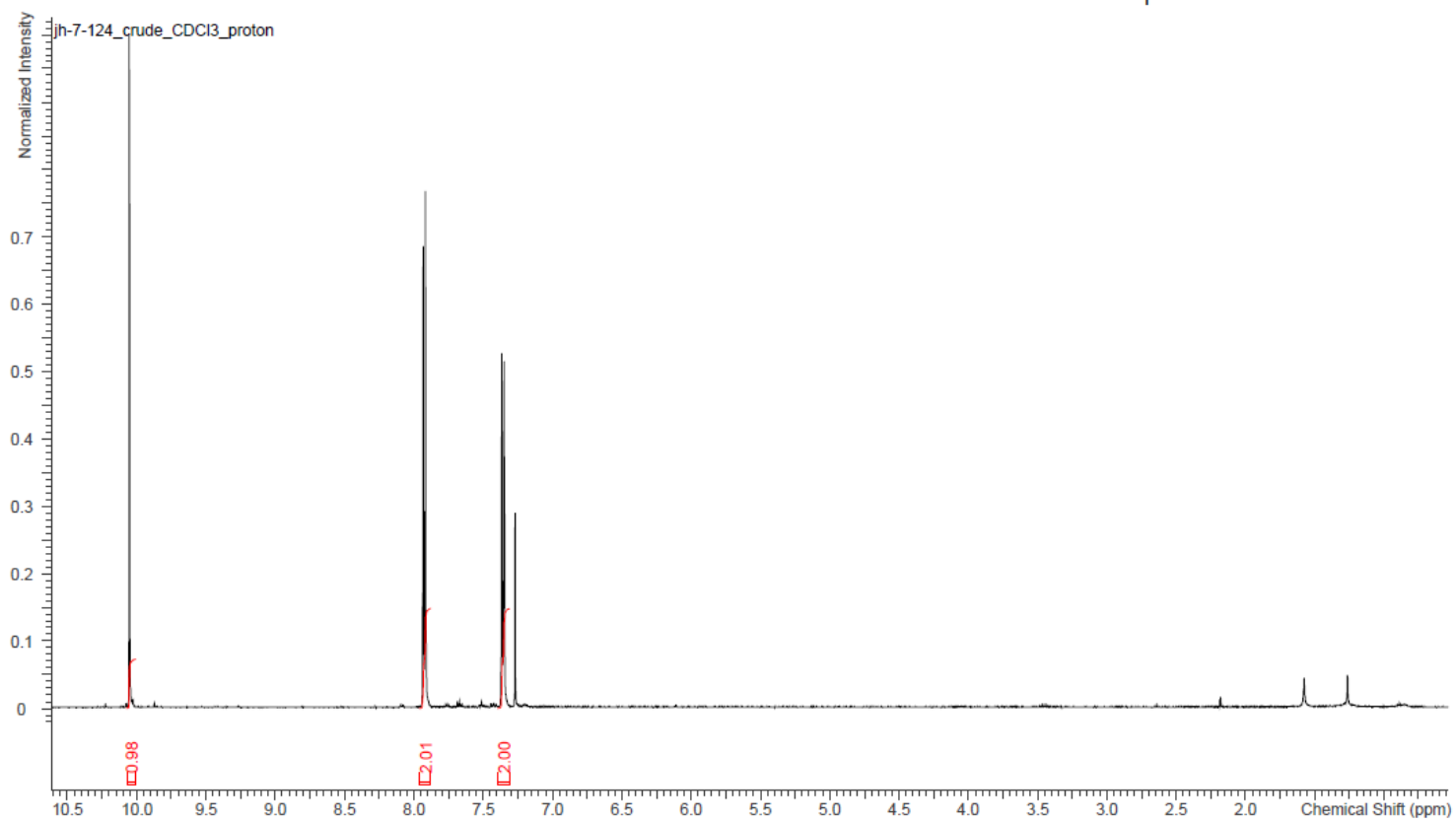
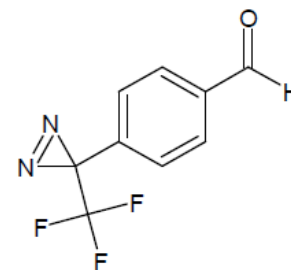


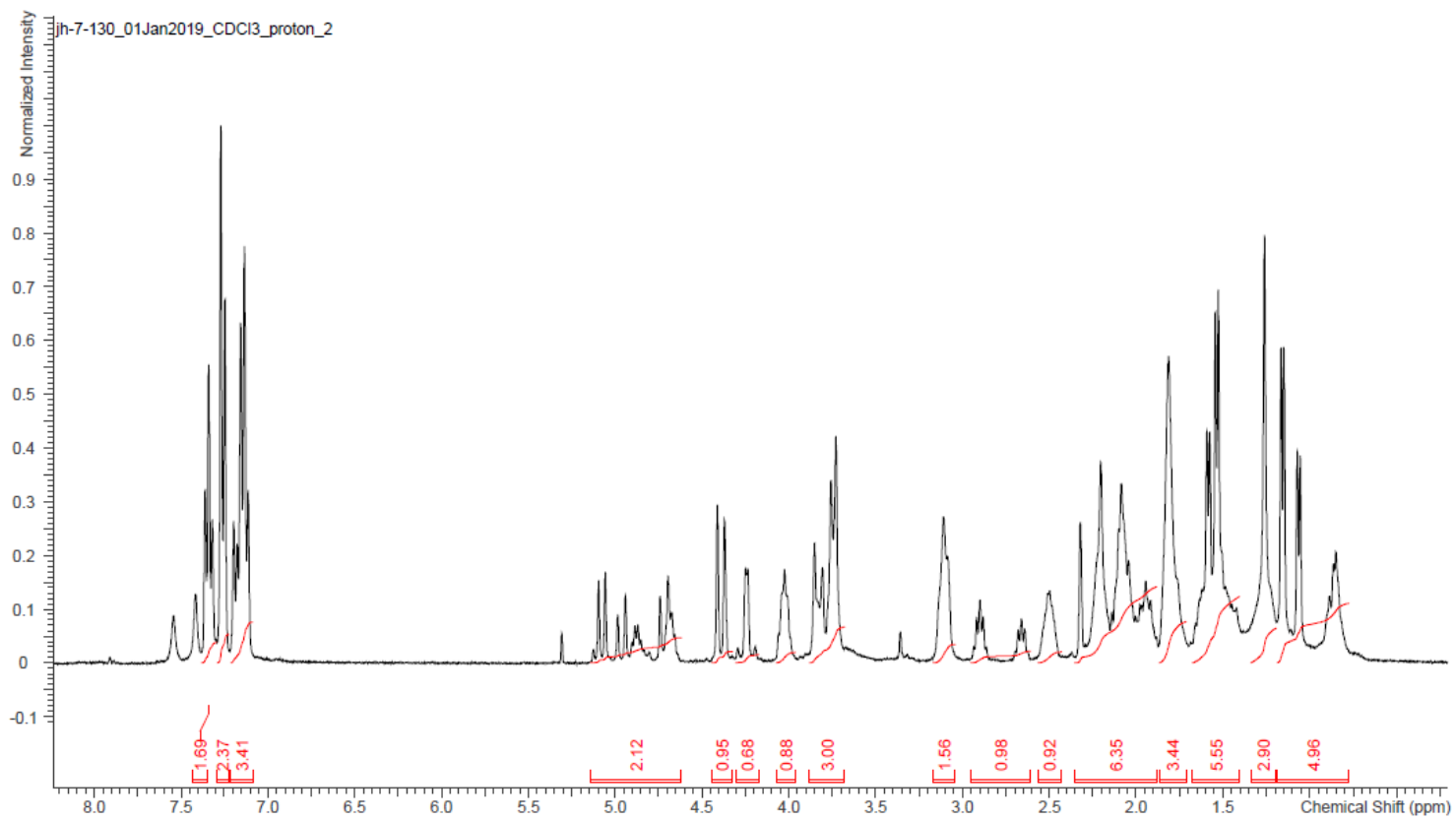
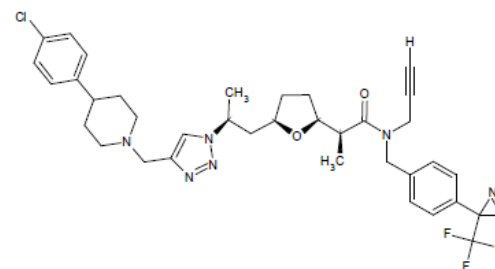


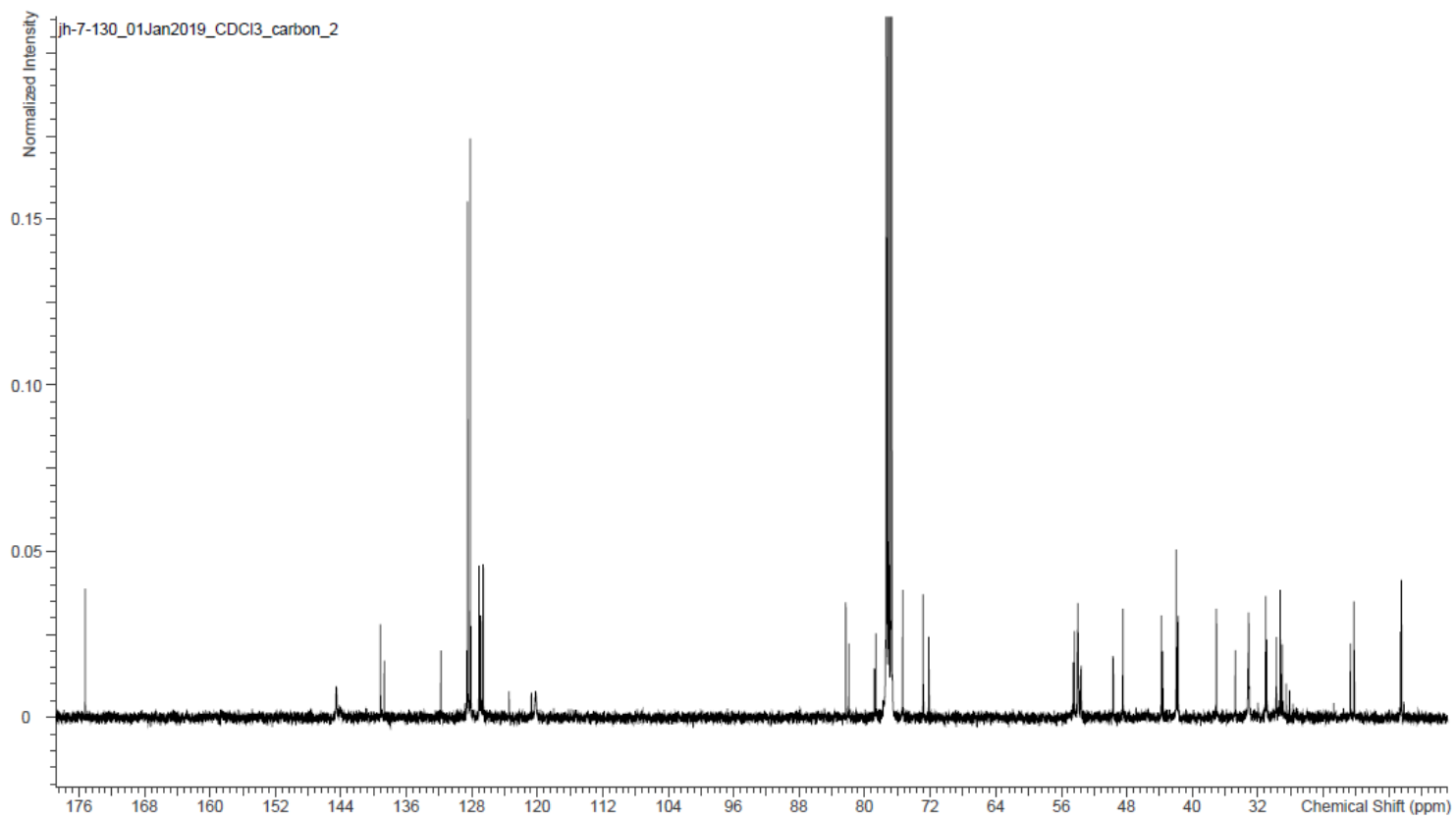
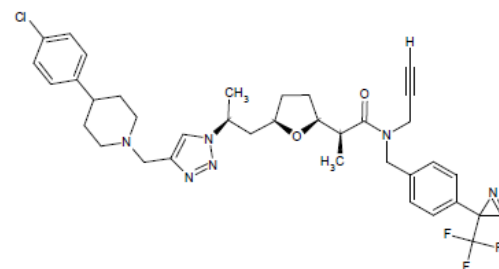


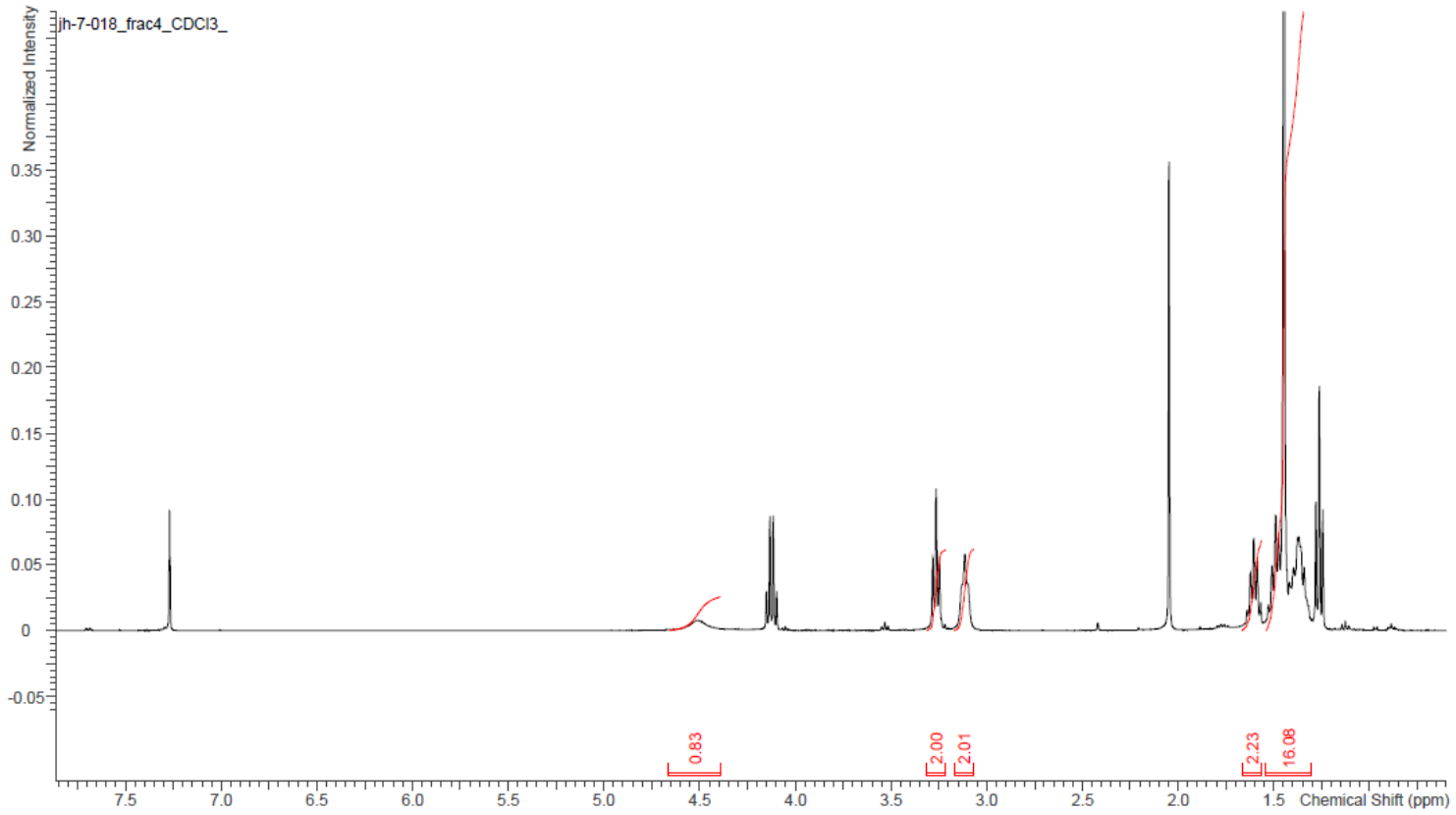
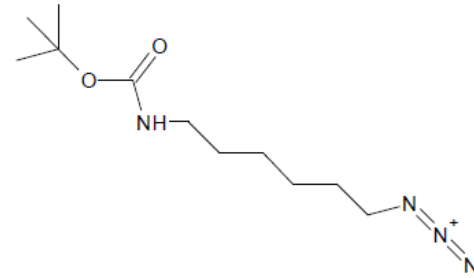


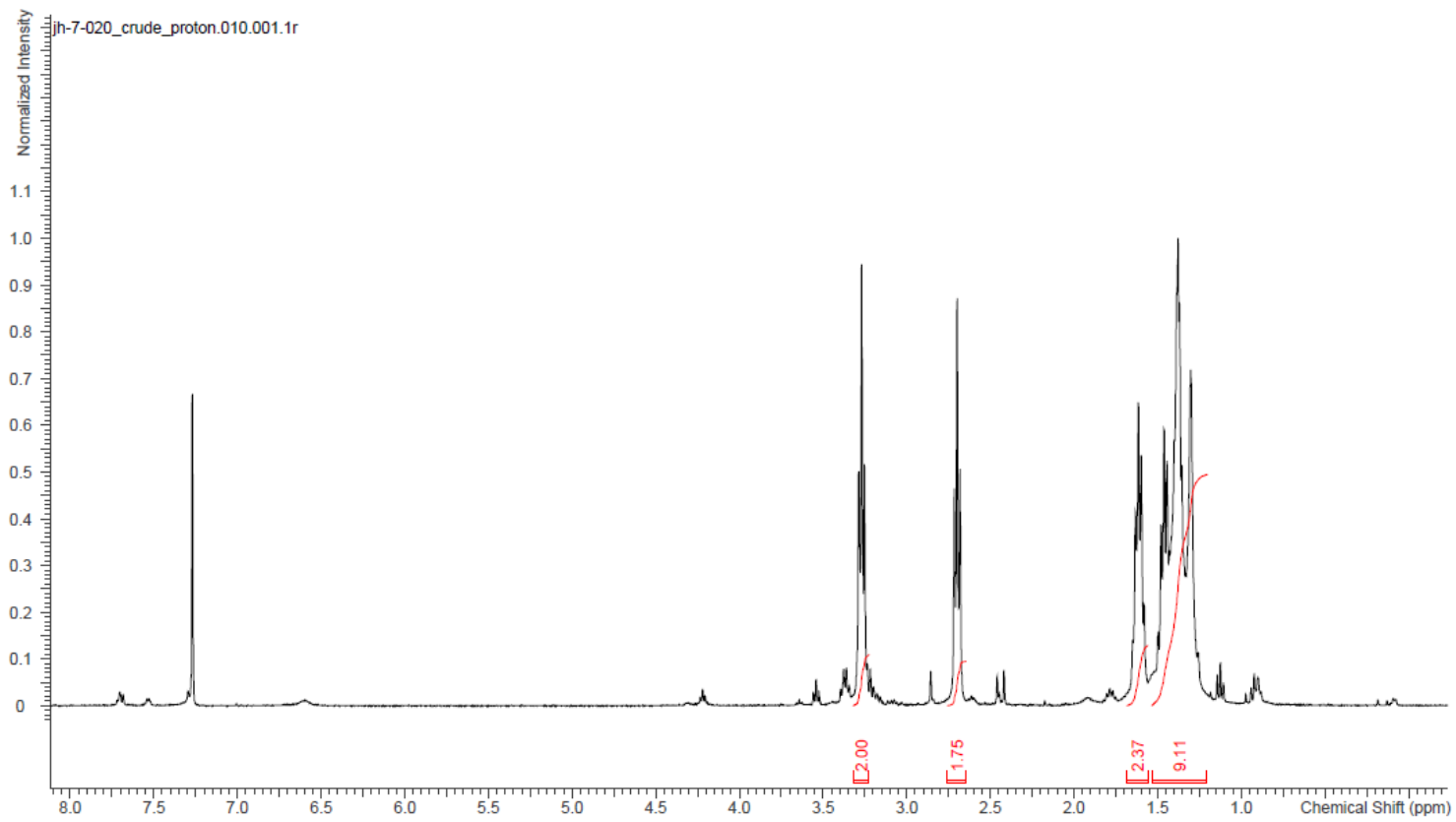
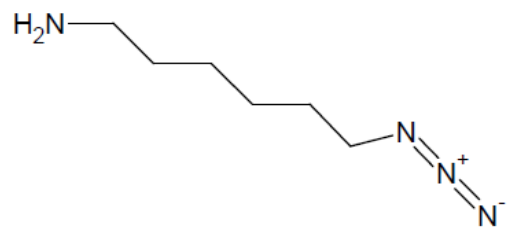


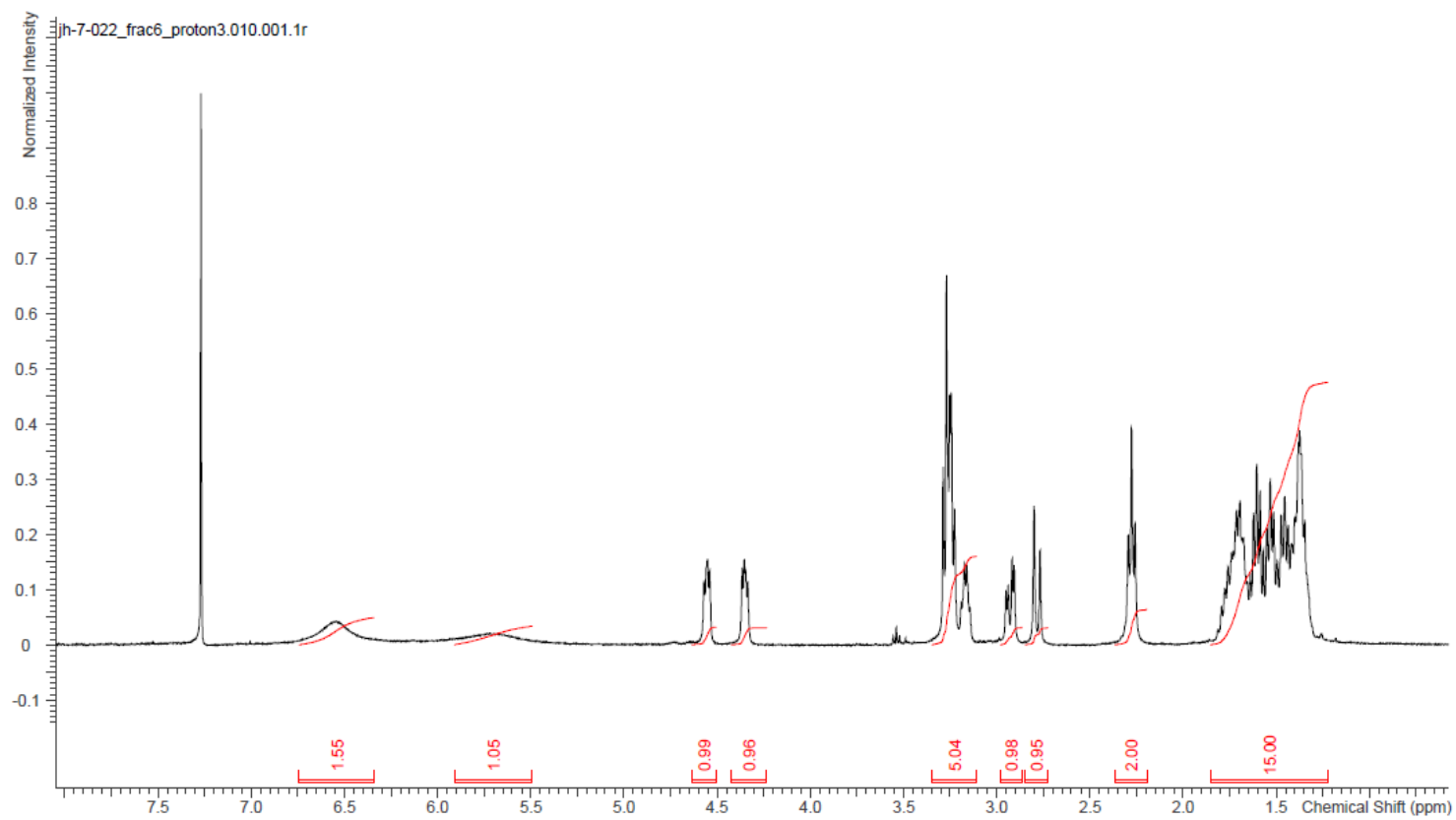
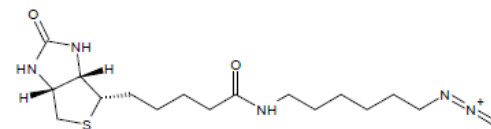


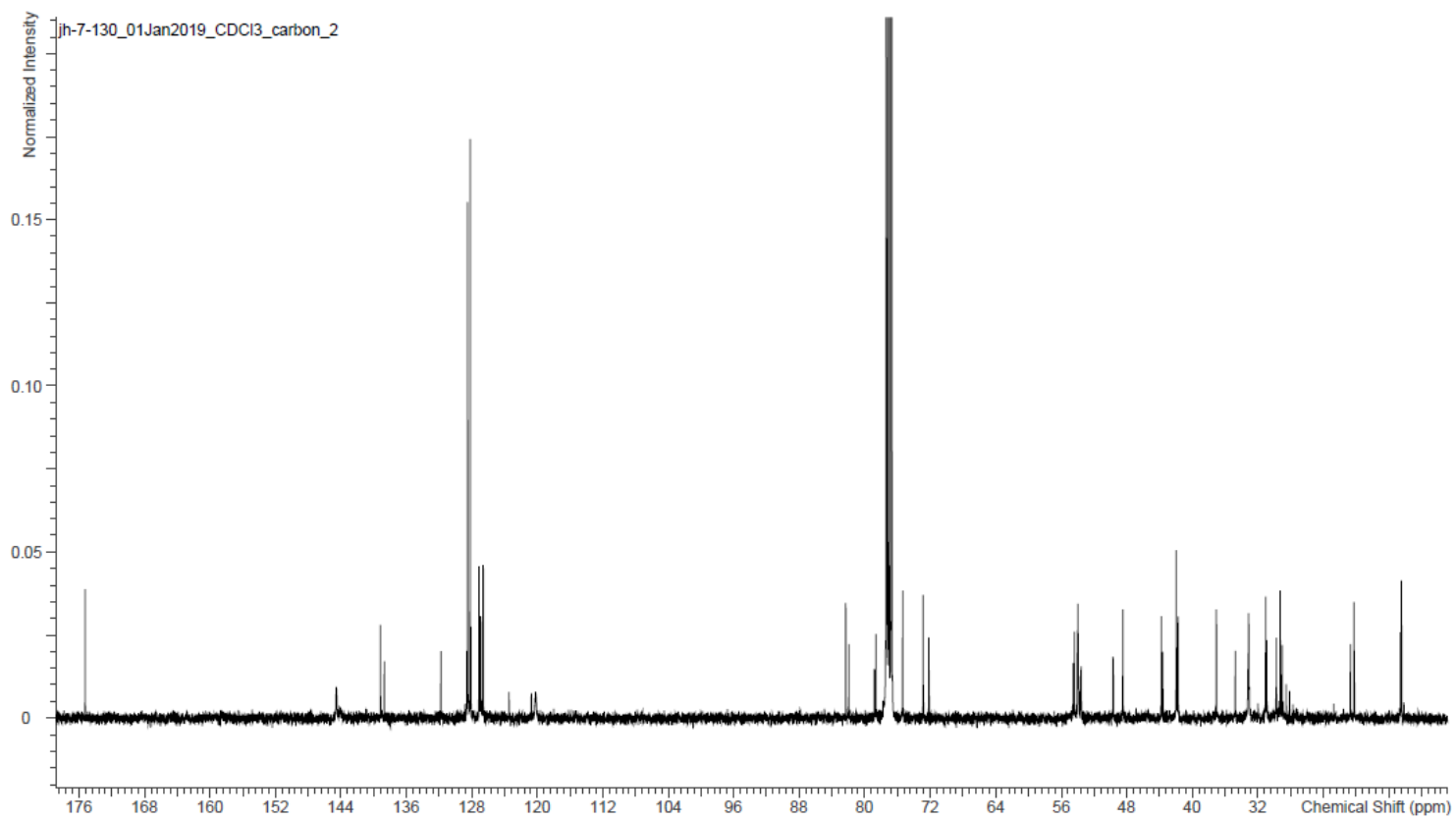
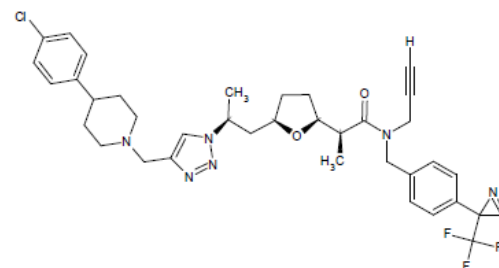












References:

1. Jindal, B. A. K., Pandya, M. K. & Khan, M. I. D. Antimicrobial resistance: A public health challenge. *Med. J. Armed Forces India* (2015). doi:10.1016/j.mjafi.2014.04.011
2. Kotwani, A. & Holloway, K. Antibiotic prescribing practice for acute, uncomplicated respiratory tract infections in primary care settings in New Delhi, India. *Trop. Med. Int. Health* (2014). doi:10.1111/tmi.12327
3. Simpkin, V. L., Renwick, M. J., Kelly, R. & Mossialos, E. Incentivising innovation in antibiotic drug discovery and development: Progress, challenges and next steps. *Journal of Antibiotics* (2017). doi:10.1038/ja.2017.124
4. Furuya, E. Y. & Lowy, F. D. Antimicrobial-resistant bacteria in the community setting. *Nature Reviews Microbiology* (2006). doi:10.1038/nrmicro1325
5. Daum, R. S. & Seal, J. B. Evolving antimicrobial chemotherapy for *Staphylococcus aureus* infections: Our backs to the wall. *Crit Care Med* (2001).
6. Maclean Smith, I. & Vickers, A. B. NATURAL HISTORY OF 338 TREATED AND UNTREATED PATIENTS WITH STAPHYLOCOCCAL SEPTICÆMIA. (1936-1955). *Lancet* (1960). doi:10.1016/S0140-6736(60)92303-5
7. Rammelkamp, C. H. & Maxon, T. Resistance of *Staphylococcus aureus* to the Action of Penicillin. *Exp. Biol. Med.* (1942). doi:10.3181/00379727-51-13986
8. Haley, R. W. *et al.* The emergence of methicillin-resistant *Staphylococcus aureus* infections in United States hospitals. Possible role of the house staff-patient transfer circuit. *Ann. Intern. Med.* (1982). doi:10.7326/0003-4819-97-3-297
9. Hiramatsu, K., Cui, L., Kuroda, M. & Ito, T. The emergence and evolution of methicillin-resistant *Staphylococcus aureus*. *Trends in Microbiology* (2001). doi:10.1016/S0966-842X(01)02175-8
10. Ventola, C. L. The antibiotic resistance crisis: part 1: causes and threats. *P T A peer-reviewed J. Formul. Manag.* **40**, 277–83 (2015).
11. Munita, J. M., Arias, C. A., Unit, A. R. & Santiago, A. De. HHS Public Access. *Mech. Antibiot. Resist.* **4**, 1–37 (2016).
12. Aminov, R. I. A brief history of the antibiotic era: Lessons learned and challenges for the future. *Front. Microbiol.* **1**, 1–7 (2010).
13. P., C. C. B. & S. B. in *Antimicrobial susceptibility testing protocols*. (ed. Richard Schwalbe, Lynn Steele-Moore, A. C. G.) (CRC Press, Taylor and Frances group, 2007).
14. Heesemann, J. [Mechanisms of resistance to beta-lactam antibiotics]. *Infection* (1993).
15. J.M., H.-M. Chemistry and biology of the polyene macrolide antibiotics. *Bacteriol. Rev.* (1973).
16. Nelson, M. L. & Levy, S. B. The history of the tetracyclines. *Ann. N. Y. Acad. Sci.* **1241**, 17–32 (2011).
17. Chopra, I. & Roberts, M. Tetracycline Antibiotics: Mode of Action, Applications, Molecular Biology, and Epidemiology of Bacterial Resistance. *Microbiol. Mol. Biol. Rev.* (2001). doi:10.1128/MMBR.65.2.232-260.2001
18. Fuoco, D. Classification Framework and Chemical Biology of Tetracycline-Structure-Based Drugs. *Antibiotics* (2012). doi:10.3390/antibiotics1010001
19. Tillotson, G. S. Quinolones: Structure-activity relationships and future predictions. *J. Med. Microbiol.* **44**, 320–324 (1996).
20. Hawkey, P. M. Mechanisms of quinolone action and microbial response. *J. Antimicrob. Chemother.* **51**, 29–35 (2003).

21. Chittapragada, M., Roberts, S. & Ham, Y. W. Aminoglycosides: Molecular insights on the recognition of RNA and aminoglycoside mimics. *Perspectives in Medicinal Chemistry* (2009).
22. Klotz, I. M. The Mode of Action of Sulfonamides. *J. Am. Chem. Soc.* (1944). doi:10.1021/ja01231a046
23. Kang, H. K. & Park, Y. Glycopeptide antibiotics: Structure and mechanisms of action. *Journal of Bacteriology and Virology* (2015). doi:10.4167/jbv.2015.45.2.67
24. Reynolds, P. E. Structure, biochemistry and mechanism of action of glycopeptide antibiotics. *Eur. J. Clin. Microbiol. Infect. Dis.* (1989). doi:10.1007/BF01967563
25. Shinabarger, D. L. *et al.* Mechanism of action of oxazolidinones: Effects of linezolid and eperezolid on translation reactions. *Antimicrob. Agents Chemother.* (1997).
26. Bozdogan, B. & Appelbaum, P. C. Oxazolidinones: Activity, mode of action, and mechanism of resistance. *International Journal of Antimicrobial Agents* (2004). doi:10.1016/j.ijantimicag.2003.11.003
27. Takenaka, T. Classical vs reverse pharmacology in drug discovery. *BJU Int* **88 Suppl**, 7–10 (2001).
28. Wohlleben, W., Mast, Y., Stegmann, E. & Ziemert, N. Antibiotic drug discovery. *Microb. Biotechnol.* **9**, 541–548 (2016).
29. Kumar, K. & Waldmann, H. Synthesis of natural product inspired compound collections. *Angewandte Chemie - International Edition* (2009). doi:10.1002/anie.200803437
30. Wetzel, S., Bon, R. S., Kumar, K. & Waldmann, H. Biology-oriented synthesis. *Angew. Chemie - Int. Ed.* **50**, 10800–10826 (2011).
31. Guha, R. In Silico Models for Drug Discovery. **993**, 81–94 (2013).
32. Riss, T. L. *et al.* Cell Viability Assays. *Assay Guid. Man. [Internet]* (2013). doi:10.1016/j.acthis.2012.01.006
33. Terstappen, G. C., Schlüpen, C., Raggiaschi, R. & Gaviraghi, G. Target deconvolution strategies in drug discovery. *Nature Reviews Drug Discovery* (2007). doi:10.1038/nrd2410
34. E.L., B., E., H., I., P. & E.J., K. Approaches to the analysis of cell signaling networks and their application in drug discovery. *Curr. Opin. Drug Discov. Dev.* (2005).
35. Lee, J. A. & Berg, E. L. Neoclassic drug discovery: The case for lead generation using phenotypic and functional approaches. *J. Biomol. Screen.* (2013). doi:10.1177/1087057113506118
36. Moffat, J. G., Vincent, F., Lee, J. A., Eder, J. & Prunotto, M. Opportunities and challenges in phenotypic drug discovery: An industry perspective. *Nature Reviews Drug Discovery* (2017). doi:10.1038/nrd.2017.111
37. Paul, S. M. *et al.* How to improve RD productivity: The pharmaceutical industry's grand challenge. *Nature Reviews Drug Discovery* (2010). doi:10.1038/nrd3078
38. Luesse, S. B. *et al.* Natural products in parallel synthesis: Triazole libraries of nonactic acid. *Bioorganic Med. Chem. Lett.* **18**, 3946–3949 (2008).
39. Nikodinovic, J. *et al.* Resolution of methyl nonactate by *Rhodococcus erythropolis* under aerobic and anaerobic conditions. *Org. Lett.* **8**, 443–445 (2006).
40. Kusche, B. R., Smith, A. E., McGuirl, M. A. & Priestley, N. D. Alternating pattern of stereochemistry in the nonactin macrocycle is required for antibacterial activity and efficient ion binding. *J. Am. Chem. Soc.* (2009). doi:10.1021/ja9050235
41. Fischbach, M. A. & Walsh, C. T. Antibiotics for emerging pathogens. *Science* (2009). doi:10.1126/science.1176667

42. Von Nussbaum, F., Brands, M., Hinzen, B., Weigand, S. & Häbich, D. Antibacterial natural products in medicinal chemistry - Exodus or revival? *Angewandte Chemie - International Edition* (2006). doi:10.1002/anie.200600350
43. WHO. Antimicrobial resistance. Global Report on Surveillance. *World Heal. Organ.* (2014). doi:10.1007/s13312-014-0374-3
44. Lowy, F. Staphylococcus aureus infections. *N. Engl. J. Med.* (1998). doi:10.1056/NEJM199808203390806
45. Tong, S. Y. C., Davis, J. S., Eichenberger, E., Holland, T. L. & Fowler, V. G. Staphylococcus aureus infections: Epidemiology, pathophysiology, clinical manifestations, and management. *Clin. Microbiol. Rev.* (2015). doi:10.1128/CMR.00134-14
46. Gerits, E. *et al.* Elucidation of the mode of action of a new antibacterial compound active against Staphylococcus aureus and Pseudomonas aeruginosa. *PLoS One* (2016). doi:10.1371/journal.pone.0155139
47. Cross, J. & Jacobs, R. F. Vancomycin-resistant enterococcal infections. *Seminars in Pediatric Infectious Diseases* (1996). doi:10.1016/S1045-1870(96)80004-5
48. Koch, G. *et al.* Evolution of resistance to a last-resort antibiotic in staphylococcus aureus via bacterial competition. *Cell* (2014). doi:10.1016/j.cell.2014.06.046
49. Butler, M. S., Blaskovich, M. A. & Cooper, M. A. Antibiotics in the clinical pipeline in 2013. *Journal of Antibiotics* (2013). doi:10.1038/ja.2013.86
50. Feher, M. & Schmidt, J. M. Property distributions: Differences between drugs, natural products, and molecules from combinatorial chemistry. *J. Chem. Inf. Comput. Sci.* (2003). doi:10.1021/ci0200467
51. Chopra, I., Hesse, L. & O'Neill, A. J. Exploiting current understanding of antibiotic action for discovery of new drugs. *J. Appl. Microbiol.* (2002). doi:10.1046/j.1365-2672.92.5s1.13.x
52. Phillips, J. B. *et al.* Natural product derivatives with bactericidal activity against Gram-positive pathogens including methicillin-resistant Staphylococcus aureus and vancomycin-resistant Enterococcus faecalis. *Bioorganic Med. Chem. Lett.* **20**, 5936–5938 (2010).
53. Gellman, S. H., Dado, G. P., Liang, G. B. & Adams, B. R. Conformation-Directing Effects of a Single Intramolecular Amide-Amide Hydrogen Bond: Variable-Temperature NMR and IR Studies on a Homologous Diamide Series. *J. Am. Chem. Soc.* (1991). doi:10.1021/ja00004a016
54. Scocchera, E. *et al.* Charged Nonclassical Antifolates with Activity Against Gram-Positive and Gram-Negative Pathogens. *ACS Med. Chem. Lett.* (2016). doi:10.1021/acsmchemlett.6b00120
55. H. Brooks, W., C. Guida, W. & G. Daniel, K. The Significance of Chirality in Drug Design and Development. *Curr. Top. Med. Chem.* (2011). doi:10.2174/156802611795165098
56. Farha, M. A. & Brown, E. D. Strategies for target identification of antimicrobial natural products. *Natural Product Reports* (2016). doi:10.1039/c5np00127g
57. Jahn, L. J., Munck, C., Ellabaan, M. M. H. & Sommer, M. O. A. Adaptive laboratory evolution of antibiotic resistance using different selection regimes lead to similar phenotypes and genotypes. *Front. Microbiol.* (2017). doi:10.3389/fmicb.2017.00816
58. Lipinski, C. A., Lombardo, F., Dominy, B. W. & Feeney, P. J. Experimental and computational approaches to estimate solubility and permeability in drug discovery and

- development settings. *Advanced Drug Delivery Reviews* (2012). doi:10.1016/j.addr.2012.09.019
59. Pankey, G. A. & Sabath, L. D. Clinical Relevance of Bacteriostatic versus Bactericidal Mechanisms of Action in the Treatment of Gram-Positive Bacterial Infections. *Clin. Infect. Dis.* (2004). doi:10.1086/381972
 60. Levison, M. E. Pharmacodynamics of antimicrobial drugs. *Infectious Disease Clinics of North America* (2004). doi:10.1016/j.idc.2004.04.012
 61. Yung-Chi, C. & Prusoff, W. H. Relationship between the inhibition constant (KI) and the concentration of inhibitor which causes 50 per cent inhibition (I50) of an enzymatic reaction. *Biochem. Pharmacol.* (1973). doi:10.1016/0006-2952(73)90196-2
 62. Smith, E. & Collins, I. Photoaffinity labeling in target-and binding-site identification. *Future Medicinal Chemistry* (2015). doi:10.4155/fmc.14.152
 63. Ruoho, A., Kiefer, H., Roeder, P. & Singer, S. The mechanism of photoaffinity labeling. *Proc. Natl. Acad. Sci. USA* (1973). doi:10.1073/pnas.70.9.2567
 64. Das, J. Aliphatic diazirines as photoaffinity probes for proteins: Recent developments. *Chemical Reviews* (2011). doi:10.1021/cr1002722
 65. Chee, G. L., Yalowich, J. C., Bodner, A., Wu, X. & Hasinoff, B. B. A diazirine-based photoaffinity etoposide probe for labeling topoisomerase II. *Bioorganic Med. Chem.* (2010). doi:10.1016/j.bmc.2009.11.048
 66. Green, N. M. Avidin. *Adv. Protein Chem.* (1975). doi:10.1016/S0065-3233(08)60411-8
 67. Marttila, A. T. *et al.* Recombinant Neutralite Avidin: A non-glycosylated, acidic mutant of chicken avidin that exhibits high affinity for biotin and low non-specific binding properties. *FEBS Lett.* (2000). doi:10.1016/S0014-5793(00)01119-4
 68. Eirich, J., Orth, R. & Sieber, S. A. Unraveling the protein targets of vancomycin in living *S. aureus* and *E. faecalis* cells. *J. Am. Chem. Soc.* (2011). doi:10.1021/ja2039979
 69. MacKinnon, A. L. & Taunton, J. in *Current Protocols in Chemical Biology* (2009). doi:10.1002/9780470559277.ch090167
 70. Ambroise, Y., Pillon, F., Mioskowski, C., Valleix, A. & Rousseau, B. Synthesis and tritium labeling of new aromatic diazirine building blocks for photoaffinity labeling and cross-linking. *European J. Org. Chem.* (2001). doi:10.1002/1099-0690(200110)2001:20<3961::AID-EJOC3961>3.0.CO;2-R
 71. Burgermeister, W., Nassal, M., Wieland, T. & Helmreich, E. J. M. A carbene-generating photoaffinity probe for beta-adrenergic receptors. *BBA - Biomembr.* (1983). doi:10.1016/0005-2736(83)90488-1
 72. Hatanaka, Y., Hashimoto, M., Nakayama, H. & Kanaoka, Y. Syntheses of Nitro-Substituted Aryl Diazirines. An Entry to Chromogenic Carbene Precursors for Photoaffinity Labeling. *Chem. Pharm. Bull. (Tokyo)*. (1994). doi:10.1248/cpb.42.826
 73. Taubes, G. The bacteria fight back. *Science* (2008). doi:10.1126/science.321.5887.356
 74. Payne, D. J., Gwynn, M. N., Holmes, D. J. & Pompliano, D. L. Drugs for bad bugs: Confronting the challenges of antibacterial discovery. *Nature Reviews Drug Discovery* (2007). doi:10.1038/nrd2201
 75. Farhat, M. R. *et al.* Genomic analysis identifies targets of convergent positive selection in drug-resistant *Mycobacterium tuberculosis*. *Nat. Genet.* (2013). doi:10.1038/ng.2747
 76. Nikaido, H. Prevention of drug access to bacterial targets: Permeability barriers and active efflux. *Science (80-.)*. (1994). doi:10.1126/science.8153625
 77. Schrag, S. J., Perrot, V. & Levin, B. R. Adaptation to the fitness costs of antibiotic

- resistance in *Escherichia coli*. *Proc. R. Soc. B Biol. Sci.* (1997). doi:10.1098/rspb.1997.0178
78. Denamur, E. & Matic, I. Evolution of mutation rates in bacteria. *Molecular Microbiology* (2006). doi:10.1111/j.1365-2958.2006.05150.x
 79. Mooney, S. D., Krishnan, V. G. & Evani, U. S. Bioinformatic tools for identifying disease gene and SNP candidates. *Methods in Molecular Biology* (2010). doi:10.1007/978-1-60327-367-1_17
 80. Wattam, A. R. *et al.* Improvements to PATRIC, the all-bacterial bioinformatics database and analysis resource center. *Nucleic Acids Res.* (2017). doi:10.1093/nar/gkw1017
 81. Zojer, M. *et al.* Variant profiling of evolving prokaryotic populations. *PeerJ* (2017). doi:10.7717/peerj.2997
 82. Li, H. & Durbin, R. Fast and accurate long-read alignment with Burrows-Wheeler transform. *Bioinformatics* (2010). doi:10.1093/bioinformatics/btp698
 83. Yang, X., Chockalingam, S. P. & Aluru, S. A survey of error-correction methods for next-generation sequencing. *Briefings in Bioinformatics* (2013). doi:10.1093/bib/bbs015
 84. Rine, J., Hansen, W., Hardeman, E. & Davis, R. W. Targeted selection of recombinant clones through gene dosage effects. *Proc. Natl. Acad. Sci. U. S. A.* (1983). doi:10.1073/pnas.80.22.6750
 85. Stephen C Bergmeier, N. D. P. Synthesis of methyl nonactate derivatives. (2006).
 86. Murali, R., Prakash Rao, H. S. & Scheeren, H. W. Intra-molecular Diels-Alder reactions of citraconamic acids from furfurylamines and citraconic anhydride: Effects of substitution in the furan ring on regioselectivity. *Tetrahedron* (2001). doi:10.1016/S0040-4020(01)00175-2
 87. John Naleway, R. H. Compositions And Methods For Targeted Enzymatic Release Of Cell Regulatory Compounds. (2006).
 88. Jianhua Cao, Youhao Dong, Eric J. Gilbert, Ying Huang, Joseph M. Kelly, Stuart McCombie, Neng-Yang Shih, P. C. T. Piperidine derivatives useful as ccr3 antagonists. (2005).
 89. Frederick Hicks, Da-Ming Gou, Salvatore Anthony Marchese, Lawrence J. Martel, Atena Necula, Richard E. Benetti, R. A. S. Method for making aryl hydrazines and substituted indoles. (2002).
 90. Lee J, Seo S, Lim E, Cho N, N. G. & Al., E. Synthesis and biological evaluation of 1-(isoxazol-5-ylmethylaminoethyl)-4-phenyl tetrahydropyridine and piperidine derivatives as potent T-type calcium channel blockers with antinociceptive effect in a neuropathic pain model. *Eur. J. Med. Chem.* **74**, 246–257 (2014).
 91. Chen, G. *et al.* Synthesis and SAR study of diphenylbutylpiperidines as cell autophagy inducers. *Bioorganic Med. Chem. Lett.* (2011). doi:10.1016/j.bmcl.2010.11.029
 92. Acquaa-Harrison, G., Zhou, S., Hines, J. V. & Bergmeier, S. C. Library of 1, 4-Disubstituted 1, 2, 3-Triazole Analogs of Oxazolidinone RNA-Binding Agents. *J. Comb. Chem.* (2010). doi:10.1021/cc100029y
 93. Weisner, J. *et al.* Covalent-Allosteric Kinase Inhibitors. *Angew. Chemie - Int. Ed.* (2015). doi:10.1002/anie.201502142
 94. Yoo, B. *et al.* N -acetylgalactosamino dendrons as clearing agents to enhance liver targeting of model antibody-fusion protein. *Bioconjug. Chem.* (2013). doi:10.1021/bc400333m
 95. Akiba, H., Sumaoka, J., Tsumoto, K. & Komiyama, M. Click Conjugation of a Binuclear

- Terbium(III) Complex for Real-Time Detection of Tyrosine Phosphorylation. *Anal. Chem.* (2015). doi:10.1021/ac5045466
96. Qin, Z. *et al.* Design and synthesis of neuroprotective methylthiazoles and modification as NO-chimeras for neurodegenerative therapy. *J. Med. Chem.* (2012). doi:10.1021/jm300353r
 97. Emer, E. *et al.* Diversity-oriented approach to CF₃CHF-, CF₃CFBr-, CF₃CF₂-, (CF₃)₂CH-, and CF₃(SCF₃)CH-substituted arenes from 1-(Diazo-2,2,2-trifluoroethyl)arenes. *Org. Lett.* (2014). doi:10.1021/ol5030184
 98. Dudutiene, V. *et al.* Discovery and characterization of novel selective inhibitors of carbonic anhydrase IX. *J. Med. Chem.* (2014). doi:10.1021/jm501003k
 99. Qiao, C. J. *et al.* Synthesis and biological evaluation of indole-2-carboxamides bearing photoactivatable functionalities as novel allosteric modulators for the cannabinoid CB1 receptor. *Eur. J. Med. Chem.* (2016). doi:10.1021/acschemneuro.6b00041
 100. Hentschel, F. *et al.* Synthesis and cytotoxicity of a diazirine-based photopsammaphin. *European J. Org. Chem.* (2014). doi:10.1002/ejoc.201301717
 101. Kambe, T., Correia, B. E., Niphakis, M. J. & Cravatt, B. F. Mapping the protein interaction landscape for fully functionalized small-molecule probes in human cells. *J. Am. Chem. Soc.* (2014). doi:10.1021/ja505517t
 102. Tantama, M., Lin, W. C. & Licht, S. An activity-based protein profiling probe for the nicotinic acetylcholine receptor. *J. Am. Chem. Soc.* (2008). doi:10.1021/ja805868x
 103. Rowland, M. M. *et al.* Phosphatidylinositol 3,4,5-trisphosphate activity probes for the labeling and proteomic characterization of protein binding partners. *Biochemistry* (2011). doi:10.1021/bi201636s
 104. Tom, C. T. M. B. & Martin, B. R. Fat chance! Getting a grip on a slippery modification. *ACS Chemical Biology* (2013). doi:10.1021/cb300607e
 105. Schenk, S. & Laddaga, R. A. Improved method for electroporation of *Staphylococcus aureus*. *FEMS Microbiol. Lett.* (1992). doi:10.1016/0378-1097(92)90596-G
 106. Pang, Y. Y. *et al.* Agr-dependent interactions of *Staphylococcus aureus* USA300 with human polymorphonuclear neutrophils. *J. Innate Immun.* (2010). doi:10.1159/000319855